Techno-economic evaluation of a waste heat assisted district heating system

M. Hansen

Techno-economic evaluation of a waste heat assisted district heating system

by

M. Hansen

to obtain the degree of Master of Science
at the Delft University of Technology,
to be defended publicly on Friday May 28, 2021 at 9:00 AM.

Student number:	4350294	
Project duration:	March 2, 2020 – May 28, 2021	
Thesis committee:	Dr. ir. C.A. Infante Fereirra,	TU Delft, supervisor
	Prof. dr. ir. T.J.H. Vlugt,	TU Delft
	Dr. ir. R. Pecknik,	TU Delft
	Ir. M. van der Werf,	Witteveen+Bos, supervisor

This thesis is confidential and cannot be made public until May 28, 2023.

TU Delft

Abstract

The purpose of this research is to find an alternative to the natural gas-fueled heating systems of dwellings for the neighborhood of Westenholte. Reasons for replacing this system include the high GHG emissions, resulting from the combustion product of natural gas (CO_2), in addition to its greenhouse effect.

As a solution to replace the GHG-intensive heating of dwellings, a district heating (DH) network is proposed. This heating system does not involve the vast amount of natural gas needed by the traditional system, leading to the desired reduction in CO_2 emissions. However, constructing and using a DH network is considered a large investment, which might be higher in total cost in comparison to the traditional, CO_2 emission-intensive, heating system. Both the cost and CO_2 emission of a new DH should be minimalized. Therefore, the following KPIs are selected for comparison of the DH network: CAPEX, OPEX, and LCOE to indicate the cost, as well as CO_2 emission to indicate the difference in GHG emissions. The KPIs of the DH of Westenholte are then compared to a reference solution: a decentralized all-electric solution, which also stands largely independent of natural gas.
These KPI of the DH of Westenholte are to be compared to a reference solution: a decentralized all-electric solution, which is also largely independent of natural gas.

Two temperature regimes of the distribution temperature of the DH are calculated and optimized for the neighborhood of Westenholte. By using a lower temperature (50/30 °C) in comparison to the more conventional temperature (70/40 ° C), the KPIs could be improved. Lowering the distribution temperature could make the heat pumps more efficient, subsequently reducing the overall cost.
Additionally, the DH can probably reduce the GHG emission and, at the same time, is cheaper by using multiple renewable heat sources. As the heat profile over time differs for all heat sources, using a combination of the energy sources is estimated to create a better match with the heat demand profile. This would reduce the required heat production, storage, and associated CO_2 emission and cost.

In this study, a DH network is divided into the different submodules – heat demand, supply, and coupling of demand and supply – and then modeled in Python. The heat demand submodule models the heat demand of the dwellings, including the domestic hot water (DHW). In the heat supply submodule, all the available thermal energy sources used are modeled: wastewater (TEWW), surface water (TESW), solar, and industrial waste (IWH). The coupling module then matches the demand and supply geographically, by modeling the distribution grid, and, in time, also by modeling the thermal energy storage.

For the DH of Westenholte, the lowest LCOE of 0.15 € /kWh was found for a 70/40 °C DH combination of 25 percent IWH, 60 percent TEWW, and 15 percent TESW in addition to a peak supply, however, generating 34.67 ton/year CO_2 emission. A DH network of 50/30 °C would provide the lowest CO_2 emission, which would use 25 percent IWH and 75 percent solar thermal energy inducing a CO_2 emission of 2.76 ton/year, nonetheless, requiring an LCOE of 0.40 € /kWh. In contrast to the all-electric reference scenario with an LCOE of 0.22 € /kWh and a CO_2 emission of 49 ton/year, the LCOE-optimized scenario proved both cheaper and dissipating lower CO_2 emissions.

Acknowledgments

This thesis was only made possible with the help of all those involved in the project. Therefore, I would like to thank, first and foremost my supervisor, Dr. ir. Carlos Infante Ferreira, for his guidance and patience while writing this thesis. His much-appreciated feedback was key to the quality of this study.
Second, I would like to give thanks to Ing. Aylin Knepper and Ir. Mark van der Werf for their guidance at Witteveen+Bos. The weekly meetings provided me with valuable new insights and enabled me to attain a steeper learning curve. Also, I would like to commend Ir. Raphaël van der Velde, among others involved, for the possibility to work on this project.
At last, I am also grateful to my family, for the support provided in the process of writing my thesis during the COVID-19 pandemic.

Mathijs Hansen
Delft, May 2021

Contents

Nomenclature

Symbols

$\dot{m}$	Mass flow rate [kg/s]
$\dot{Q}$	Heat flow [kW]
A	Surface area [m^2]
a_0	Linear regression parameter [°C]
a_1	First variable FPC specific term [m^2/(K*J)]
a_2	Second variable FPC specific term [m^2/(K^2*J)]
c_p	Specific heat [J/(kg * K)
E	Energy density of water [KJ/m^3]
f	Function with input heat load and output KPI
f_d	Fanning fiction factor [-]
G	Solar irradiance [kWm^2]
n	Lifetime of the technology [years]
r	Discount rate [-]
T	Temperature [°C]
t	Time [s], lifetime
A	Heat demand for calibration year [kWh]
B	Behavior of occupants in dwellings [%]
b	Linear regression parameter [-]
c	Constant
D	Diameter
f	Friction factor [-]
Gas	Cubic meters of gas [m^3]
H	Height [m]
h	Height dependent on time [m]
K	Minor loss factors [-]
k	Ratio of specific heats [-]
LMTD	Log mean temperature [°C]
N	Number
P	Timeseries [t^{-1}]
p	Pressure [Pa]
p_t	Time-series
Q	Energy [J]
Re	Reynolds number
SMA	Simple moving average filter for a time-series with N steps
U	Overall heat transfer coefficient [kW(m^2 * K)
V	Volume [m^3]
V	Volumetric flow [m^3/s]
v	Velocity [m/s]
W	Work [kWh]
w	Width [m]

Subscripts

a	Ambient
air	Air to water variant
array	Array of FPC
avg	Average
bio	Biological capacity [g/day]
capex	CAPEX
cold	Cold side
compressor	Compressor
d	Demand
DHW	Domestic hot water
DN	Nominal diameter of piping
dwelling	Per dwelling
eff	Effective
effl	Effluent
el	Electric
Extra	Extra cost
field	Field of FPC

FPC	Flat plate collector
gas	Combustion efficiency of gas
head	Head of pump
HEX	Heat exchanger
hl	The heat losses
hot	Hot side
HP	Heatpump
i	Hour
IJssel	Property of the IJssel
inside	Within dwelling boundaries
j	Specific archetype
l	Levelized, total values equals on of the time-series
m	Average
major	Major part
max	Maximum
minor	Minor part
outside	Outside dwelling boundaries
pipes	Piping
pump	Pump
river	River property
s	Heat required to supply the DH system
Secondary	Secondary cost
seg	Segment of neighborhood
SMA	Simple moving average filter used
Solar	Solar specific
st	Storage
stored	Stored
sw	Surface water
tank	Tank used to store
TES	Thermal energy storage
th	Thermocline
Total	Total
unforeseen	Previously unforeseen cost
w	Water
yearly	Per year

Greek symbols

α	Linear factor
β	Linear factor
Δ	Difference
ϵ	Pipe roughness [m]
η	Efficiency [-]
ρ	Density [kg/m^3]
τ	Operation time [s]

Acronyms

ATES	Aquifer thermal energy storage
C-TES	Chemical thermal energy storage
CAPEX	Capital expenditure
CHP	Combined Heat and Power
COP	Coefficient of performance
DH	District heating
DHW	Domestic hot water
EMM	Energy management model
FPC	Flat plate collector
GHG	Greenhouse gases
HDPE	High-density polyethylene
HEX	Heat exchanger
HHV	High coloric values
HT-ATES	High-temperature aquifer thermal energy storage
IWH	Industrial waste heat
KPI	Key Performance Indicators
LAW	Leidraad Aardgasvrije Wijken
LCO_2	Levelized CO_2 emission
LCOE	Levelized cost of energy
LH-TES	Latent heat thermal energy storage
LMTD	Log mean temperature
LT-ATES	Low-temperature aquifer thermal energy storage
MT-ATES	Medium-temperature aquifer thermal energy storage
OPEX	Operational expenditure

P-HEX	Plate heat exchanger
PB-h	Bonded polyurethane
PE	Polyethylene
PUR	Polyurethane
PV	Photo voltaic
PVT	Photovoltaic thermal hybrid solar plate
RES	Renewable energy sources
SCOP	Seasonal coefficient of performance
SH	Space heating
SH-TES	Sensible heat thermal energy storage
SMA	Simple moving average over period N [h]
SPF	Seasonal performance factor
SS	Stainless steel
ST	Sewage treatment
ST	Steel
STE	Solar thermal energy
TES	Thermal energy storage
TESW	Thermal energy of surface water
TEWW	Thermal energy of waste water
TRL	Technology Readiness Level
TS	Heat transfer station
WH	Waste heat

1

Motivation, research question methodology

1.1. Motivation

The European Union acknowledges global warming as a result of the emittance of greenhouse gases (GHG), such as CO_2 and CH_4, causing the greenhouse effect. Subsequently, the EU aims to stop its contribution to the greenhouse effect by 2050 as part of the European green deal (European Commission, 2019) following the Paris agreement signed in 2016. The Netherlands, as part of the European Union, has adopted the goal of 95 percent reduction of CO_2 emissions by 2050, which is ratified in the "Klimaatwet" in July of 2019 ("Klimaatwet", n.d.). This same law states that, by 2050, most of the energy supply in the Netherlands needs to be from renewable energy sources (RES) (Sociaal-Economische Raad, 2018). RES are defined as energy sources that are not depleted when consumed (for example energy from wind) or sources that renew themselves constantly (for example excess biomass from crops). RES produce little to no CO_2 emission and are supposed to be a net-zero contributor to GHG emissions.

An additional consequence of the "Klimaatwet" is the termination of the most commonly used fuel for heating, natural gas, as of 2050. Because natural gas is a GHG on its own and the burning of natural gas causes CO_2 emissions, it is perceived as an effective measure against global warming. The Netherlands is for 76 percent (Segers et al., 2019) of all heating nation-wide dependent on natural gas. The largest heat user in the Netherlands (1008 PJ) is the built environment with 47 percent of the total heat usage in 2017, of this amount, 60 percent is gas-fired. The natural gas consumption of dwellings consists mainly of space heating (SH) and domestic hot water (DHW) of the dwellings and buildings. Together SH and DHW amount for 98 percent of gas usage of dwellings (Segers et al., 2019) and this heating is done with individual gas-fired boilers. The second-largest user is the industry sector representing 42 percent of the total Dutch heat consumption, of which 44 percent is produced by natural gas. Combined, these two sectors need to find a solution to fill the heating gap of 469.4 PJ of gas-fired heat.

Zwolle, a city in the Netherlands, is now faced with the problem of replacing natural gas used in supplying the heat demand of dwellings and industry with RES as a consequence of the Klimaatwet. To be proactive in the shift towards new energy, the city set the main goal as becoming energy neutral by 2050, providing clarity and directions for its citizens. In their view, energy neutrality implies an equal amount of energy is used locally as is being produced by RES.
A possible solution for replacing the heating of dwellings with natural gas and facilitating local RES is district heating (DH). These are systems using a grid of heat supplying pipelines to which dwellings and buildings are connected, making it possible to use centralized RES to provide for heating of dwellings or other purposes. Hoogervorst (2016) and Paardekooper et al. (2018) both pledges for DH in areas where heat demand is high and heat sources are relatively close, as is found in urban areas. Paardekooper et al. (2018) especially pledged for use of industrial waste heat (IWH), as excess heat is currently being dumped. Next to that, IWH is dumped at higher temperatures compared to most RES, making it energetic more rewarding to use compared in terms of ease of use and accessibility.

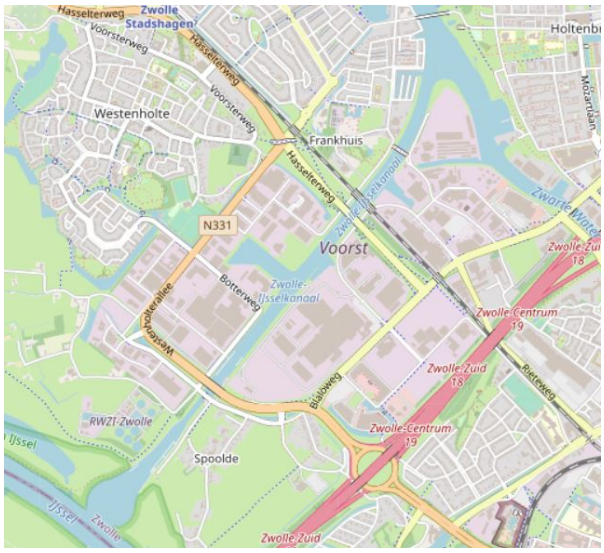

Figure 1.1: Industrial area Voorst and neighborhood Westenholte (Afstandmeten.nl, 2020)

In figure 1.1 the district Westenholte and industrial zone Voorst of Zwolle can be found relatively close to each other, making it a logical choice for DH based on IWH. The neighborhood of Westenholte used 3.386.000 m^3 of natural gas (gross calorific value equivalent of 0.12 PJ) (CBS, 2018) over 2.177 dwellings (allecijfers.nl, 2020) making it 1555 m^3 (gross caloric value of 54.7 GJ) per dwelling, which is slightly more than the average consumption of 1270 m^3 per dwelling in 2018 (CBS, n.d.).

Uncertain is the amount of waste heat available at Voorst, as privacy concerns prevent this data from being released publicly. To supply the total heating demand, it is worth looking at other RES near Westenholte, taking into account the unpredictable fluctuation of IWH and the amount of heat, which might be lacking. Thermal energy from waste water (TEWW) can be utilized at the local sewage treatment plant and thermal energy of surface (TESW) water could be used as RES. With enough room, solar thermal energy can also be an option. From these sources, solar thermal energy and TESW are considered RES, while IWH and TEWW are seen as forms of waste heat (WH).

A consortium was formed, led in engineering by Witteveen+Bos, to further investigate the feasibility of a DH network using RES with the use of technologies showing a high (>6) technology readiness level (TRL) to ensure achievable design, and compare it to other solutions. Examples of other solutions are the ones proposed by ''Leidraad Aardgasvrije Wijken" (LAW), which are supported by the government as alternatives to DH. Based on the key performance indicators (KPI): capital expenditure (CAPEX), operational expenditure (OPEX), levelised cost of energy (LCOE) and CO_2 emissions, the feasibility of the different heating solutions will be measured. The LCOE is defined as the total sum of cost over the entire lifetime, divided by the amount of energy produced. This is more frequently used as an indicator to evaluate RES (Doracic et al., 2018; Hansen, 2019; Lensink, 2020).

The feasibility of RES in DH is often greatly influenced by the low source temperature and fluctuating supply (Li & Nord, 2018; H. Lund et al., 2014; Mazhar et al., 2018). The low source temperature requires more power for the heat pump to upgrade it to the supply temperature. As a solution, the supply and return temperature of the DH are lowered in order to decrease the power consumption of the heat pumps used to upgrade the heat and reduce thermal losses of the distribution grid. However, the total volume flow of the DH must be increased to deliver the same amount of heat, which on its turn increases pumping cost. Both the pumping cost and thermal losses are proven to be the main factors in the OPEX of a DH network (Mazhar et al., 2018), implicating a correct balance needs to be found.

Using multiple heat sources for DH has been seen as a key development by some of the most relevant works in that area (H. Lund et al., 2014; Mazhar et al., 2018; Rezaie & Rosen, 2012). Combining different

thermal RES for heat, might lead to a lowered impact of the fluctuations from the RES (Pieper et al., 2019). However, the integration of multiple heat RES is complex, as each source has a varying supply profile over time and is hard to control. Storage, daily as seasonally, has been found as a solution to accommodate the varying supply of heat. Daily storage is used as a way to provide for daily occurring peaks (solar irradiation during the day) and seasonal storage for surplus heat produced in summer. For example: solar energy, TESW, and TEWW, to be used in winter when demand is higher and supply lower. Common seasonal storage has low efficiency, making use of RES less efficient as well. Because of the scale, an integral approach is expected to provide a better LCOE than using the RES individually (Kruit et al., 2018).

Modelling DH networks is a common method to determine the feasibility of DH networks. Vesterlund et al. (2017), Wang et al. (2018), Descamps et al. (2018) and Dénarié et al. (2018) developed DH models addressing multiple heat sources using various simulation and optimization methods for operation and design. A model of a large multi-source DH network with seasonal and daily storage, using different temperature regimes, covering the optimal feasibility and feasibility benefits of using multiple sources, has not been identified in the current literature, which leaves to wonder if the expected lower cost is realistic.

1.2. Objective

This thesis aims to determine the feasibility of currently available (TRL) DH networks, composed of multiple sources and storage, by developing a model for calculating its common economic and environmental indicators: CAPEX and OPEX (Sarbu et al., 2019), LCOE and CO_2 emissions. The main research question of this thesis, therefore, is:

What are the LCOE and CO_2 emissions of multi-source DH systems with supply/return temperatures of 70/40 °C and 50/30°C and decentralized all-electric heat pump systems for space heating and DHW heating of the 2177 dwellings of Zwolle's district Westenholte?

To answer the main research question, a DH model will be built, using the RES TESW, TEWW, solar thermal and electrical energy and IWH, assisted by thermal energy storage (TES), to measure the feasibility in terms of LCOE and CO_2 emissions for two different temperature levels: medium temperature with 70/40 °C for supply and return and low-temperature levels with 50/30 °C as supply and return temperature of the distribution grid. Additionally, for the IWH, a boundary condition has been set that not all waste heat may be used internally. Supporting questions of the main research questions are:

Sub question consumer end :

1. How can the demand of domestic buildings, set for 2022 and the near future, be modelled for the temperature regimes low and middle on an hourly basis for three or more years?

Sub questions heat supply :

2. What is the state of the art of components for the different RES used to acquire energy for DH?
3. What is the most suitable modelling method for each individual RES?

Coupling of demand and supply :

4. What is the most optimal type of distribution network to supply heat to consumers?
5. What is the most optimal type of storage to compensate for the mismatch in heat supply and demand?
6. How can an optimal configuration of the different heat sources be found, minimizing CO_2 emissions and LCOE?

1.3. Methodology

In chapter 2, a literature review is given regarding the state of the art of decentralized heating and renewable multi-RES DH heating. Different subsystems are identified within a DH system: the demand, the supply and the coupling of demand and supply. For all the subsystems demand and coupling of demand and supply,

equipment best suitable to provide the lowest LCOE will be selected. Literature research will be used to determine which modelling methods exist for the subsystems of the DH, including the equipment than found. The models will then be evaluated on input, accuracy and computational time required. Based on the literature review, a methodology will be elaborated.

In chapter 3, the demand is determined and validated, answering sub-question 1. Once the demand has been identified, the amount of heat necessary for the supply can be established, which is discussed in chapter 4, answering sub-questions 2 and 3. The models found in chapter 2 will be used to estimate the local energy production and associated cost for Westenholte and Voorst after which they will be validated in chapter 4.

The coupling of the supply and demand is done by the distribution grid, including heat transfer stations and storage. In chapter 5, sub-question 4 and 5 will be resolved, leading to an optimal distribution grid including TES. The whole DH model is now complete and will be put together in chapter 6. The model of the alternative decentralized solution for heating will also be proposed in chapter 6 and integrated into the DH model after which the final validation of the model will take place.

Optimization of the DH will be done in chapter 7 to determine the lowest LCOE and CO_2 possible for the system by running different scenarios, answering sub-question 6. In chapter 8 conclusion and recommendations will be presented. A schematic overview of the thesis can be found in figure 1.2.

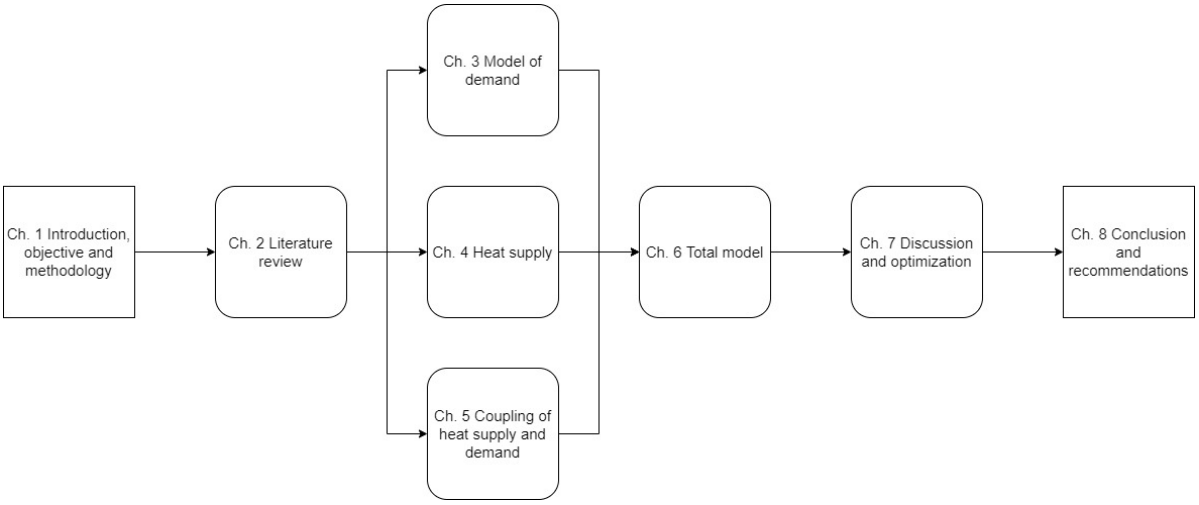

Figure 1.2: Schematic thesis overview

2

Literature review of demand and supply of renewable DH networks

2.1. Introduction

To determine the state-of-the-art of multi-RES DH, first, the history of conventional DH will be studied concerning purpose, global functioning of the system, and key advantages and disadvantages leading to an evaluation in the state-of-the-art of DH. Once DH state of the art has been identified, a schematic overview will be given of the multi-RES DH. The DH system is then subdivided and the components and models for the different subsystems will be selected to come to an optimal system in terms of CO_2 emissions and LCOE.

2.2. History

Each DH network is a complex network of piping, distributing a medium that carries heat to the consumer. Since the 14^{th} century (Mazhar et al., 2018), DH has been around as a method for providing buildings with heating. Compared to conventional decentralized heating, DH offers a set of advantages in safety, efficiency, and reliability of the energy source, depending on the network. H. Lund et al. (2014) defined four generations of DH based on the distribution medium, supply and return temperature and purpose to determine the challenges for future DH networks.

The 1^{st} generation DH networks were created to replace dangerous individual boilers. This generation DH is operated by distributing steam, which is generated by centralized fossil-fueled boilers. By distributing steam with high temperatures through pipes, large heat losses occurred. This steam-based DH was used untill 1930 and has been classified as outdated, mainly because of the large heat losses and inefficient transport. Additionally, safety issues, such as the dangerous release of steam, occurred frequently and sometimes piping exploded.

The inefficiency of steam leading to higher overall cost in the 1^{st} generation DH functioned as the motivation for a 2^{nd} generation of DH. Therefore, the aim of the 2^{nd} generation was fuel saving by the use of a combined heat and power (CHP) system, and the increase in efficiency by using pressurized water to deliver heat. Typically the pressurized water transported through pipes in concrete ducts was over 100 °C, decreasing heat loss and preventing dangerous releases of steam. A disadvantage of this system is the large shell and tube heat exchangers (HEX) that are necessary, material-intensive heavy valves, and lack of controllability, because of these valves. This heating system is currently available in several countries in Europe, including the Netherlands.

The 3^{rd} generation DH networks, introduced in the 1970s, was designed to become less dependent on foreign fossil fuels used as the heat source. By replacing foreign-dependent fossil heat sources with secure local and sometimes cheaper heat sources such as WH, biomass or fossil coal as well as some RES, independence could be achieved. Simultaneously, this generation has been using temperature levels in pressurized water lower than 100°C, decreasing heat losses even further. This network was the first to use prefabricated

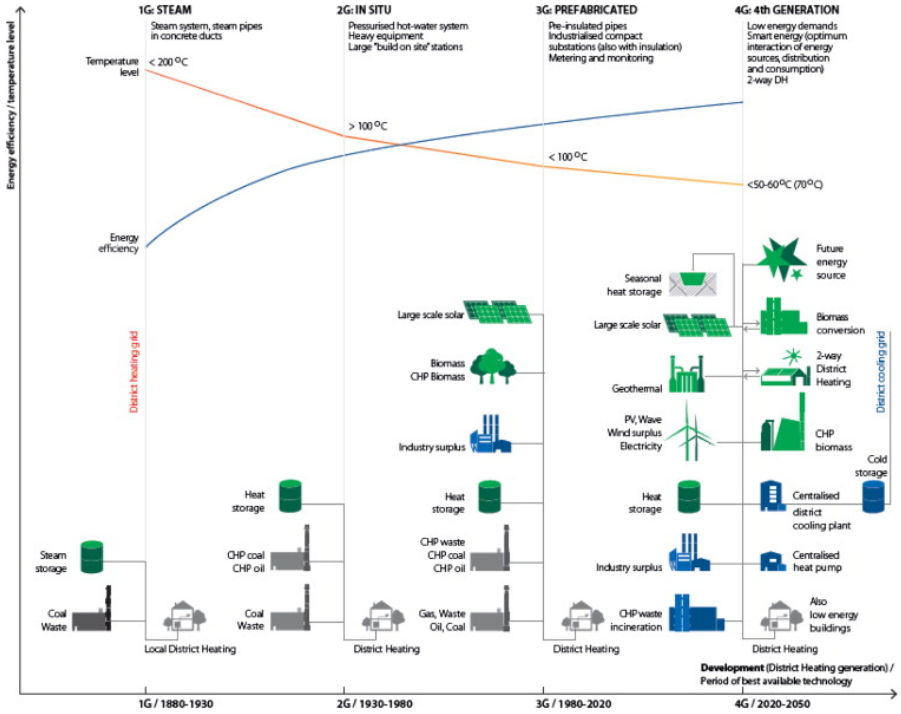

Figure 2.1: Four generations of DH according to H. Lund et al. (2014)

insulated tubes and other material lean components to reduce cost drastically.

Where the 3^{rd} generation different heat sources were used to become less dependent on foreign fossil fuels, the 4^{th} generation DH aims to reduce overall emission of GHG. The new generation DH will be part of a future energy system, where synergies between different energy sectors, such as electricity and heat, are stimulated and exploited. This new network is called a smart thermal grid and is defined by H. Lund et al. (2014) as:' a network of pipes connecting the buildings in a neighborhood, town center or the whole city, so they can be served from centralized plants and several distributed heating or cooling production units, including individual contributions from the connected buildings'. The future generation of the heating network is to be built from 2020 until 2050. An overview of all generations of DH is presented in figure 2.1 (H. Lund et al., 2014). The new 4^{th} generation DH, as defined by H. Lund et al. (2014), will continue to reduce the distribution temperature to decrease thermal losses in the grid and use more prefabricated, material lean, components to reduce cost, as was the trend in earlier generations.

2.2.1. Low-temperature DH

The new 4^{th} generation DH with a smart thermal grid can create local jobs, as the construction and operation of multiple local heat sources become necessary (Schweiger et al., 2019). However, this new system faces challenges to be constructed in the future. One of the two larger challenges of this new system is facilitating the usage of more than one or multiple low-temperature RES or WH. The other challenge is the fluctuating nature of the sources (Li & Nord, 2018; H. Lund et al., 2014).

To accommodate low-temperature heat sources, the distribution temperature of the DH grid is lowered. The lower distribution temperature will cause lower operating costs, as heat pumps have higher efficiency when the difference temperatures become smaller according to the Carnot efficiency principle. Simultaneously, heat losses of the distribution grid will also decrease with a decrease of the distribution temperature according to Newton's law of cooling. The heat losses of the DH grid account for 5-20 percent of the delivered energy and are considered a major expense (Mazhar et al., 2018).
However, since the heat density per volume of water in the distribution grid has decreased, a higher pumping cost is to be expected for identical heat loads (Mazhar et al., 2018). More expensive material for insulation

in dwellings is needed to limit flow rates. To prevent the flow from increasing drastically to compensate for the lowered heat density, demand regulation measures can be taken. Insulation of the buildings could lower the consumption, meaning pumping cost will remain the same, however, this will require additional cost. The government does partially give subsidies for the insulation of dwellings. With these partial subsidies, it is reasonable to expect a decrease in the demand which might switch the preference of using a medium temperature to a low-temperature DH. A local balance between the insulation cost, material cost and source efficiency needs to be found.

To provide an overview of possible best suitable distribution temperatures of DH networks, they have been categorized in ultra-low, low, medium, and high. The consumer demand of SH and DHW sets the lower boundary temperatures of the supply flow for each category (Østergaard, 2018). For the Netherlands this would be 65 °C for the storage of DHW in tanks, to meet the medium temperature storage. For low-temperature DH, the minimum temperature must be 50 °C for the storage of DHW in taps and as found in the work of (Østergaard, 2018) 30 °C for ultra-low temperature as minimal required temperature to heat low heat demand homes. A typical temperature difference of 30–45 °C has been found for the medium temperature, 25–35 °C for low-temperature networks, and 20–30 °C for ultra-low networks as researched by Østergaard (2018). These temperature regimes have been summarized in figure 2.2.

A costly problem arises when the lowered temperature of a low-temperature distribution grid cannot release enough heat into the house, which depends on the temperature used and the surface area of the radiators. For ultra-low temperature specially designed low-temperature radiators must be installed. This could also be the case for low-temperature DH. However, in a well-insulated dwelling, the distribution temperature could be lowered to 35-55 °C as the system is over-sized and peak demand is hardly necessary as found by Østergaard (2018). These finding should be put in perspective of the country of origin, as the experiment was performed in Denmark. His work reports a test in which the current installed high-temperature radiators were used with supply water between 40-50 °C and could keep the room temperature steady at 20 °C year-round. Østergaard (2018) therefore showed expensive replacement with low-temperature heating systems can be prevented. Currently installed radiators are often over-dimensioned (Kennisinstituut voor Installatietechniek, 2012). Even though the research took place in Denmark, the results might still apply for the Netherlands as the building's heating systems are designed to supply enough heat to fulfill peak demand, disregarding external heating from surrounding houses/rooms.

The effects of using different temperature regimes are still unclear and might be affected by local conditions of the buildings heated as seen in the following literature. R. Lund et al. (2017) compared low-temperature DH (55 °C/25 °C) with ultra-low temperature DH using electric boosting (45 °C/25 °C) and ultra-low temperature DH with heat pump boosting (35 °C/25 °C) in which grid losses, production efficiencies, and building requirements where compared in EnergyPlan showing low temperature have the lowest cost. Best (2018) also performed an economic comparison of medium temperature (70 °C) and low temperature (40 °C/25 °C) DH systems for new, low heat demand buildings in Germany. Heat distribution efficiency increased and favorable conditions were found for renewable energy sources. No economic disadvantages were found. However, ultra-low temperatures require the housing stock to have an exceptionally low heat demand, needing thorough interference in dwellings. Therefore, only medium and low temperature will be further up for research, as these require little to no interference for the dwelling.

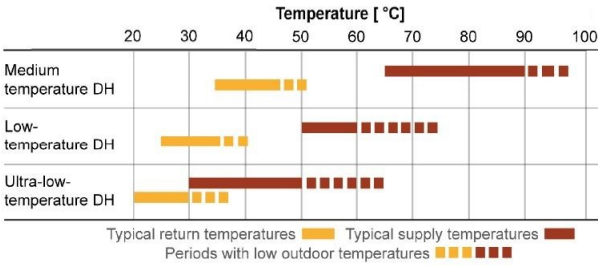

Figure 2.2: Three different temperature regimes DH, including temperature demands of dwellings according to Østergaard (2018) (adapted graph).

Table 2.1: Advantages and disadvantages of TES (Guelpa & Verda, 2019).

Advantages	Disadvantages
Increase in production flexibility	Large thermal losses
Reduction of pipe diameter	high space requirements
Decrease OPEX	Increase CAPEX

2.2.2. Fluctuating heat sources

To expand the technical challenges to cover all area's challenges that arise when facing the low-temperature DH, Guzzini et al. (2020) have performed a survey under experts to identify key advantages and disadvantages of low-temperature DH. Low heat losses and easier integration of renewable heat sources were identified as key advantages by the experts. Key disadvantages of this type of network were identified as: a necessary change of DH business model and specific technological solutions which are needed to ensure existing supply conditions. The latter disadvantage is simultaneously the second major problem of using multiple low-temperature RES as a result of fluctuations in these RES.

The second major problem encountered when using multiple RES's and WH is the fluctuations of each source (Guzzini et al., 2020; Li & Nord, 2018; H. Lund et al., 2014). Historically, the demand determined the amount of heat that was produced as seen in generations one to three as defined by H. Lund et al. (2014). With the new heat sources, this will no longer be the case as the heat production RES and WH can hardly be controlled. The fluctuations of the heat sources can vary from daily to a more seasonal base or are scheduled depending on availability in the case of IWH. A solution has been found in using TES to store and regulate the heat supply in order to meet the, also time-dependent, heat demand.

TES are available in the order of daily, weekly, and even seasonal storage and can provide the match between demand and supply. Other benefits include a reduction in piping diameter as well as an increase in the overall performance (Guelpa & Verda, 2019). These advantages, however, come at a price: the additional investment costs are significant depending on the type of TES. The storage of heat itself is also not considered efficient as large heat losses occur, particularly for long-term storage (Guelpa & Verda, 2019). Additionally, TES requires vast amounts of space which must meet strict requirements and is not always available near a DH (Guelpa & Verda, 2019). The primary advantages and disadvantages of TES have been summarized in table 2.1, a more elaborated table will be given in section 2.5.1. With the use of multiple RES and WH, the first investment cost relative to the amount of heat stored can be lowered, as the total amount of heat supplied is increased.
Combining different RES might reduce the financial burden of using TES. Instead of each RES having to use its storage, a collective one can be installed. Since the price per kW energy stored decreases when size increases, this can offer a substantial financial benefit. The size of the storage necessary can also be decreased as each source will provide at different times of days which can decrease the overall heat supply fluctuation (Pieper et al., 2019).

Nonetheless, in order however, to seize the benefit of a proportional decrease in cost and overall lower cost, optimal use of storage for multi-source DH must be done with help of predictions to be useful, according to Descamps et al. (2018) who researched the use of TES without a control scheme in a multi-source DH. To probe the effect of such a control scheme, the sources need to be modelled accurately, as a DH performance is highly sensitive to heat source fluctuations (Wang et al., 2018).

Other problems of multi-source DH are the feed-in options for the heat sources, as found in the work of Li and Nord (2018) on finding a suitable location for obtaining multiple RES. Table 2.2 summarizes the three distinct possibilities for the feed-in and the advantages and disadvantages. For finding a beneficial location for placing a DH, the sources have to be in close proximity to a high-density heat demand environment, as heat transport costs are high.

2.2.3. Fourth generation multi-RES DH

A schematic view of a 4^{th} generation DH grid is illustrated in figure 2.3. The diagram illustrates the proposed thermal energy distribution of a DH where the heat sources TEWW, TESW, Solar thermal energy and IWH

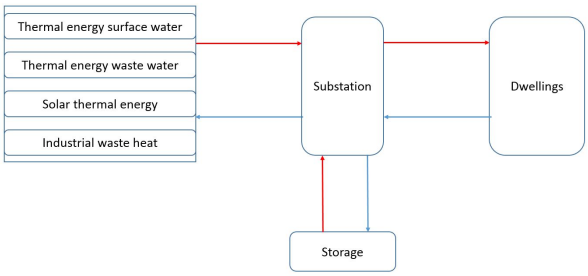

Figure 2.3: Schematic overview of DH model

Table 2.2: Feed into DH network of heat sources and their advantages and disadvantages (Li & Nord, 2018)

Connection variants	Extraction from the return line and feed-in into the supply line	Extraction from the return line and feed-in into the return line	Extraction from the supply line and feed-in into the supply line
Features	The temperature difference is dependent on operating conditions and grid operator. The pressure difference is high and depends on the actual location in the grid	The temperature rise is commonly set by the DH operator, the pressure difference is relatively low	The temperature increase is prescribed by the grid operator, the pressure difference is relatively low
Advantages	The return temperature is unchanged, which avoids temperature strain on return pipes, and the influence of heat extraction efficiency of other heat sources	It is preferable for heat sources with high efficiencies for lower temperatures	-
Disadvantages	High energy demand for the mandatory feed-in pumps	The return temperature is raised, which increases the grid heat loss, and influences the efficiency of other heat sources	The supply temperature is raised, which increases the grid heat loss, and influences the efficiency of other heat sources

provide heat. Substations seen in figure 2.3 regulate the thermal energy flow. This overview provides the basic idea of the proposed 4^{th} generation DH for Westenholte.

Figure 2.3 also illustrates a distinction of subsystems manifested in the heat supply, heat demand, and the coupling of supply in demand in the form of a distribution grid and storage. These subsystems are normally used to divide the DH, after which the individual subsystems are constructed to form a larger model. The mathematical description of the system is seen in equation 2.1, where the DH network is a kind of hydronic system. A hydronic system transfers heat by circulating a fluid in a closed system of pipes, loading and unloading its thermal energy. Herein the demand of a DH must always be matched by supply. During transport from supply to demand, thermal losses occur. The heat supply also needs to compensate for these losses.

$$\int_0^\tau \dot{Q}_s dt = \int_0^\tau (\dot{Q}_d + \dot{Q}_{hl}) dt \tag{2.1}$$

Equation 2.1 provides the energy balance for the system at any moment in time. $\dot{Q}_s$ is the heat required to supply the DH system in kW, $\dot{Q}_d$ is the consumer heat demand in kW, τ the amount of operation time in seconds, t is time in seconds and $\dot{Q}_{hl}$ are the heat losses of the entire network in kW. Equation 2.1 states that the demand and heat losses should equal the supply at any given moment in time.
The use of storage can mathematically be expressed by adding a new variable to equation 2.2 showing a new energy balance as presented in equation 2.2:

$$\int_0^\tau (\dot{Q}_s + \dot{Q}_{st}) dt = \int_0^\tau (\dot{Q}_d + \dot{Q}_{hl}) dt \tag{2.2}$$

This balance demonstrates the usage of storage to balance the thermal energy, where $\dot{Q}_{st}$ gives the surplus

heat which is being stored or the heat which is given back to the network from storage. Figure 2.4 illustrates the heat flows and how they influence one another. The main influences are depicted as the local weather, as this predominantly determines the heat demand of the dwellings and heat supply of the RES. The design of

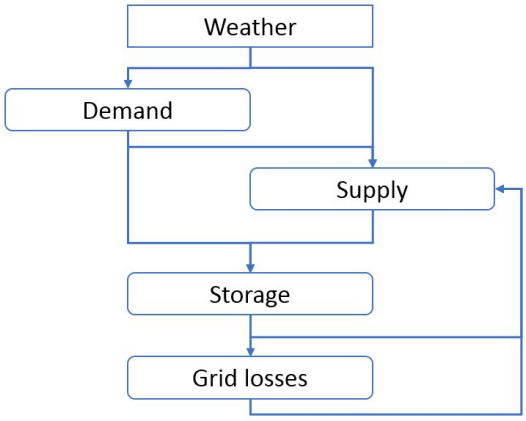

Figure 2.4: Flowchart of heat-flows where mean input on heat flows is weather

the DH is based on the expected demand of the DH. With this demand, a strategy is determined to estimate the total supply necessary. The main factors in determining the supply are the weather, the storage used, and the expected grid losses. This way of modeling the DH system is one of two ways where the other one is based on the hydraulic equilibrium present. A combination of both hydraulic and energetic balance is necessary to come to the result. This study will primarily use the energetic balance method (Talebi et al., 2016). As equation 2.1 demonstrates, balancing demand and supply depends on time and therefore is a dynamic process. The DH needs to be evaluated for each moment in time to maintain the balance. Various simulation and design programs have been developed for DH (Knepper, 2019; Schmidt et al., 2017).
Obvious from most models is the complexity of the dynamic process. This complexity continues in the number of calculations made, which is significantly high. As the model intends to research dynamically the properties of multiple sources compared to just one source for the average simulation/design model, the amount of calculations already increases significantly. As is common for this research, an hourly time step will be used (Descamps et al., 2018; Knepper, 2019; Pieper et al., 2019) to facilitate the hourly differences of the RES and WH, leading to a significant increase of calculations made. For this reason, where possible the computational time must be limited, whilst still producing accurate results.

2.2.4. Key performance indicators

Looking at previous research, the lowest CO_2 emission can be achieved using as much RES as possible. For the DH, the major source producing CO_2 emissions is the electricity used in the pumps and heat pumps (Bayer et al., 2012) which might not come from a renewable source. To calculate the CO_2 emission, the average CO_2 emission per kW is used (Bayer et al., 2012). However being part of a smart electricity grid the price and CO_2 production might vary per moment in the future, depending on the RES electricity production. The new smart distribution grid should aim to create synergies with the smart electricity grid. For example, aim to use cheap electricity when RES electricity production is high to reduce cost and save CO_2. As the cost and CO_2 emission are inversely related, the cost is used to limit CO_2 demand (H. Lund et al., 2014).

CO_2 will predominantly be created by the use of peak supply and electricity. When peak heat demand occurs during the limited amount of hours of the year, often still fossil fuel-powered heaters are used to provide this heat as this is the cheapest solution. Electricity used might still be produced with the burning of fossil fuel. In order to prevent this CO_2 pollution, the hours in which the fossil fuel peak supply must be limited. Dénarié et al. (2018) performed a multi-criteria analysis on a multi-source DH. Among others, the multi-criteria analysis was performed based on renewable-energy ratio, investment costs, net present value, payback time, CO_2 emissions and land use. Different scenario's using a varying percentage of RES per scenario implicated

that the scenario with the highest share of RES and storage capacity emits the least amount of CO_2, but with the consequence of the highest overall payback time showing the importance of CAPEX versus OPEX. Since the RES investment cost or OPEX are higher compared to conventional types of fossil fuels and RES have a net zero-emission, this result was to be expected.

The LCOE is based on a combination involving both the CAPEX and OPEX, which are combined to be evaluated against the yearly discount rate $r = 6\%$. The LCOE can therefore also be expressed by the following equation:

$$LCOE = \frac{\sum_{t=1}^{n} \frac{CAPEX_t + OPEX_t}{(1+r)^t}}{\sum_{t=1}^{n} \frac{E_t}{(1+r)^t}} \tag{2.3}$$

The LCOE can thus provide in one parameter the CAPEX and OPEX combined and has been used as a primary indicator for many renewable energy technologies. Predominantly, the total OPEX is higher compared to the total CAPEX. The LCOE is a way of making the cost over time, in order to show the actual amount of energy produced versus the cost made over the financial lifetime. By doing so, the varying OPEX of the new RES and WH versus the more steady OPEX of historical fossil sources becomes an irrelevant factor, making a comparison possible. It however does not validate the actual profitability of the project and is normally used to make comparison cases between projects Colla et al. (2020).

For DH Mazhar et al. (2018) indicated the primary source of the OPEX are the heat losses and the pumping cost when using sources that are not dependent on heat pumps. When operating costs are optimized, Vesterlund et al. (2017) implicated that the usage of the cheapest source is preferred for a multi RES DH network, which is interpreted as a preference for the source with the lowest LCOE. The increase in pumping cost for lowering the supply temperature to facilitate the RES was small compared to thermal distribution losses. Wang et al. (2018) showed that the pumping costs are strongly influenced by the fluctuating heat of the RES. The sensitivity analysis performed, showed a 1 percent fluctuation of RES can result in between 0.16 percent and 7.56 % fluctuation in pumping work, which might make this decision more complex. An accurate prediction is also proven necessary by Descamps et al. (2018) who developed a one-dimensional dynamic multi-source model with storage supplying a peak load of 50 kW. The RES used are solar energy and heat pumps, directly increasing the temperature of the return stream. The result of the four scenarios implicate a relatively high usage of electricity and gas as a heat source. This might be prevented when an optimal control strategy, including a predictive factor for storage, would be used. Additionally, Colla et al. (2020) reason that TRL should be used as an indicator for the success of a heat source after evaluating different physical, environmental, social, and economic indicators.

In conclusion, in order to come to the best result, the source temperature and accompanied lowest LCOE for each heat source and the whole system will be determined to establish the cost and to find a balance with lowering of the distribution temperature. Fluctuations of RES and WH can have a significant impact on the pumping cost, and therefore accurate models are needed to predict the fluctuations. Additionally, the models will be evaluated on the complexity and completeness of the input data to guarantee a fit with the area of Westenholte and Voorst.

The different subsystems heat demand, heat supply and coupling of supply and demand will be researched separately to come to the optimal feasibility of the proposed DH. The first components for the subsystem will be evaluated based on expected LCOE per source and expected cost, along with maximizing energy output. The LCOE and cost will be determined by comparing different business cases of the varying heat sources, where the withdrawn energy is divided by the specific economic cost per source, leaving the distribution grid out of the comparison, as was done by Lensink (2020). The LCOE can vary on components and placement of the components in the DH area deeming it necessary to evaluate each source individually for a new DH. The associated models predicting the heat input will then be evaluated, based upon input and accuracy.

2.3. Heat demand model

The demand, $\dot{Q}_d$ as found in equation 2.1, is formed by the customers of the DH and needs to be predicted, in order to determine the feasibility of the DH network. Normally the maximum demand is used to determine

Table 2.3: Four main methods of demand evaluated as found by Talebi et al. (2016)

Method used	Historical	Deterministic		Stochastic predictive
		Complex	Simplified	
Demands on input	low	high	medium	high
Computational time	low	high	low	medium
Accuracy	low/medium	high	medium	high
Highest accuracy encountered [%]	9-66	4	8	

the dimensions of the piping used in the DH network (Mazhar et al., 2018), implying an appropriate estimation is crucial for correct dimensioning and therefore the feasibility of a DH. The prediction of demand also forms the basis of the quantity of heat and storage needed. Various models have been developed to predict the heat demand of both the DHW and SH for all buildings present. An accurate model used to predict demand, therefore, has an impact on both CAPEX and OPEX of the DH system, as it determines dimensions and operation of the system.

The different methods existing for modelling the heat demand for dwellings have been categorized by various works. According to Talebi et al. (2016), three principal methods are differentiated based on the output: historic, deterministic and predictive methods. The following description of the different models is largely based upon the review made by Talebi et al. (2016).

A simple historic system that can be used is the degree-day method. In this method, the heat losses are calculated based on the difference in temperature between the in- and outside temperature and are often used for smaller dwellings. The heat infiltration rate of the building serves as an input for the system. However, the availability of this type of data is low, and this method is considered inaccurate. Then again, the greatest limitation of all the historic methods is the lack of available data.
Another popular historic approach is the typical dwelling or archetype building modeling. This method requires a classification of the buildings. Next, for each class, a typical building for that specific class is constructed on which the values are based. Using the classification, a regression analysis can be performed and used in order to define the most useful parameters.

Deterministic methods calculate the heat demand based on physical models of the buildings. The methods within this approach are categorized into complex and simplified models. Complex models simulate the heat demand based upon all parameters involving heat loss. The input for this type of model is very demanding, not widely available and high. The resulting heat demand is, however, very accurate. Drawbacks of using this method are the computational time and the high demands of the input data required.

The simplified deterministic method uses specific key parameters to come to a relatively accurate result, considering the number of calculations made in comparison with the normal deterministic method. The input data of this method is thus very selective and still difficult to obtain, but computational time is decreased drastically.

Predictive methods, including artificial intelligence, use weather and demand data to predict the new demand. The inputs for this type of modeling are hard to obtain because of common gaps in data, as they should be consistent. They also experience an over-fitting problem, which is hard to eradicate and is considered as one of the major downsides of using this method.
The methods involve an extensive amount of computational time, predictive methods and complex deterministic methods. All of them have strict demands and require large amounts of the input data, and are not seen as viable options, which leave the historic and simplified deterministic method. Since the historic method varies in accuracy per method and simplified deterministic method can be accurate but has less available input data, the latter would be the best option for modeling the DH demand of both the dwellings as the larger-scale buildings for a small number of dwellings as computational needs are larger than the historical method. The historical method is thus left for evaluating the demand for a large number of dwellings. An overview of the properties of the different methods is found in table 2.3.

In chapter 3 the combination of the typical dwelling, with the simplified deterministic method will be further researched and evaluated based upon the specific inputs found in Westenholte, after which a method will be determined.

2.4. Heat supply using RES and WH

The heat supply of a DH is centralized and was normally created as a demand deemed necessary. For example, if more heat was needed, more fuel was burned to fulfill this demand. The heat from the supply was then carried away by the distribution network from a centralized generation site. With the new low-temperature smart thermal network, multiple renewable heat sources or WH sources will be used in a decentralized manner throughout the network in a few concentrated generation spots. The RES and WH was chosen in Westenholte are IWH, TEWW, TESW, and solar heat. These are all hard to control and varying in heat generation, LCOE and source temperature. To come to an optimal LCOE and CO_2 emission for the DH, the criteria quantified in section 2.2.4, on which to assess the different heat sources, are used to set up physical and financial models.

Figure 2.5 shows the expected annual heat demand curve according to Thomsen and Overbye (2016), based on the predicted heat demand sorted on the amount of heat demand. As can be seen, the majority of the hours are covered by a heating supply seen as 'base load' in the figure. It would be illogical to design the system to supply the peak load, as the investment cost to cover these small amounts of hours is significant (Thomsen & Overbye, 2016). Predominantly, the peak load is covered with a heat source low in CAPEX such as a boiler, either on electricity or gas or a biomass furnace. Figure 2.5 is thus used in establishing the quantity of heat required for a DH.

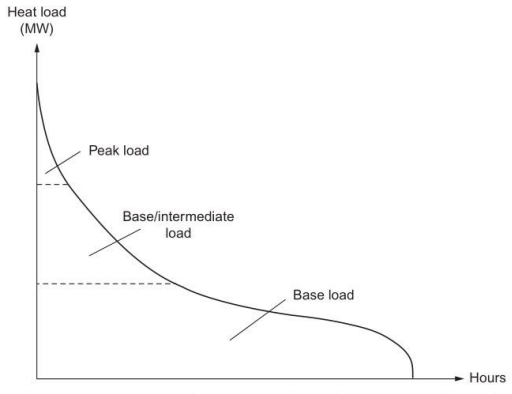

Figure 2.5: Indication load (Thomsen & Overbye, 2016)

To come to the best heat source the cover the base loads, table 2.4 shows the different RES and WH with their main influence factors and LCOE. For the optimal use of each source, further literature research focusing on the design and modeling will show the best method to utilize each source. Lensink (2020) presented the LCOE of different energy sources, based on case studies made of a similar approach. These case studies were done in order to determine the subsidy, each energy source needs to meet the future set by the government. As the studies are the most resembling studies found, the LCOE calculated provides a relevant indicator for the energy sources as found in DH for an average case of the Netherlands. However, the LCOE of the RES is strongly locally dependent as, for example, the distance to the DH can cause the price to increase drastically as a result of heat loss, resulting in a necessity for local evaluation.

2.4.1. TESW

TESW is a low-temperature mature (TRL 9 (Niessink, 2019)) heat source. By using an HEX, heat is drawn from surface water. For this heat to be useful, a heat pump is used to upgrade the temperature to the DH distribution temperature.

Usually, a counter-current HEX is used in order to exchange heat. The countercurrent HEX has two flows,

Table 2.4: Different heat sources evaluated on expected cost, source temperature and main influence of availability. For TESW, the use of a storage method has already been taken into account.

Source	Basic price assumed by Lensink (2020) [€/kWh]	Temperature range [°C] (Church, 2016)	Weather dependent	Mean (weather) predictable dependency
Thermal energy of surface water	0.115	10 - 50	Yes	Season
Solar thermal energy	0.08	70 - 130	Yes	Season and daily rhythm
Thermal energy of waste water	0.077	0 - 40	Yes	Season
Industrial waste heat	0.044	90 - 200	No	Production schedule

separated by the HEX material, flowing countercurrent next to one another. Maximum exchanged heat can be approximated using equation 2.4, in which the amount of heat $\dot{Q}_{sw}$ is calculated using the specific heat capacity of surface water $c_{p,sw}$[kJ/kg/°C], the mass flow of water $\dot{m}_{sw}$ [kg/s] and the temperature difference in the surface water ΔT [°C].

$$\dot{Q}_{sw} = c_{p,sw} * \dot{m}_{sw} * \Delta T \tag{2.4}$$

The fluid used to absorb the heat is lower in temperature than the surface water, in order to make it possible to absorb the heat. The heat is transferred by heating the fluid inside the HEX a few degrees, however since the temperature of this fluid is lower than the surface water, a heat pump must be used to upgrade the temperature level to the distribution temperature level.

Spitler and Mitchell (2016) categorized TESW in open-loop systems and closed-loop systems. The open-loop system pumps water from the sources through a heat exchanger and then returns it to the source. A closed-loop system has a heat exchanger placed in the surface water through which water is circulated. The water is cooled down by 3 -6 K (Kruit et al., 2018), preventing a drastic impact on the biosphere of the surface water. Most likely, similar regulations will be set for in the future as found by IF and Stowa (2018), which state that the waterbody should not reach a temperature lower than 12 ° C when the used water is dumped back.

Because of the large scale of the DH, an open-loop system is recommended by Spitler and Mitchell (2016). Another advantage of an open-loop system is the prevention of a mixture of the cooled surface water, which would decrease efficiency (STOWA, 2018) and, in turn, play a more significant role for larger heat removal.

An open-loop system consists primarily of piping, filters, pumps and heat pumps as illustrated in figure 2.6. In this set up the pump, HEX, heat pump, circulation pump and location are key factors in LCOE. The circulation pump in this set up is the largest energy consumer because it needs to pump the most mass flow with the highest head (Spitler & Mitchell, 2016).

Another indicator of the OPEX is the coefficient of performance (COP) of the heat pump, which is the output of added energy divided by the working load. A higher COP indicates a lower LCOE, as less energy is required to upgrade the heat to the desired temperature level of the DH network. Heat pumps are often designed for a specific project (Spitler & Mitchell, 2016). The COP for TESW heat pumps has not been reviewed in current literature, but Hepbasli et al. (2014) researched it for TEWW. They found COP values between 1.77 and 10.63 of which the systems show much resemblance to TESW. STOWA (2018) estimated the COP of the used heat pumps around 3-7. Historically, the COP also stayed in this range.

Also used for the system, instead of the COP, is the seasonal COP (SCOP), which is the heat output over a whole year divided by the electricity used. This parameter is used as the COP varies with the temperature difference between the source and the DH. Niewold (2019) shows the cost and associate SCOP for different projects throughout the Netherlands using TESW. A proportional inverse relationship is found inherently between the quantity of heat produced and LCOE. In the Netherlands, open-loop TESW are predominantly used in combination with aquifer thermal energy storage (ATES). ATES is an open form of storage in which hot water is pumped into the ground to be later redeemed. Niewold found a proportional inverse relationship

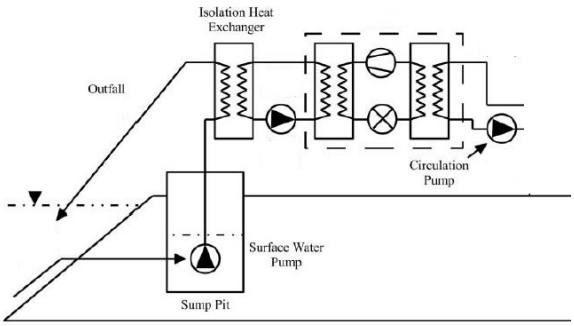

Figure 2.6: Typical open-loop set up using thermal energy of surface water adapted from Mitchell and Spitler (2013)

between the quantity of heat produced and the LCOE. However, the relationship as found by Niewold (2019) has to be put in perspective, as the cost of storage also decreases with increasing size (Guelpa & Verda, 2019), which might cause a stronger inverse proportional causality.
The location influences the LCOE since the locally available mass of surface water can vary. For a smaller mass flow, less heat will become available driving up the LCOE as the CAPEX is the same. The temperature of the water used equally depends on the location, resulting in less or more obtainable heat.

In order to obtain the local LCOE, all the different components of TESW are modeled independently by using simple equations, as has also been done by Lensink (2020). By then applying the cost as found in Niewold (2019) the CAPEX, OPEX and LCOE are determined for different scales of TESW. However, since the LCOE evaluation performed by Lensink (2020) was for a typical small-scale operation and since the same methodologies have been applied for all the different types of sources, the LCOE shown in section 2.4 must be reevaluated for a new DH.

To model the available heat from TESW and get a better estimate of the LCOE on location, a simplified deterministic method is used. As previously explained in 2.3, a deterministic model is based on resembling all physical relationships in mathematical equations to model the specific phenomenon. In this simplified deterministic method, not all physical parameters are considered reducing calculating operations of the model, well still coming to an accurate result. For the simplified deterministic model of TESW, first, the temperature of the river needs to be modelled. In combination with the heat pump operational cost and the pumping cost, the OPEX can be approached.

Modeling of rivers can, as heat demand, also be done using historical or statistical, stochastic or deterministic methods. The historical or statistical methods have been proven accurate (Dugdale et al., 2017) and are mainly used for large spatial scales when the data requirements for process-based modeling become too large (Caissie, 2006). The stochastic methods are often very accurate for predicting daily water temperature when only the air temperature is available (Caissie, 2006). Both these methods revolve around the relationship between air temperature and water.

Deterministic methods can also provide the data on an hourly basis (Caissie, 2006), have the lowest inaccuracy and are built around an energy and mass balance. Caissie (2006) states that a model is often chosen based on the aim and data requirements. As hourly data is preferred, the deterministic method seems the best fit. However, this requires extensive calculation as the input data used is large. A regression method also can determine the hourly temperature, although the latter is not common.

Important factors for the temperature of rivers, as identified by Caissie (2006) are the following four dominant groups factors: atmospheric conditions, topography, stream discharge and stream bedding. The emphasis lies on the atmospheric conditions as an influential group, they are responsible for the process taking place on the surface of the river. Dugdale et al. (2017) reviewed various methods and modelled the river based on solar radiation (separated in long and shortwave radiation), evaporation or condensation, convec-

tion or conduction, river bed and groundwater factor accompanied with heat convection and dispersion to the shore. Surface fluxes typically dominate the temperature of the river and are the aim of most of the models used.

The output of the temperature model should be an hourly temperature level of the river for the inlet of the TESW installation. For calculating the temperature one, two, or three-dimensional models can be used. The one-dimensional model is advised as the water temperature does not need to be modeled in three dimensions. The one-dimensional model operates with nodes placed along the river where meteorological data is collected from. The resolution of these nodes is highly dependent on the available input data for the inputs. It is recommended to only model the river for the principal axis, as transversal temperatures rarely occur when above depths of 4-5 m (Caissie, 2006).

In conclusion, a historical and a simplified deterministic method are used to approach the hourly temperature of surface water. The model used the temperature in this study will be further defined in chapter 4.

2.4.2. TEWW

TEWW is very similar in working principle compared to TESW in components used and has thus probably the same TRL. Just as with TESW, the thermal energy is gained from water using HEX and, depending on the source temperature, a heat pump that increases the source temperature to the DH distribution temperature. The biggest difference can also be found in the HEX used. Wastewater from houses or industry contains thermal energy, which is harvested in several ways for different locations, each requiring an unique design of HEX, as the contamination determines the kind of HEX. Wastewater has an advantage over normal water as it has a higher temperature year-round, as shown in figure 2.7.

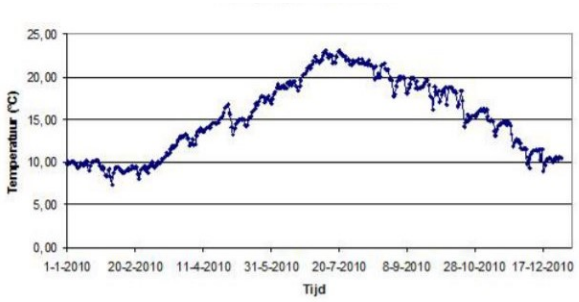

Figure 2.7: Temperature profile wastewater 'Vrijverval' sewage in Zwolle (Kluck et al., 2011)

The higher year-round temperature is, among others, caused by waste heat used in domestic housing, of which 40 percent is released back into the sewer (Sayegh et al., 2018). Additional heat is created inside the sewer by yeasting and other biological processes.

There are three ways to recover heat from wastewater: first, it can be collected at the source; domestic buildings and industry. Second, it can be recovered in the sewer system. Third, it can be collected at a local sewage treatment plant. Each of these locations varies in source temperature, fluctuations of source temperature and heat, and needs different equipment.

For all the locations, an HEX is used to regain the heat from the waste water. Once the heat has to be regained, a heat pump is necessary to upgrade the temperature level, to guarantee the temperature meets that of the distribution temperature level. Figure 2.9 depicts a classification map for a different type of systems of waste water HEX. As this research focuses mainly on the construction of a centralized DH, the first system does not meet this qualification. The second and third option therefore remain, and will first be set apart based on the type of HEX and then evaluated on use for a DH.

A sewer recovery system has been found to use three main types of HEX (Weeren et al., 2018): first, integration in new sewage construction system, second, standardized build-in systems for sewage lines and

third, pressure sewer system for which the HEX is built around the sewer pipe for construction reasons. In figure 2.8 all three systems can be found. In the bottom two images, the pressure sewage systems are found. The system on the bottom left shows a spiraled HEX outside of the sewage pipe. The image on the bottom right shows a double-sided stainless steel (SS) HEX, where SS is used to withstand the pressure, as a polymer system would fail.

For the sewage treatment plant, HEX's are placed in the treated effluent. Only bigger TEWW sources will be able to provide year-round heat. If the wastewater used lacks quantity, the daily fluctuations will become higher. As the DHW use rises in the morning and the evening, because of bathing by the population, the temperature and mass flow of the wastewater increases. These fluctuations make for a less steady source of heat and increase complexity, by requiring larger storage solutions.

For the systems to regain heat from waste water, different HEX's are used and different locations are found. However, for all mentioned concepts, the CAPEX varies between 2 and 3 thousand euro per kW generated heat and having a payback time between 8 and 12 years, dependent on renovations and investment cost according to Weeren et al. (2018), who provided a portfolio of TEWW already occurring in the Netherlands where wastewater was the primary source of heat.

Hepbasli et al. (2014) performed an extensive review for regaining heat from wastewater, with the use of heat pumps. These heat pumps primarily use a vapor compression cycle. The COP values encountered are within a spectrum of 1.77 to 10.63, which is large. For this reason, it is hard to make an estimation of which heat pump will be used and the cost of the expected heat pump.

Where the heat pumps vary in COP, the differences in CAPEX and the payback time found in the Netherlands, as seen by Weeren et al. (2018), are not significant enough to base a design on, the system needs to be further explored. The work of Hepbasli et al. (2014) concluded the fouling of wastewater HEX and heat pumps as key disadvantages to using TEWW. This fouling influences the CAPEX, but more significantly the OPEX of the equipment, so the placement after the sewage treatment is the best option. OPEX is also varying with location as the temperature level determines the amount of energy required for the heat pump. The larger the temperature differences, the greater the energy consumption of the heat pump. To determine the max heat potential of the waste water, the temperature and mass flow profile over time are the leading factor in placing the TEWW system.

Kretschmer et al. (2016) set out a method to come to a favorable situation in which, first, a preselection is made, after which measurements are taken of the stream used. The first step is based on the assumptions that the wastewater temperature is highest at its source, after which it cools down by interaction with surrounding soil temperature. Other assumptions of the temperature made are that the soil temperature of urban areas is higher compared to open terrain and as rainwater increases volume flow of the waste water but decreases, only use of the dry weather flow is considered for potential.

These assumptions can be traced back to a local sewage system found in Zwolle. The temperature of the wastewater is researched by Kluck et al. (2011) who showed that waste water from dwellings cools down rapidly in the winter after being released in the sewer (13 °C in 100 m) while in the sewer itself until the sewage treatment plant the waste water barely cools (1.5 °C in 2.5 km).

The measurements should be taken to include the dry-weather flow, as rain water decreases temperature while there is an increase of flow, according to Kretschmer et al. (2016). The potential is determined by multiplying the specific heat of the waste water with the water flow and the temperature difference, in order to come to the heating potential. The final steps include following a set of four planning principles stating that an optimal position needs to be found far enough from a sewage treatment and close enough at the source to prevent cooling in the sewer, versus placement far enough along the wastewater stream to get a steady temperature and multiple inflows.

A more defined temperature level and mass flow of the waste water can also be estimated by using a deterministic two-dimensional model, such as one set up by Dürrenmatt and Wanner (2014a). The input used for this model consists of sewer pipe properties, soil properties, and influent and ambient conditions.

Figure 2.8: Different sewer heat recovery systems. Picture 1 shows a new sewage integrated construction system, picture 2 a standardized sewage build-in system and pictures 3 and 4 a pressure sewage system adaptation (Weeren et al., 2018)

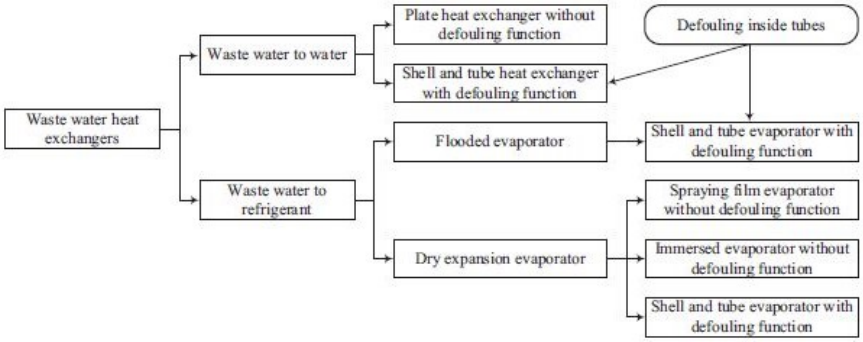

Figure 2.9: Classification of different waste water heat pump systems by Hepbasli et al. (2014)

However, a sewage HEX set up would influence the sewage treatment plant significantly, when in a proximity of 1-2 km. The lowering of the temperature level decreases the efficiency of the sewage treatment significantly. IF and Stowa (2018) therefore made the following assumptions for the possibilities of TEWW in the proximity of a sewage plant: within a kilometer of the sewage treatment plant, only a 1 K change in temperature should occur. When using the effluent, a 5 K temperature change is allowed, increasing the potential significantly. Also, increases 0.7 – 1.1 K when passing the sewage treatment. Previous research also indicated the sewage treatment plant has the maximum heat potential (Kluck et al., 2011). For the previous reason stated, the sewage treatment effluent is chosen as a heat source.

The LCOE, as determined in Lensink (2020), has also been performed on the average effluent of normal sewage treatment in the Netherlands, providing a good indication of the associated cost. As also stated by Kluck et al. (2011) who performed an extensive review of a sewage treatment plant in Zwolle, the costs of each project are very different locally, as the scale of the specific operation is of key importance. The work of Kruit et al. (2018) shows this for TESW, which has many similarities in cost construction as TEWW.

To estimate the heat potential of the effluent of the sewage treatment, models are used. In literature only one model estimating the effluent temperature per hour could be found, which was done by Wells et al. (2005) who used the meteorological data air temperature, dew point temperature, wind speed and direction, and solar radiation to estimate the effluent temperature. Their one-dimensional deterministic model assesses the heat gains and losses for the aeration basins resulting in the effluent temperature. Dürrenmatt and Wanner (2014b) distinguished four different parameters in modeling their two-dimensional deterministic model comprising of an one dimensional balance equation describing the phenomena of changes and flow direction, water temperature, air temperature and water vaporization accompanied by an one-dimensional radial equation describing the balance of temperature of the soil pipe wall and water temperature over time. Hart and Halden (2020) also noted the lack of modeling without the use of location-specific elaborate data and

proposed a method to estimate the monthly main temperature on a combined historical and deterministic model. The model estimates the soil temperature based on a deterministic model based on a dynamical lumped capacity model, after which the temperature is corrected by historical data over a period of thirty years and assumed source temperature data.

However, looking at historical temperature profile development as found in effluent of sewage, it changes over a time step of a couple of hours is significantly low, making the required input data and calculations necessary for the temperature reluctant. A simpler lumped model as established by Hart and Halden (2020) has therefore a better balance between computational requirements and accuracy. The models showed good comparison to real-time data with Pearson coefficients of P=0.81 and 0.76 for maxima and minima. The model found by Tessel and Pijl (2006) showed even greater values, where the majority of the 48 researched sewage treatments a determination has been found between 0.9 and 0.95 (19) and >0.95 (12). In comparison, the Pearson coefficient squared equals the determination coefficient and is for the model of Hart and Halden (2020) 0.66 and 0.58. A similar model as used by Tessel and Pijl (2006) will be evaluated for use in chapter 4.
However, the volume flow modelling of the effluent seems to be absent in literature. What exists abundantly are models aimed at predicting the influent flow. Martin and Vanrolleghem (2014) reviewed the most common methods used to estimate the influent flow. The solutions were classified in the following classes: completing an incomplete dataset about the quantity and among others of the influent, translating quality measurement into activated sludge models, identifying the uncertainty in quality and quantity of wastewater.
The second class identifying and characterizing the influent based on parameters required for the activated sludge model is well established. The third class uses autoregressive functions to represent uncertainties in the quality and quantity of the influent. This method still needs more back up and research to model the effects of the causalities leading to the formation to the effluent.
Based on the description of the classes provided, the first class has the most appropriate fit. For the first class, a subdivision is made for a solution based on harmonic functions or by establishing a wastewater generation system. Fourier generators have proven very useful for describing daily and weekly patterns. Translating of measured values offers lower computational requirements. Another method looking promising is using a deterministic model including physical factors such as the amount of inhabitant, sewer network, type of industry, rainfall and temperature profile among others. The latter model can easily be extrapolated to other sewage treatment plants for which the influent needs to be modelled as it can use characteristic data found for that location.

The first model, based on harmonic functions, is predominantly aimed at describing dry weather patterns and interpolating hourly data of daily provided flows and uses a small number of measurements to come to a fairly accurate result making it cheap to use. The deterministic model however is more easily adaptable as it can use data from the local area to come to results. This model also has the best fit with the model estimating the temperature making this the most appropriate fit for this study.

However, when using one of these models, the effluent shows different patterns of outflow and temperature compared to the influent. First of all, the sewage treatment plant can add somewhere between 0.7–1.1 °C to the effluent temperature. Secondly, as observed from data in the existing literature, the effluent released into nature is characterized by a buffer function of the sewage treatment plant, as the effluent has been proven to have a far lower standard deviation compared to the influent (Langeveld, 2004).

As for the sewage treatment plant to maintain its function, it will be necessary to maintain a constant volume with some playroom to accommodate changes in the influent. In the Netherlands, sewage treatment plants are designed according to dry weather and rainy water discharge, which is the average and maximum the sewage treatment plant can handle. With these figures, a dynamic analogy of the sewage treatment plant acts as a buffer, as was also made for the temperature by Wells et al. (2005). A key parameter for this is to approach the standard residence time, as it is considered a chemical plant with multiple continuous batch reactors. These reactors are easily modelled when their volumes and residence times are known and seem the best fit as an initial approach for modelling the effluent temperature and flow rate.

The total model estimating the LCOE based on the proposed equipment using simulated flow and temperature will be constructed for Westenholte in chapter 4.

2.4.3. Solar thermal energy

Solar thermal energy is a frequently occurring heat source for DH. The technology for gaining heat from the sun is therefore considered mature (TRL>9) (Mazhar et al., 2018). Many DH systems exist where solar thermal energy is the primary energy source. These DH are almost always assisted by some form of TES since the seasonal and diurnal or daily differences are significant. Gaining heat from the sun is done with the help of solar collectors. The collectors absorb the light into a medium, which is heated and then transported to its ultimate destination; an HEX or heat pump, depending on the temperature of the medium, which varies depending on the collectors used.

TES is used to optimize the use of the functioning of the collectors. The solar fraction, the total amount of heat that is gained during one day, is a prime indicator for determining the amount of storage required. When the solar fraction is lower than 50 percent, storage is required. Three types of collector and storage set ups have been defined by Mora et al. (2018): completely decentralized, block heating and centralized heating. Where decentralized does not have storage, block heating might include storage and centralized includes storage. As this work uses centralized heat sources, fully decentralized solar heating will not be dealt with in detail in this work.

Centralized oriented solar thermal systems have a large, ground-mounted, field of collectors, of which a system delivering above 350 kW is rare. However, of the larger systems, sizes up to 50 MW is found in Europe, so they are already proven technology. The centralized systems often come with storage and can therefore deliver heat parallel to other heat sources. The block heating oriented system often consists of roof-mounted solar collectors and can have both centralized as decentralized TES. An advantage that so far has only been experienced with the centralized orientation, is that the scaling up of the system enhances performance and decreases investment cost per area.

For the solar thermal system, two groups of collectors are differentiated, non-concentrating collectors and concentrating collectors, which are not common for domestic heating and are therefore disregarded in this study. The advantage of the non-concentrating collectors is that they can use all light (diffuse and direct irradiation) present and not only the direct irradiation from the sun. However, the temperatures for these collectors are lower compared to the concentrating collectors as a major drawback, potentially requiring a heat pump in order to reach the distribution temperature.

Of the non-concentrating collectors, flat plate collectors (FPC) are predominantly found in Europe thanks to development source to increase quality, efficiency and cost print. Heat-pipe based collectors have also been used as collectors. Thanks to a double glass wall with a vacuum in between, heat losses are lower leading to higher efficiency than FPC.

Photovoltaic thermal hybrid (PVT) collectors simultaneously produce electricity and heat and are found the best overall performance according to Tian et al. (2019) who evaluated them based on their electrical output as thermal output. However, the high CAPEX which is double that of PV panels, and lacking manufacturing sites prevent them from being used in DH. Additionally, some argue that photovoltaic (PV) panels in combination with a heat pump provide a cheaper alternative.

It has been shown that for a cold climate in Iran, the use of an evacuated tube collector is economically preferred. The capital expenditure of the evacuated tube collector is higher, however yearly useful energy gain is 30 percent more. However, bursting and overheating are severe and result in massive amounts of operation and maintenance work. The FPC collectors have far less maintenance requirement due to their simple structure, and low installation cost (Huang et al., 2019), additionally, for DH these have been found to have a higher yearly efficiency compared to the evacuated tube collector because of limited capacity to absorb hours of high intensity compared to FPC.

For the non-concentrating non-PV panels, Van Miltenburg (2016) argued that by using evacuated tube collectors the overall solar gain is lower compared to FPC. In order to compare the PVT and FPC, Pakere et al. (2018) reviewed the use of PVT for DH and concluded an LCOE of 0.0341 € / kWh is achieved for a solar field of 3000 m^3. Comparing this to the LCOE of normal ground-mounted FPC, which is 3-5 € / kWh (Mora et al., 2018) perhaps the use of PVT might be beneficial as the ground price in the NL is relatively high. However, as

the production of this technology is still in a low stage of development, normal FPC would satisfy the needs as set by the consortium. Using PVT increases complexity, requiring a larger difference in cost to be used. It is also not sure yet if using PV panels in combination with a heat pump is not cheaper than using a PVT Panel.

Furthermore, Mora et al. (2018) indicated that the solar collectors are mounted in many different ways, but the main locations found by Mora et al. (2018) are either ground-mounted or roof-mounted. Roof-mounted collectors occur when space is limited and costly but is more expensive. When ground space is cheap and available, ground-mounted solar collectors are used, which are lower in cost as larger collectors can be used and simpler mountings among others.

In chapter 4 further research will be done to evaluate if ground or roof-mounted collectors might be more beneficial.

Modelling methods providing the output temperature of FPC are categorized into three groups according to Tagliafico et al. (2014), who performed a review on the different modeling methods and found the following in their work: steady-state, lumped capacity, and discretized. The first approach, the steady-state method, is the simplest and therefore also computational the fastest method, but can only provide accurate results with long time-averaged data. The lumped capacity model is the simplest of the dynamical models and can provide accurate results, but this feature depends on the weather conditions, as only small inertia effects are accounted for. Cloudy days cause errors in the results. The last approach, the discretized approach, has the highest accuracy. The higher accuracy however comes with an equally higher price: the method is more complex and requires more computational time.

The lumped capacity method and steady-state method are the most interesting for larger-scale DH, as these both require the least computational demand. The lumped thermal capacity method is based on the thermal capacitance of the FPC, in which a differential equation describes the energy balance of the system. The models can be separated into 1-point, 2-point or 3-point lumped models, where the number of points resembles the separation of the lumped capacities. It is shown with a 1-point approach the temperature fluctuations are overestimated and with a 2-point approach, the temperature fluctuation is underestimated. As extra fluctuations require an overestimation of the amount of FPC and storage, this seems more appropriate for the proposed DH model, as this will lead to an overestimation of the required storage. Additionally, it is expected the calculation time of the 1-point lumped capacity method is less computationally expensive, since only one differential equation needs to be solved, reducing complexity and requiring the least amount of data. For the steady-state approach, the lumped capacity is neglected and a simple singular value for the heat coefficient for the entire collector is used, average plate temperature, and outside influences such as weather. This model has also been integrated into the testing of FPC in compliance with the European Union in code EN 129751:2006+A1:2010. Equations 2.6 and 2.6 shows how the heat absorbed is calculated, as deployed by the European Solar Thermal Industry Federation (2012).

$$\dot{Q} = A * G * \eta_{FPC} \tag{2.5}$$

$$\eta_{FPC} = \eta_0 - \frac{a_1 * (T_m - T_a)}{G} - \frac{a_2 * (T_m - T_a)^2}{G} \tag{2.6}$$

For which A is the active surface area of the panel [m^2], G the irradiance [J/m^2], η_{FPC} the efficiency of the panel, T_m the average temperature [$°C$], T_a the outside temperature [$°C$] and η_0, a_1, a_2 FPC specific factors. Since the proposed model of the DH needs a quasi-steady state prediction as the time step is set to an hour, the steady-state method is used (Sakhaei & Valipour, 2019). Computational time and complexity are to be limited, as this is part of the entire modelling process the dynamical processes are disregarded. In chapter 4 the model will be set up for Westenholte.

2.4.4. IWH

IWH is excess thermal energy of the industry. The usage of IWH is a mature (TRL-9) technology, as an internal cooling and heating structure is found in most industrial plants. However, IWH has huge unrealized potential, (Fang et al., 2013; H. Lund et al., 2014; Mazhar et al., 2018; Yang et al., 2018), as 50 % of the industrial energy is wasted as low-grade waste heat suitable to be used in DH, (Fang et al., 2015). Preventing this from being used is the lacking infrastructure and politics. Using IWH can reduce the cost of waste disposal and

limit GHG emissions and water usage (Fang et al., 2013). For the Netherlands, this would account for roughly 100 PJ per year. Of this, about 57 PJ might be used for the heat supply of households which is about a sixth of the Dutch household consumption as defined by Schepers and van Lieshout (2011).

However, not all waste heat can be used in other industrial processes, resulting in the dumping of heat into the environment. Preventing IWH to be used, is the lack of infrastructure connecting waste heat to DH, the mismatch in time of domestic demand and IWH heat supply, instability as a result of severe weather conditions, failure of equipment, economic market effects and an unfortunate topography Li and Nord (2018). Utilization of IWH must be done with precaution to meet safety demands for cooling of equipment, making it even more difficult (Fang et al., 2015).

Typically, the heavy industry cannot be found in close proximity to residents for safety reasons. For the Netherlands, this has been established in the laws set by the government dependent on the type of industry. Setting up the infrastructure to carry away the heat gained from these processes is thought to introduce such a high amount of additional cost (CAPEX increase from pipeline construction and pumps, OPEX increase from pumping cost, heat losses) (Fang et al., 2015; Fang et al., 2013), that it is disregarded. Industry within 5-10 km (Fang et al., 2013) is recommended, however, this can greatly vary per location.

Because of the varying supply for the different industries, quantity and quality are important factors to estimate the potential. Several studies have been conducted to determine potential IWH available on an international scale, national scale, and local scale. For these studies, first, the properties of IWH need to be defined in terms of heat available (quantity) and temperature (quality). When these parameters have been found, an evaluation can take place, which determines the amount of excess heat present in the industrial area. Once this analysis has been performed, the equipment can be determined, resulting in available heat and also the price of the heat. HEX capable of processing the different WH present are typically used, as can be seen in table 2.5.

The reason why temperature is used as parameter to validate the excess heat is because, when using a higher temperature WH, it also offers the possibility to be used elsewhere in the industrial process present. This would be more beneficial compared to it being used in a DH, because of the following reasons: first, high temperature heat is harder to produce, compared to low degree heat, so it requires more energy to produce. Second, the transport of high degree IWH to the consumer will be more expensive than it is used locally as CAPEX of installing the piping and heat losses will be higher compared to the small trajectory of it being used on site.

The studies performed on international and national scales were likely to use different categories for the different industries and associated temperature levels, after which the average amount of waste heat was used to assess the potential WH available (Chowdhury et al., 2018; McKenna & Norman, 2010; Papapetrou et al., 2018). As this macroscopic process differs greatly per location, this method is not sufficient to use for the case study, where more accuracy is required to come to an economical evaluation.

Local approaches are more based on the specific industries present and their associated processes. Ajah et al. (2007), Bonilla-Campos et al. (2019), Fang et al. (2015), and Fang et al. (2013), Woolley et al. (2018) described different methods in order to estimate the potential of WH. Ajah et al. (2007) used specific data offered by the IWH provider to make an economical assessment for the DH of Delft, after which a heat pump was used to upgrade the temperature to useful temperature for the DH. An Aspen simulation provided the amount of heat available. A cascade heating network is proposed by Fang et al. (2013) to simultaneously decrease the heat consumption of the industrial area and only the heat with no other purpose would be used. Fang et al. (2015) then provide a method for the design of such a system, by providing a methodology similar to the pinch analysis already in use. This method requires the amount of heat necessary with the associated temperatures from the source. Woolley et al. (2018) developed a four-step method comprising a waste heat survey, followed by an assessment of the data after which the technology is selected, leading to the final decision and its supporting arguments. Bonilla-Campos et al. (2019) used a similar, but more extensive approach compared to Woolley et al. (2018) in order to model the IWH production, their method involves a seven-step plan, using measurements to support the modeling.

Table 2.5: Kind of IWH according to Fang et al. (2015) with examples, all can be found at the location of Voorst except for slag/residue

Temperature	Kind of IWH	Examples
High	Flue gas	Flue gas from the exhausts of cyclones in cement plants
	Steam	Steam from waste heat boilers in ferrous smelting factories
	Slag or residue	Slag from the blast furnaces in iron works
	Product	Steel slabs from casting workshops & strong sulfuric acid in copper smelters
	Combustible gas	The sensible and combustion heat of blast furnace gas in iron works
Medium	Product	Steel slabs from casting workshops and strong sulfuric acid in copper smelters
Low	Condensation water	From waste heat power generation turbines in smelting factories.
	Cooling medium	Circulating cooling water in the walls of the blast furnaces of an iron works

Depending on the cooperation's experience with involved partners, a method for estimating the potential can be chosen. Regional key figures can also be used to estimate the waste heat potential. Miró et al. (2016) evaluated three leading methods in the literature and used key figures. However, these methods do not incorporate the hourly profile of the IWH production.

As the method used by Bonilla-Campos et al. (2019) requires extensive iterative communication between model and real-world data in form of on-site measurements, a model based on Woolley et al. (2018) is more suitable for this study. The reason is that the scope of the work consists of a more integral approach including many partners, which results in extensive amounts of communication, for which partners involved have not shown interest.

Woolley et al. (2018) methods use the following steps: first, a surveying step is executed, to identify sources and sinks with their associated temperatures and processed heat present on site. The second step includes an assessment to determine the IWH to get to a quantitative assessment. The quantitative assessment is based around the principle of exergy, and spatial availability. The third step involves a selection of the equipment to be used. For the proposed cascade heating network HEX are used. When the resulting IWH is of a temperature lower than the DH network, a heat pump needs to be used to increase the temperature. In the fourth and last step, an analysis is performed to improve the economic and environmental factors such as the overall payback period, the net financial benefit, and also the CO_2 emission reduction. In this stage the LCOE can also be calculated, using the method proposed by Doracic et al. (2018) for levelised cost of excess heat. This however does not include heat pump cost.
As far as literature is concerned, methods estimating the potential of waste heat are abundant, although they lack temporal hourly profiles for industries.

Once the excess IWH has been identified, the cost can be determined based on the equipment necessary for utilization. The model of the heat and the expected LCOE of the IWH are thus inherently connected, as first a pinch analysis needs to be performed to determine the excess heat where its temperature and quantity are both necessary.

2.5. Coupling of supply and demand

The coupling of the supply and demand through a medium- to low-temperature distribution network presents two main issues in the forms of a time difference and a location difference. The time difference is found in the mismatch which occurs because of physical factors, such as weather and seasonal differences, on the supply and demand and/or economic factors. The second issue arises in the feasibility of transporting heat from supply to demand as thermal losses and pumping costs carry a high OPEX. Minimization of the piping used reduces the cost and thermal losses. Feasible areas can be found when the energy density of demand and supply is high. The distance between the heat sources and demand is relatively is small to normal for a large-scale DH when demand and supply are within 200-300 m away from the consumers (Talebi et al., 2016).

2.5.1. Thermal energy storage

To resolve the time-dependent issue separating heat supply from demand, TES is used, which offers an increase in performance of the DH. By increasing the flexibility of demand and supply, matching of supply and demand is done more efficiently, resulting in a reduction of total cost and CO_2 emissions. The reduction is

Table 2.6: Advantages of using TES with DH (Guelpa & Verda, 2019)

primary advantage \specific advantages	Energetic	Economic	Environmental	Other aspects
Reducing generation unit size/number of unit		Avoid investment cost for further units		Reduce system complexity
Thermal peak shaving and valley filling	Increase the system performance by reducing use of low efficiency plants	Decreases cost by enabling use of more convenient plants and maximizing profits in electricity selling	Reduce emissions by decreasing the use of low efficiency plants	Better management of undesired events (such as pump failure or leakages)
Relieve intermittence of RES	Reduce primary energy needs by increasing RES exploitation	Allows exploiting plants with low operating costs	Allow exploiting zero-emission energy plants	
Smaller pipe size		Reduce the investment costs		Perception of a lower impact on the urban layout
Network (transport and distribution) management flexibility	Reduce primary energy needs by increasing RES exploitation	Reduce pumping cost	Reduce the emission related to pumping power production	Better management of undesired events (such as pump failure or leakages)

made possible as the TES acts as a buffer on the supply and demand. For the supply, this means the peaks of the heat source are stored which would otherwise go to waste decreasing the total heat necessary. This storing of heat also enables more efficient use of RES decreasing CO_2 emissions. The daily and seasonal fluctuations of RES must be flattened out to suffice more efficiently in the demand. For the demand, the peaks which are found daily and seasonally are covered, decreasing the required overall heat. This buffer also has been found to decrease the pipe diameter and overall pumping of the distribution network. Table 2.6 summarizes the results of all these effects and is an adaptation from Guelpa and Verda (2019).

In order to select the best applicable TES dealing with the fluctuations of heat supply and demand, a preliminary selection needs to be made between the historically used TES, disregarding specific geological specifications. TES previously used for DH are categorized based on a timescale, a physical method used to store the heat and centralized or decentralized use Guelpa and Verda (2019). Common physical methods to store heat are: sensible (SH-TES), latent (LH-TES) and chemical (C-TES). These methods are used in the following fashion: SH-TES uses difference in temperature of the storage medium to store heat and is of TRL of 7-9, LH-TES uses phase changes in the storage medium, which has reached TRL of 4-7 and C-TES thermal energy is stored in the bonds between atoms or by absorption/absorption reactions which have reached a TRL of 4-6. To come to a selection of which method to use, the time scale, geographical location, and available space play key roles. However, this thesis aims to provide results for a readily available, renewable multi-source DH. Therefore, only SH-TES will be further assessed as this has a minimum of TRL-7, implied that the technology has been demonstrated and has already been used in an operational environment.

Most DH prescribe the use of two different time scales of heat storage: short-term and long-term or seasonal storage. Short-term storage has a range from a couple of hours to a day to store excess heat when demand is low and making heat available when demand is high during the day. Seasonal storage is mainly oriented on providing storage from timescales of multiple weeks to entire seasons. The scale is such that surplus heat is large, for example, during summer when TESW is used and ATES stores heat to be used in winter when heat demand is high. When comparing short and long-term SH-TES the key points to test are mainly the application but also the space required and heat source used.

To compare the application, at first the use in terms of location has to be determined: centralized or decentralized. Decentralized TES first, will encounter multiple problems, when placed in dwellings as addi-

tional investments and approvals are necessary to install this system as space is a key issue for all TES (Guelpa & Verda, 2019), also contradicting the aim of this thesis. Second of all, has been shown that flexibility is lower compared to centralized TES Guelpa and Verda (2019). Third, large centralized storage shows a decrease in price when the storage volume is increased in an inverse proportional relationship where decentralized installments will most likely have a lower inversely proportional relationship. For these three reasons, centralized storage will be further used in this study.

SH-TES centralized storage is possible for short and long-term storage, which are not per definition mutually exclusive. However, they have slightly different purposes, as previously described, but also in cost, space, thermal losses and quantity of heat stored. Guelpa and Verda (2019) emphasize short term storage is mainly used when daily demand and supply have a significant mismatch, for example: solar thermal energy is only available when daylight is available whilst the heat demand is largest in the evening. This short-term storage can level the supply to meet the demand. It can also be used in, for example, in a DH network where a CHP is used to better exploit the electricity price. The long-term is primarily used when sources have different heat production moments, such as the RES or WH, to store excess heat.

Since the to-be-designed DH will have a varying supply of heat during the year, both of the storage methods are to be used for the ultimate design.

Short-term SH-TES comes in two major forms: directly connected pressurized water tanks and atmospheric pressure water tanks. Directly connected pressurized storage is mainly used for high-temperature DH systems where the pressure must be higher than the saturation pressure. It also has the advantage of storing a temperature difference of 50-55 °C and replacing the pressure vessel needed to maintain pressure in the DH system. Atmospheric pressure water tanks are indirectly connected to the DH and have a maximum temperature gap of 30 - 40 °C. The atmospheric tank has a lower investment cost and therefore is a better choice when operation time is limited. In chapter 5 a decision will be made between these two options for the proposed DH. The location of the short-term SH-TES can vary, it is possible to place one large tank or several smaller tanks.

Long-term SH-TES are significantly large and are classified according to the temperature used, or interaction with the ground, which is either a closed (a storage vessel containing water) or open (directly pumping and extracting water into the soil) storage solution. Common methods for storing heat are in a closed container such as a water tank, pits and boreholes. In open storage, groundwater mixes with the water storing heat. The method mentioned is called the aquifer thermal energy storage (ATES). The sensible heat of water injected in the ground is then used as a storage solution.

Guelpa and Verda (2019) advice taking the following environmental factors as the base for determining the best system possible between thermal losses and reliable discharge, recovery efficiency and CAPEX cost, based on: space available, geological location characteristics, other storage sites and groundwater usage nearby. Considering the finances of the geographical storage, a famous graph illustrated in figure 2.10 shows the investment cost for the different kind of seasonal storage systems, as created by Mangold et al. (2004). The chart served to estimate the cost of seasonal TES for a project in Germany.
Figure 2.10 shows that the cheapest types of seasonal storage are duct and aquifer storage for which the geological demands are the highest. For this case, the ATES is used, as was predetermined by the consortium formed by Witteveen+Bos and others. In perspective with the other long-term TES solution it is known that the ATES is more dependent on the geological location as the storage medium, water, must be stored in between two impermeable ground layers to contain the water. Unlike the tank pit, it also often requires a heat pump, as most ATES are low temperature. As the advantage, the ATES has the lowest investment cost, as seen in figure 2.10, low space requirement and short payback time. It has also been proven that ATES can decrease the energy consumption of a DH network between 40 to 70 percent compared to conventional storage according to Fleuchaus et al. (2018).

ATES differ between low-, medium- and high-temperature. In low-temperature ATES (LT-ATES), water at 30 °C is pumped to around to max 400 meters below ground level (mbgl). In 2016, 2200 permissions have been an issue for ATES in the Netherlands of which more than 90 percent were LT-ATES. Medium-temperature ATES (MT-ATES), 30 °C-60°C, and high-temperature ATES (HT-ATES), >60 °C have not been found feasible yet

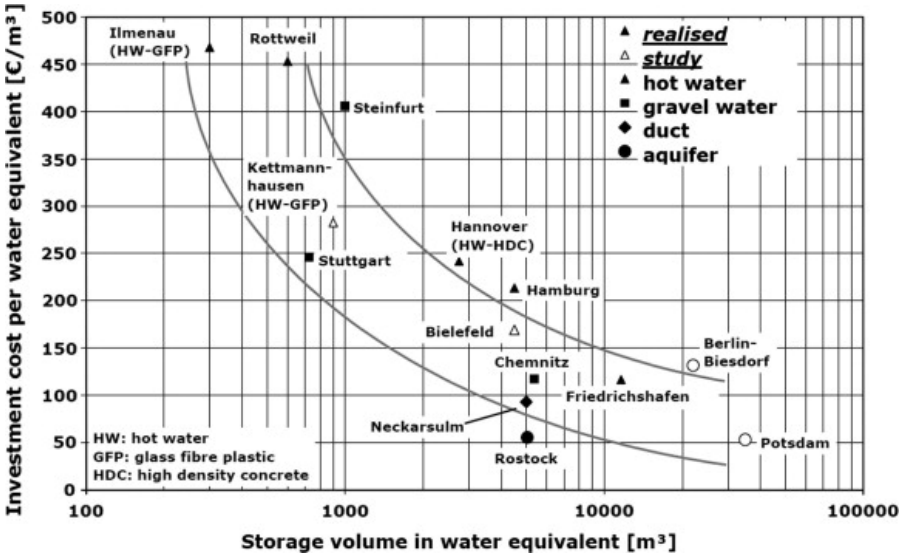

Figure 2.10: Investment cost of different seasonal TES (Mangold et al., 2004)

and struggle to get permissions from the government due to unproven destruction of the biosphere. This implicates a heat pump must be used in order to upgrade the heat to the distribution temperature, significantly increasing the amount of water that needs to be stored.
For both short and long-term storage, various models have been developed before a storage solution can be selected. The exact functioning of the short term storage solution selected will be explained and modelled. Secondly, the LT-ATES physical functioning will be explained. Lastly, models will be introduced based on accuracy, input and time step.

The short-term storage solution consists of a pressurized tank filled with water which is stratified into different temperature segments, so both hot and cold water is stored in the tank. When a surplus of heat is present, the cold water flows out of the tank and hot water is added into the appropriate segments using diffusers to prevent the water from mixing. Vice versa, the same happens when heat is necessary. Now, the hot water is being extracted and cold water is added to the tank. The separation in temperature or stratification remains intact by the use of diffusers, which should add the water, and also should be designed to prevent turbulence to maintain the stratification zone.

Since the direct connection of the pressurized storage tank will also make it function as a pressure vessel, the functioning of the storage tank will be controlled automatically by pressure. The pressure is a direct function of the demand, as normally in a DH when the pressure of the system is kept at a constant level. When demand decreases pressure will increase and water is drained from the network into the vessel. When demand increases the opposite happens and the vessel is discharged. Figure 2.11 shows the functioning of this type of storage.

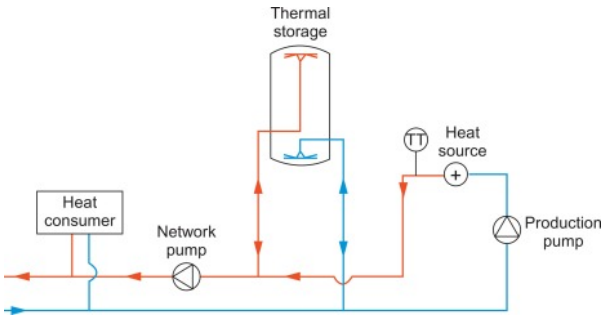

Figure 2.11: Operation of short term directly attached storage (Thomsen & Overbye, 2016)

As the pressurized vessel storage functions automatically, the operation and volume of the storage are of key importance to its operation as this will determine the operation of the vessel. The pressure difference depends on the location, where the vessel is placed thus deciding when the storage is charged and discharged. The volume in equation 2.7 dictates the amount of heat that is stored.

$$E = c_{p,w} * \rho_w * \Delta T \tag{2.7}$$

In which the amount of heat E[kJ] is calculated, using the specific heat capacity of water $c_{p,w}$[kJ/kg/°C], the density of water ρ_w[kg/m^3] and the temperature difference in the storage ΔT[°C].
Pinel et al. (2011) created a large number of designs in order to model the heat storage and its efficiency of water tanks. The most extensive models solves the full Navier Stokes equation in 3 dimensions to accommodate heat transfer, buoyancy, and diffuser activity, while the easiest ones are the plug flow models. A common approximation is a one-dimensional model in which the temperature gradient is assumed to only be present in the vertical axis, based on the assumptions the tanks have a high level of insulation and the longitude direction heat transfer is not present. Some analytical models also exist, where the same assumptions are made as for the one-dimensional equation, and often only two stratification layers are considered.

The long-term storage however is more difficult to model as many factors are involved. For this problem often finite element modeling is used. For optimization, this however involves a significant amount of calculations. The most basic method involves an adaptation of equation 2.7 where the property of the soil and the water are used as an average and a simple efficiency coefficient which slowly increases over years as the ATES charges. The best solution must be in between those two approaches. Pinel et al. (2011) indicated that under some circumstances, simplified methods give acceptable approximations for preliminary feasibility studies.

A review performed by Lee (2010) showed the general procedure for design and emphasized the complexity of the ATES. Oftentimes, numerical simulations are used in order to design and simulate the ATES. These calculations are based on either the finite-element method, integral finite difference method or a hybrid of the latter. Simplified models exist and can be found in the work of Kranz and Bartels (2010), who developed a simplified model which only considers the thermal behavior of a flow field of a single well. However, this model is still relying on the finite difference method, making it too time-consuming to be used in the large system model.

A new simplified model should be developed for Voorst and Westenholte in order to minimize computational time. This simplified model will be developed in chapter 5.

2.5.2. Distribution network

As previously mentioned, the coupling of the supply and demand faces two different problems: one of timescale and one of topographical location. The latter can be solved by utilizing pipes that transport heat from supply to demand. A variety of options exists for this distribution network: piping characteristics, heat pumps, pumps, and heat exchangers.

A selection can be made for a DH to transport heat directly from the heat source or to divide the DH into two networks: the primary, from the heat source to heat transfer station and the secondary network from the heat transfer station to dwellings. The latter option will be chosen, as this is more suitable for large networks. The so-called 'heat transfer substation' divides these networks. This part will focus on the secondary network. The options for the grid structure are Y-network, ring network or a combination of both. Historically, DH is built-in Y-network. In this scheme, dwellings are connected in parallel to the heating source. The demand in the network determines the mass-flow going through the pipes. In the dwellings themselves, valves are found to control the supply.

Benefits of Y-network according to Kuosa et al. (2013):

- Simple structure
- Construction is easy

Disadvantages of Y-network according to Kuosa et al. (2013):

- Slow control system
- Lower energy efficiency compared to the ring topology
- Different lengths of pipes between dwellings resulting in large local pressure differences

An alternative network was researched in an attempt to prevent large pressure drops, with the ring network as a result. In this network each consumer has its mass flow control, meaning pumping on demand. Changing from valves to pumps, changes the network in such a way that all consumers now have an equal pipe diameter. In this system, the supply and demand temperature of the heating network vary depending on the outside temperature.

Advantages of ring network (Laajalehto et al., 2014):

- Increased control
- Lower pressure drop
- Equal pipe diameter everywhere
- Decreased OPEX
- Decreased heat loss

Disadvantages of ring network (Laajalehto et al., 2014):

- Increased CAPEX
- Complex distribution model

The decreased heat losses are because the flow rate is higher and as a result lower delay as found in the model of Laajalehto et al. (2014). As a disadvantage, it has increased CAPEX, because the longer distance in piping has to be covered, and a different, more sophisticated, model for the coupling of the outside temperature to the supply temperature is used. Only when the latter is applied, does the heat loss decrease substantially.
A hybrid solution between the Y and ring topology is also possible. The security of the delivery is, therefore, the highest, though the CAPEX and heat losses are greater.

The piping is one of the key factors, determining the cost of DH heating, as the distance is long and most heat losses occur during transport. For a 4th generation network, it is proposed to use prefabricated flexible twin piping or polymer piping (H. Lund et al., 2014). The first choice to be made is to either use prefabricated insulated flexible twin-piping or individual piping. Polymer piping has the advantages of less heat loss, less expansion, as well as less space required. The disadvantage of the twin-piping is a reduction in flexibility and the influence of the piping on heat transfer between supply and return pipe, as they are placed alongside each other.

de Boer (2018) developed a master thesis on heat losses of piping in Dutch DH systems. He compared three types of tubes: steel tube insulated with PUR and protected by a PE layer; ST/PUR/PE, ST/PUR/PE with thicker insulation and twin-pipeline, where both tubes are embedded in a single PUR layer. The heat losses and cost were calculated for a temperature range of 70 °C to 40 °C and as a result, the thicker insulated tube had an advantage of 14.6 percent and the twin-tube even 39.7 percent heat loss reduction compared to a less insulated single pipeline. Financially, the twin-tube was also the better option even though the investment will increase with costs for placement and welds. The reason for this is that only half of the piping needs to be installed and the costs of heat loss far outweigh the increased maintenance cost associated with twin piping.

The network can be modeled in various ways, however, the design of the network will not be the focus of this thesis. To design the network either the model as developed by Witteveen+Bos will be used or the guidelines provided by Kennisinstituut voor Installatietechniek (2012).

2.6. Alternatives of DH

The “klimaatakkoord” is the law that dictates a disconnection of dwellings from the gas grid while offering other solutions than DH to stop using natural gas as well. (Hoogervorst et al., 2020) extract five strategies from this law:

1. Individual electric heat pump
2. DH with middle to high supply temperature heat sources
3. DH with low-temperature heat sources
4. Green gas, gas with a net carbon emission of zero
5. Hydrogen as energy carrier

These are just some solutions for heating dwellings. However, since the government considers these to be valuable options, this selection of solutions will be assessed by the government in the LAW.

The two DH solutions do not differ from the proposed DH, leaving three solutions. Of these three solutions, numbers four and five are debated for their role in the transition. In both of these solutions, replacement of fossil natural gas with a more sustainable gaseous option is not expected soon. Weeda and Niessink (2020), researched the use of hydrogen for heating dwellings in the Netherlands and found that the hydrogen solution still is lacking experience, as safety issues are major. For both solutions, the availability of the proposed gas is too low for such a large-scale operation.

The first solution is thus remaining as a decentralized solution. This solution implies the use of decentralized heat pumps for dwellings with a high degree of insulation. The source medium from which the heat pump will draw its heat will be the groundwater or outside air. Of these two heat sources the air heat source has lower CAPEX but higher OPEX (Hoogervorst et al., 2020). The ground source heat pump requires drilling to become functional. The soil must be fit for this kind of heat pump. Additionally, the drilling is invasive for the home owners (Hoogervorst et al., 2020). Because the installment of the ground source heat pump is considered invasive, this solution falls outside the scope of the research, leaving the less invasive air-source heat pump.

2.7. Methodology based on literature study

After the literature research, the most appropriate models have been selected for modeling the multi-RES DH of the neighborhood of Westenholte and the industrial area of Voorst. In the following chapters each of the models will be constructed for this DH network, after which the flowchart as seen in figure 1.2 will guide the results and conclusion. First, the following paragraphs will summarize the decisions made in the literature study.

2.7.1. Heat demand

The literature study found that the temperatures, as proposed in the DH network, are suitable for the currently installed heating systems in dwellings. However, regulations apply for DHW, necessitating the installation of additional equipment for consumption. After evaluating different models to calculate the heat demand of the DH system, after which the reference building based model came out as the most appropriate model available.
In chapter 3, this model will be set up for the neighborhood of Westenholte and the industrial area of Voorst. Methods available for the model will be compared after which a simplified model is constructed for each reference building.

2.7.2. Heat supply

Using the heat demand, the heat supply will be established based on the required peak supply. After which the necessary supply will be determined. Finally, for each source, the LCOE will be simulated and the amount

of heat that it must use will be established.

TESW

For TESW, an HEX and a heat pump will retrieve usable heat for the DH system. An assessment of the location will be made on where the equipment is most likely to provide the lowest LCOE. After this evaluation, the temperature of the surface water will be modelled using a historical model.

TEWW

Similar to TESW, an HEX and a heat pump will be used to redeem heat. The HEX will be placed so it can use the effluent as a heat source. The effluent volume flow and temperature will be estimated by using a simple historical model.

Solar heat

FPC will collect the solar heat which is then if needed upgraded by a heat pump. A simple steady state model will calculate the heat provided by the collectors. A comparison will be made which LCOE is lower, ground-mounted or roof-mounted.

IWH

A method similar to the method proposed by Woolley et al. (2018) will estimate the potential of IWH after which a pinch analysis will be performed to estimate the excess heat of the industrial zone of Voorst. In case information of the companies cannot be redeemed, a guess will be made using literature data indicating the amount, time and temperature profile of IWH that is expected and in which phase of matter. When the amount is known, a calculation will be made which HEX and heat pump can be used, leading to the LCOE.

2.7.3. Coupling of supply and demand

Storage

For the short-term storage, a pressurized water tank will be used, which is approximated using standard thermic properties of water. Afterward, an optimal design and operation strategy will be obtained from the current literature.
For the long term storage, a central LT-ATES will be used for which a simplified model will be developed.

Distribution grid

The distribution grid will be constructed using either steel or polymer piping and designed as set by Kennisinstituut voor Installatietechniek (2012) after which standard calculations for the hydronic system will model the system.

2.7.4. Total model

All the models will be joined together resulting in the finished model. The alternative method determined in chapter 2 will be integrated into the main model, making use of the model of demand.

2.7.5. Optimal use of the available sources

Strategies will be developed to optimize the cost and come to the lowest LCOE and CO_2 emissions. The resulting different scenarios per distribution temperature will be compared. The optimal solutions for the latter will then be contrasted to the decentralized alternative. The results will lead to the answer to the main research question, which will also include a discussion.

3

Model of demand

3.1. Introduction

The DH network must be able to satisfy the heat of the consumers by providing the right amount of heat. Historically, heat demand prediction methods generate the quantity of heat necessary at a given time. With help of the heat demand, the quantity of heat supply over time can be provided by the heat sources. Here, the heat demand model will provide the input, the heat demand, indicating the amount of heating that is required at a given time.

Various models have already been analyzed in chapter 2, to obtain the best heat demand model for the neighbourhood of Westenholte. A bottom-up approach based on a model of a typical dwelling meets the criteria set in chapter 2. The bottom-up uses a model which calculates the heat demand for each typical dwelling of a category, using a partly deterministic model based on the heating degree-day method. For groups of dwelling similar in heat consumption an ideal dwelling is assumed, for which the heat demand is calculated. By summing, the heat demand of the individual dwellings will then provide the total heat demand.

Stretching the model of the heating demand somewhat further, the additional cost of equipment needed for the dwellings to be fit for a DH will also be included. The heat demand model will thus provide a total picture of the consumers of the DH network, including the demand and cost. These additional costs will include insulation and electrical boiler, which adds heat to the DHW to increase the temperature. When the distribution temperature used for the DH is set to 50/ 30 °C, insulation and an electrical boiler are required for all dwellings. The insulation is necessary, as the used distribution temperature would likely not be able to deliver enough heat. The mass flow could be too high to be economically feasible as this largely determines the price of DH (Mazhar et al., 2018). The electrical boiler is necessary as by law the water needs to be stored at 60 °C (Kennisinstituut voor Installatietechniek, 2012). To calculate the cost, and provide a consumer model, the typical model is used as input, making it logical that these costs are part of the demand model.

First, however, the method used for estimating the heating demand of a single dwelling must be formulated. Secondly, using the heating demand from each dwelling, establishing the total gross heating demand of the neighbourhood of Westenholte is covered. For the gross heat demand, the neighbourhood of Westenholte will be simulated as-is. Assuming no insulating measures or further adaptations to the dwellings. Third, the associated cost when a low distribution temperature is used for DH will be configured. Lastly, the different results are presented and evaluated on accuracy.

3.2. Method: Typical dwelling based model

The typical dwelling method is based on the idea that dwellings can be grouped on heat demand, as previously mentioned. The basis of most typical dwelling models consists of grouping dwellings on the geometry of the building, in combination with the year of construction. Combined, these form the outer shell, which is dominant in the heat exchange to the surroundings of the dwelling. Data generated for the outer shell are supplemented with other parameters, such as occupancy, affecting the total heat demand of the typical

dwelling. The total system is best described by the occupancy of the dwelling and weather, as has been previously stated in section 2.3. This is because the occupants have the final decision in the heat they desire and the weather determines how much heat is required to supply the occupants desire.

The occupancy factor, for example, is seen in the thermostat settings. Thermostat settings are set per dwelling, based on residence time and personal preference, but are also directly reflected in the DHW consumption. The required energy for SH is then dependent on heat gains and losses. Newton's law for cooling accounts for the different heat losses resulting from the demand, using the difference in temperature, the surface area, and the insulation factor. The temperature set by the occupants of the dwelling and the outdoor temperature is a direct input for the heat loss model, illustrating the significance the occupancies make.

Next to Newton's law of cooling, another physical phenomenon is described as influencing the heat flows of a dwelling: the solar heat gain. This has also been found by Van Miltenburg (2016) to play an important part in solar DH because solar panels will increase in heat production at the same time demand of the dwellings decreases as a result of solar radiance. Concluding, by grouping the dwellings based on their outer envelope, the heat demand can be described using the occupancy, solar gains and outside weather combined with Newton's law of cooling to describe the desired heat.

3.2.1. Typical dwelling model adaptation

To calculate the total heat demand of a typical dwelling, the heat demand is thus divided into two sections: SH and DHW demand. The SH demand is then further divided into heat losses according to Newton's law of cooling and solar heat gains. As the solar heating gains will reduce the total heat demand for space heating, these must be subtracted from the heat loss leading to heat SH demand. Equation 3.1 illustrates this subdivision.

$$\dot{Q}_{d,i,j} = \begin{cases} \dot{Q}_{hl,i,j} + \dot{Q}_{DHW,i} - \dot{Q}_{Solar,i,j} & \text{if } (\dot{Q}_{hl,i,j} - \dot{Q}_{Solar,i,j}) > 0 \\ \dot{Q}_{DHW,j} & \text{if } (\dot{Q}_{hl,i,j} - \dot{Q}_{Solar,i,j}) < 0 \end{cases} \tag{3.1}$$

The total heat demand], $\dot{Q}_{d,i,j}$ in kW, for hour [i], of the typical dwelling [j] consists of the heat losses to the surrounding, $\dot{Q}_{hl,i,j}$ per hour per typical dwelling [kW], the heat demand for DHW per hour [kWh/h] $\dot{Q}_{DHW,i}$ and $\dot{Q}_{Solar,i,j}$ are the solar gains per typical dwelling [kWh/h].

Equation 3.1 shows that the heat demand can be separated into three factors; heat loss, heating of DHW and solar gains. First solar gains will be estimated, after which the DHW demand and heat losses are estimated. The solar gains are determined based on the total solar irradiance of a flat surface $G_{i,j}$ in [kW/m^2] and the effective surface area per typical dwelling $A_{Win,j}$. As the window area per typical dwelling differs, this will provide different heat gains per dwelling. The total window area of the dwellings however does not equal the effective surface. The efficiency factor η_{win} represents the loss of a vertical window compared to a flat surface, for which the irradiation is known. η_{win} is set to 20 percent as it is estimated that only half of all solar irradiation will reach the window since it has a vertical position and only 80 percent of the light will be able to penetrate the window without being reflected. Equation 3.2 illustrates these findings.

$$\dot{Q}_{Solar,i,j} = G_{i,j} * A_{win,j} * \eta_{win} \tag{3.2}$$

The heat demand of $\dot{Q}_{hl,i,j}$ is based on the total heat needed per hour as found by Elshof (2016) and illustrated in figure 3.1. DHW is thought to be independent of outdoor weather and typical dwelling type. The amount of DHW in respect to the total yearly heat demand is 4.27 GJ for the average dwelling in Westenholte (Friedel et al., 2014). The total DHW heating demand is simulated according to equation 3.3, in which $\dot{Q}_{DHW,j}$ is the yearly total heat consumption per dwelling type for DHW and B_i is the behaviour profile of DHW per hour of the year. The behaviour profile is divided into weekdays and weekends, to represent the main difference in occupation, similar to the temperature profile.

$$\dot{Q}_{DHW,i,j} = \dot{Q}_{DHW,j} * B_i \tag{3.3}$$

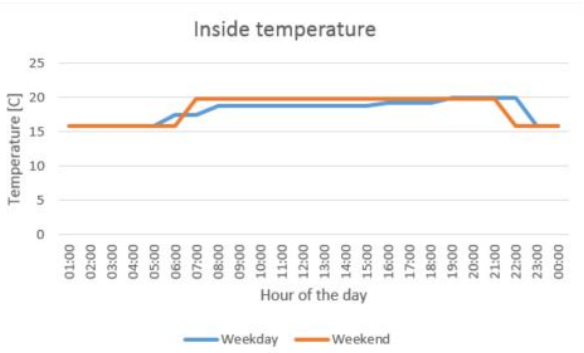

Figure 3.1: Set thermostat temperature (Bedir, 2017)

For the heat loss, Fouriers law for one-dimensional heat conduction will be used for an estimation on an hourly basis, as shown in equation 3.4. For this law, the hourly outside temperature ($T_{outside,i}$ [°C]) and inside hourly temperature ($T_{inside,i}$ [°C]) are used as input parameters to come to an hourly heat loss profile, dependent on the heat transfer coefficient (($U * A_t)_j$ in [W/K])] per typical dwelling.

$$\dot{Q} = (U * A) * (T_{inside,i} - T_{outside,i}) \tag{3.4}$$

Keeping in mind that heating is not at all time required, for example during summer, some additional requirements are set for this equation. A heat demand will only be generated if the outside air temperature drops below comfort level, which is 18 °C on average and is lower than the inside temperature. However, since internal gains are responsible for roughly 2 °C of heating (Kemna & Acedo, 2014), the outside temperature may drop to 16 °C before heating is required. Since the dwellings also have a thermal mass, a drop to 16 °C for merely a few hours does not require the central heating system to be activated. This effect is compensated by only generating a heat demand when the average over the past 24 hours is below 16 °C.

Boundary conditions

For the typical dwellings used, the total heat demand is equal to the total gas consumption. Since the average gas consumption per year is available for Westenholte, this can be used as a reference. For this year. Equations 3.5 and 3.6 set the boundary conditions for that year.

$$\Sigma_i Q_{d,i,j} = Gas_{d,j} * HHV_{gas} * \eta_{gas} \tag{3.5}$$

$$\Sigma_i Q_{DHW,i} = 4,27\ GJ \tag{3.6}$$

In equation 3.5 the total heat demand of a single dwelling must be equal to the heat consumption expressed in a cubic meter of gas $Gas_{d,j}$ [m^3] of that period, adjusted by the efficiency of gas combustion (η_{gas} = 94.2 percent (Energy Matters, 2014)). To initialize the values for Westenholte, the average gas consumption and combustion efficiency per dwelling of 2010 will be used as an exit point to calibrate the value of the insulation, using equation 3.4 and equations 3.2 and 3.3 as well as boundary condition 3.6.
The gas consumption of 2010 is used, as this year has the highest gas consumption in the past 15 years, leading to a slight overestimation of the heat demand. The total demand per dwelling is then subdivided into a constant DHW part of 21 percent in 3.6, as stated by (Segers et al., 2019) as an average for Dutch dwelling dependent on heat from natural gas. The rest of the heat demand is formed by the heat losses subtracted by the solar gains. The established amount of heat required by DHW for the reference year is used for all years the model will cover, making it independent of time.

3.2.2. Neighborhood model

So far, a method for constructing prototypes is based on the construction period and window area, which are considered dependent on the envelope. To get to a functioning method for heat demand, all the dwellings

have to be assigned to a particular typical dwelling. Agentschap NL (2011b) model of typical dwellings based on construction period and envelope for all dwellings in the Netherlands. Within a total of 30 typical dwellings, 7 types are based on dwelling envelope and approximately 4 on construction periods, this leads to many different types of typical dwellings. To simplify assigning dwellings of Westenholte to a typical dwelling, the average distribution of building envelopes used to form prototypes is only based on the construction period.

Based on the typical method using only the construction period, the number of dwellings per construction period needs to be estimated. To start, the neighborhood is divided into segments based on the year of construction, as illustrated in figure 3.3 leading to tables 3.1 and 3.2. Next, the surface area per time slot is multiplied by the dwelling density per surface area. At last, the total heat demand per segment is then calculated according to equation 3.7 for each construction period. Here, n is the total number of addresses per segment in Westenholte and $Q_{avg,seg}$ is the heat demand of the average dwelling for the specific segment dependent on the construction period, as illustrated in section 3.2.1. With the heat demand per segment, the total heat demand can be estimated.

$$Q_{seg} = n * Q_{avg,seg} \tag{3.7}$$

3.2.3. CAPEX and OPEX of dwellings

Depending on the distribution temperature of the DH, the dwellings should be insulated. For the low-temperature DH as set in the main research question, all the dwellings should be insulated. The cost of insulation is already calculated by the Agentschap NL (2011b). Another consequence of the low-temperature DH is the requirement of an electric boiler for the DHW. When the temperature of the DH is below 60 °C the temperature of the DHW must be upgraded to be used by law (Kennisinstituut voor Installatietechniek, 2012). The cost of an electric boiler is approximately €600,- excluding installation cost. When including €400,- installation cost, the total cost will approximately be €1000,- per dwelling, excluding project cost (Boilermarkt.nl, 2021). The OPEX of an electric boiler is calculated for an efficiency of 95 percent.

3.3. Data used

To use the developed model, various types of data are required. For each equation, the data used will be presented and evaluated. First, the data leading to the heat flows of the dwelling will be provided, after which the neighbourhood model data will be elaborated.
Starting with the major input for all heat flow; the weather conditions are from KNMI (2020) and are withdrawn for the location of Heino which is approximately 14 km away from Westenholte. The data provided are the temperature [°C] and total solar irradiance [kW/m^2].

Moving inside the dwelling, the occupant behaviour is subdivided into thermostat setting and DHW usage. The thermostat setting of an average dwelling is provided in figure 3.1. The DWH consumption is illustrated in figure 3.2 in percentage for a full day. The data for the typical dwelling used is set up by Agentschap NL (2011a) and let to table A.1 found in Appendix A. The distribution of the envelopes for the Netherlands is provided by Agentschap NL (2011a). Using both the typical dwellings and the distribution, the four building types based on the construction period can be constructed according to section 3.2.1.

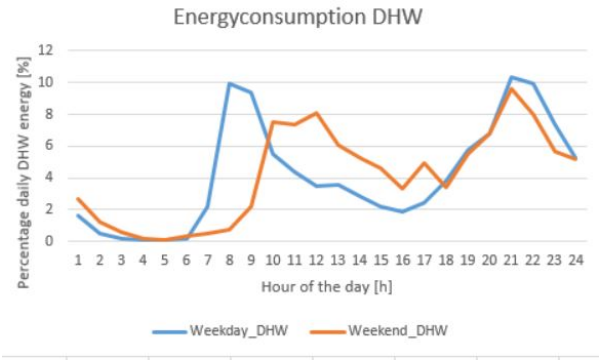

Figure 3.2: Percentage per hour of daily energy use of DHW (Ahmed et al., 2016)

Table 3.1 shows the gas demand and the improved gas usage for the four different typical dwellings found in Westenholte, accompanied by the cost of the upgraded insulation. Table 3.1 also illustrates the average heat parameters for a time slot according to Agentschap NL (2011a) upon 2005. Since the average gas consumption of the specific neighbourhood is corrected with the local average gas consumption per dwelling, as seen in equation 3.5, this should not make a large difference.

Table 3.1: Heat demand data for average dwelling in natural gas per construction period with associated window area, including the renovated heat demand with more insulation and the cost of insulation.

Construction period	<1964	~1970	~1980	>1992
Gas consumption [m^3]	2785	2177	1878	772
Gas consumption after renovation [m^3]	974	1069	1238	709
Improvement cost [€]	10404	9344	11233	1073
Window area [m^2]	24	27	27	15

Westenholte

In table 3.2 the number of dwellings is based on the dwelling density per surface area. With the number of dwellings, the construction period has been estimated based on figure 3.3.

Table 3.2: Construction period and number of dwellings per segment of Westenholte, as illustrated in figure 3.3

Segment	Part of the total surface	Construction period	Amount of dwellings
1	12%	>1992	260
2	11%	<1964	244
3	9.2%	>1992	204
4	2.9%	~1970	64
5	13%	~1970	295
6	23%	~1980	502
7	6.4%	~1980	142
8	9.1%	>1992	202
9	14%	~1980	300
Total	99,7 %		2215

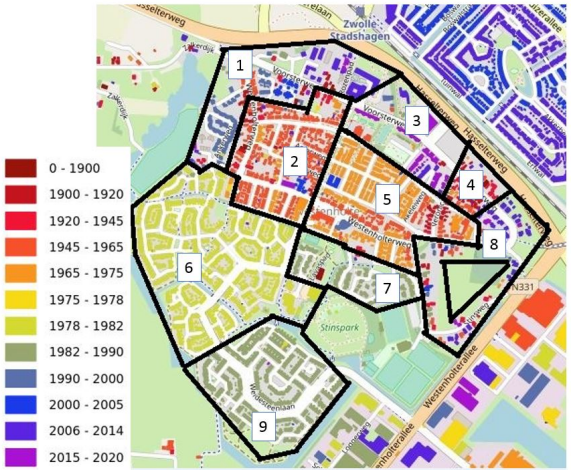

Figure 3.3: Segmented Westenholte based on year of construction (EDUgis, n.d.)

3.4. Final heat demand

Implementing all the equations and data, the following output was created: figure 3.5 delineates the heat demand profile for the typical dwelling based on the construction period, while figure 3.5 depicts the total heat demand of Westenholte. The graph illustrates the different profile dependency on temperature and light differences due to solar flux for each category of dwellings.

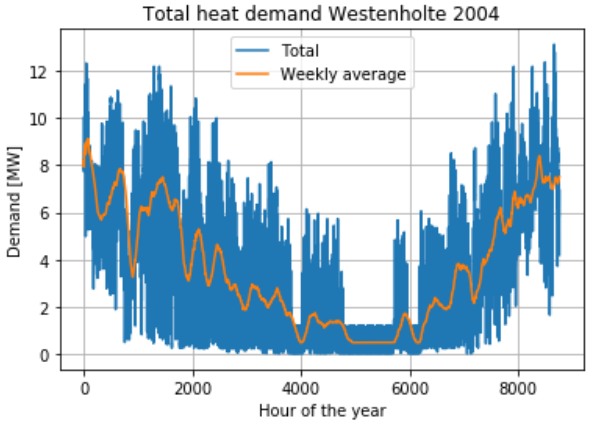

Figure 3.4: Calibrated heat demand graph of 2004 of Westenholte over hours of the year, depicting the total demand in blue and weekly average in orange.

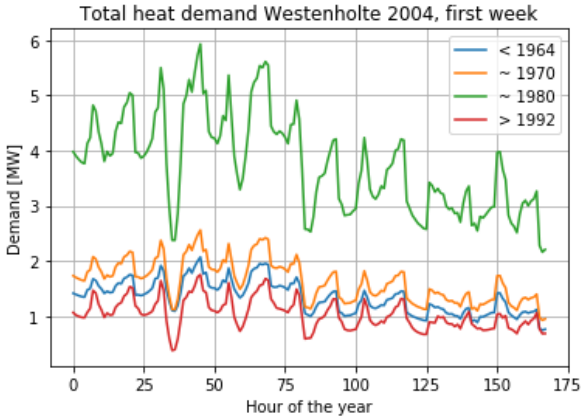

Figure 3.5: Total heat demand divided per dwelling for the first week (168 hours) in 2004 for Westenholte

Validation and calibration

To access the accuracy of the results, the total heat demand for Westenholte will be compared on the highest and lowest consumption per year over the last 10 years of an average dwelling. Additionally, the DHW consumption will be evaluated, as well as solar heating, based on the literature.

In 2010, the highest energy consumption and thus total heat demand can be found with, on average, 1900 m^3 of gas used per dwelling (CBS, 2020a). As the model is calibrated to 2010, the total error is only +3 percent or 56 m^3 of gas in comparison to the actual gas used. The year in which the least amount of gas is consumed is 2019, where the error was 19 percent too high, with on average 222 m^3 consumed more than the real-time data. To get a more accurate prediction, the average of the errors is subtracted from the average of 2010, levelling out the margin of error to -8 percent for 2010 and +8 percent for 2019. In the year 2019 the least amount of gas was consumed; 1200 m^3 on average. The model, however, predicted 1280 m^3 of gas, which is a difference of ± 6.7 percent.

4

Heat supply

4.1. Introduction

The renewable heat sources used for the DH of Westenholte are TESW, TEWW, and solar heat, accompanied by WH source IWH, as the preliminary heat sources. The cost of the heat sources, CO_2 emissions and their LCOE will be individually calculated to determine the total cost of the heat supply and their CO_2 emissions, in order to answer the main research question.
The main research question stipulated that this approach should include all the effects of the design parameters. This means that the distribution temperature of the DH should be able to vary and the fluctuations of heat supply over time must be captured. Differences in supply and return temperature directly influence the cost of the heat sources, as heat pumps are more efficient in use when the temperature difference between source and sink is smaller. The fluctuations on their part make for the requirement for storage to meet demand. Eventually, the goal is to optimize the model to provide the cheapest heat in terms of LCOE. Distributing the desired heat demand over the different sources allows an optimal balance between the costs of an individual heat source, the source temperature, and required heating profiles. Additionally, CO_2 emissions can also be a boundary condition to which optimization can take place.

To get to the cost and CO_2 emissions of all the heat sources together, they first need to be evaluated per heat source. To do so, first, the total demand provides an initial guess for the total supply needed. Second, the total supply per heat source will be determined by modeling the available heat per source and the maximum total capacity of each source. Third, the costs, LCOE and CO_2 emissions per source are calculated for when the heat demand is met by the heat supply. Finally, the results of the previous steps are validated with the data from the literature of real cases.

4.2. Total heat supply

To get the total heating supply required, the heating demand of all the consumers is used, as well as the expected heat losses of the DH system. Heat losses are predominantly encountered in the storage (Guelpa & Verda, 2019) and transport of heat (Mazhar et al., 2018). The heat losses should also be accounted for in the overall heat production.

In a multi-RES DH system, the heat demand is distributed over the different sources. In distributing the heat supply over the final sources, historically, a division is made between peak load and baseload. The peak supply is used only roughly 1,000 hours per year, as seen in figure 2.5, while the baseload is used throughout the year. This distinction is made, as it is economically more viable to use a peak load than increasing the existing capacity of the baseload in order to feed the DH. That is because the CAPEX per produced kWh would not be economically viable for a source that is only used for a very small portion of the year. For the DH network here, the baseload is filled by the previously defined RES and WH. The peak load should be filled with a different source that has a low start-up time and can run at any given hour of the year. Additionally, the CAPEX should be low to keep investment costs low while the OPEX might be somewhat higher, as its use is limited to a very small portion of the total heat. Often, a boiler is used for the peak load (Mazhar et al., 2018).

To simplify the already complex model, a boiler will also be used here for peak supply. The boiler which is to be used will cost approximately €50 000,- without installation cost based on the internal database of Witteveen+Bos. This amount will be compensated by later explained project risk cost, illustrated in equation 4.22 . The OPEX is €23,705 per GJ (Statline, n.d.), the raw price of natural gas divided by the burner efficiency of 95 percent.

The baseload will be filled with the RES and WH sources. The ratio of the sources to be used must now be determined based on the cost and availability of heat per source. Initially, the sources will be designed to a maximum of a quarter of the heat demand, which later will be adapted for optimization. For explanation purposes, the design of TESW and TEWW are modeled first, as these are simple heat sources. First, the maximum heat that will be obtainable for each source is determined, after which for both, simultaneously, a business case is developed. The method previously established for both heat sources involves a combination of an HEX, a pump, a heat pump, and piping to retrieve heat. These similarities indicate that it is beneficial to develop a method that estimates the cost for both of these heat sources simultaneously.

For solar thermal energy, the same approach as for TESW and TEWW will lead to the final cost and CO_2 emission. First, the total available heat is determined, after which a business case is built. To get to the available heat, as space equals heat for solar heat sources, the area in which the solar panels can be placed will be selected. The functioning of the solar panels is then simulated, after which a business case is built similarly to TESW and TEWW.
IWH, however, requires a more original method to obtain an accurate estimation of potential heat, since IWH is not weather-dependent. A new method is developed to estimate the heat potential, based on the gas usage of the postal code and public information of the local companies.

4.2.1. Validation of heat sources

To guarantee accuracy in the models used, all the heat sources will be validated against the current literature. The validations will be made in the two main properties of the sources, the heat profile and the associated LCOE. Two types of errors are defined; those of a single value and those of an entire profile/time series. The latter is called a continuous error, such as the available heat from solar light. For the continuous error, the Pearson correlation coefficient or R-value is used for the models, where applicable. The heat profile is hard to compare, as no reference is available for the given area, therefore only parts of the model will be validated, including the temperature profile of the heat source. The mean absolute percent average will be used for the static error based on reference data found in the literature and expresses the percentage difference from the reference value to the KPI of the source, for example for the LCOE.

4.3. Model of TESW and TEWW

4.3.1. Introduction

Summarizing from section 2.4, heat can be withdrawn from surface water and wastewater. A model reflecting the operation of obtaining the heat will be based on figure 2.6, where to obtain the heat, water is guided through an HEX extracting the heat. Heat pumps then upgrade the temperature of the available heat for use in the DH network. The amount of heat that is withdrawn, depends on the allowed temperature difference between the water and the output of the HEX and the amount of water present. The location, ergo which body of water is used and where, to gain water from should therefore optimize both parameters. For TESW, this means source positioning so that the mass flow and temperature are maximized. The effluent is found to be the best location as a heat source for TESW. Effluent is allowed to be cooled down the most in respect to influent and other wastewater sources, whilst still being a centralized source.

Thermal energy from surface water and wastewater presents great similarities. Firstly, both have a form of contaminated water as their heat source. Secondly, the temperature range of the sources both dependent on the weather with the air temperature as the main influence (Caissie, 2006). Thirdly, the temperature of dumping surface water after the regaining of heat cannot be lower than 12 °C, to comply with expected future regulation, according to IF and Stowa (2018). As a result of these similarities, the equipment used for both sources is relatively similar.

As previously stated, the temperature and volume flow available from the source water and the heat de-

mand of the DH will be leading in the TESW design. To start, a model of the available heat for both heat sources will be constructed. For the case of TESW, this will be done by first estimating the available volume of the available surface water; the IJssel. Next, the temperature of the IJssel will be approximated using a model based on linear regression, based on the air temperature. Combined, these will provide the available heat according to Newton's law of cooling.

To estimate the available heat of TEWW, first, the volume flow will be determined. The "dry-weather" effluent production will be used to estimate the total volume flow of effluent. After the volume is quantified, the temperature will be approximated with a linear regression model similar to TESW. Combined, these will lead to the total heat available for TEWW.

Finally, for both heat sources, the equipment will be designed by solving the energy balance and mass balances. The equipment will be designed in such a manner that the design process can be easily corrected for changes in the final heat output of the heat sources, as this is a design parameter. With the equipment and heat and mass flows, the final heat profile and cost can be approximated, including the CAPEX, OPEX, LCOE and relative CO_2 emission.

4.3.2. TESW heat model

Equation 4.16 determines the amount of heat available from TESW is determined by volume and temperature, as stated in section 2.4.1. The volume flow and temperature of the source water should be as high as possible at the location used. Two reasons exist to maximize the available volume and temperature of the surface water: Newton's law of cooling dictates that the volume is linearly correlated to the amount of heat, and regulations for dumping the water back into surface water depend on volume and temperature. Used water can only be fed back into nature if it influences the temperature of only 10 percent of the waterbody, while that body's mean temperature is 12°C or higher. This boundary condition is set in accordance with the regulation expected by IF and Stowa (2018). Only when meeting these regulations, heat can be withdrawn from the surface water. A larger body of water thus means a larger buffer and longer operation times. Additionally, a higher average temperature of the body of water enables more water to be extracted from the surface water, thus providing a longer time window.

For the volume flow, this means finding a river with the largest steady water supply. It is well known that for the Netherlands, the volume flow of surface water is seasonally dependent, where during the summer the least amount is available. As during the summer, available heat most likely has the lowest price, because of the increased efficiency of the heat pump, and is thus desired. This raises a first boundary condition on the location: during the summer, the volume flow of the water should be high enough so desired heat can be withdrawn from the surface water body. Simultaneously, the temperature of the water should be as high as possible as well. However, higher temperatures often indicate a large temperature swing of the seasons, meaning there will be less time to gain heat. Concluding, to maximize both the temperature and volume flow, a river with a large and steady volume flow is preferred, which simultaneously has a more steady temperature profile.

For Westenholte, the IJssel is picked as the most suitable of the surface waters nearby. The volume flow of the Ijssel is higher than the nearest surface water available: the Zwolle-IJssel channel making it the most suitable body of water. The volume flow of the Zwolle-IJssel channel is restricted by a channel lock and is not to be considered a steady flow. For this location, it has been found to have an average volume flow of 340 m^3/s and have a low flow of 140 m^3/s. The maximum capacity which can be withdrawn for the Ijssel is based on the second currently largest installed capacity of a TESW installation in the Netherlands (Kruit et al., 2018) and estimated to be 600 m^3/h or 0.16 m^3/s, Additionally, this amount of water as a heat source is not expected to significantly change the biosphere, which must be met by law, as only 10 percent of the lowest flow is available (IF & Stowa, 2018).

Temperature

The available heat is only affected by temperature in one way: the amount of hours during which the TESW can harvest thermal energy from the IJssel is limited by the temperature of the IJssel. Regulations must

be met when releasing the used water of the IJssel back into the IJssel. The exact guidelines, as set by IF and Stowa (2018), state that the temperature of the mixing area can be a maximum of 10 percent of the body of water, and the water must be 12 ° C after mixing. The temperature difference oftentimes is 3 to 6 K and depends on the waterbody's temperature. However, the source temperature influences the efficiency of the heat pump when upgrading the temperature of the surface water, as the COP fluctuates with temperature. As a result, the temperature of the IJssel has an inverse proportional relation to the associated energy required to upgrade the heat and thus influences the OPEX of the heat pump. The temperature of the IJssel is thus of great importance for assessing the maximum amount of heat available per year and the final OPEX.

Key influences on the temperate are considered: atmospheric conditions, topography, stream discharge, and the stream bedding, for which the atmospheric conditions have a dominant factor. A historical or deterministic model was recommended in the literature research executed in 2.4.1. This deterministic model should account for the variety of previously mentioned physical factors along the IJssel. The extra computational power required is most likely not justified for use in this model, as the temperature does not significantly vary during the day, making no significant impact on the total heat production. Additionally, the statistical models usually only use one point to determine the temperature, making this method superior. The most simple methods for predicting river temperature only use the outside air temperature using a linear relation, as illustrate in equation 4.1. In this equation $T_{river}(t)$ is the temperature of the river [°C], a_0 is the offset [°C], b the casual linear constant [-] and $T_{air}(t)$ the air temperature of that hour [°C].

$$T_{river}(t) = a_0 + b * T_{air}(t) \tag{4.1}$$

However, this method lacks accuracy when used with hourly data (Caissie, 2006). Even though the general trend of the air temperature is similar to that of the temperature of the IJssel, the deviation of that trend is high. A method to stabilize this variation of the air temperature is by taking the average over the week also known as the simple moving average (SMA), as illustrated in equation 4.2, in which N is the number of hours and p the time-dependent variable. This idea of taking the average temperature makes sense when realising that the thermal mass of the Ijssel is very large. Since a large thermal mass takes a long time to change temperature, the hourly fluctuations of the air temperature will have little effect in comparison to the weekly trend.

$$p_t = \frac{\Sigma_{i=t-N/2}^{t+N/2} p_i}{N} \tag{4.2}$$

Comparing the stabilized air temperature with the actual temperature of the IJssel shows a high correlation (Pearson coefficient of 0.96 for 7 years). Now, as a linear regression model seemed appropriate, a linear regression analysis is performed using the least squared method. a_0[° C] and b [-] are estimated in Python by using the module proposed by Virtanen et al. (2020) called the optimize.curve_fit function. The relationship found is shown in equation 4.3, with a covariance of -0.5*10^{-5} for the SMA of the air temperature of N = 168 hours (1 week).

$$T_{IJssel} = 1.06 + 1.61 * SMA(T_{air}, N = 168) \tag{4.3}$$

Concluding, the IJssel will serve as the volume of water. The heat can then be determined by the volume and temperature. The volume of the IJssel will greatly exceed the required water volume, posing no limiting factor, which therefore does not have to be modeled. The temperature will be limiting in terms of regulation and is modeled by a linear model based on air temperature.

4.3.3. TEWW heat model

The heating capacity of the effluent of the sewage treatment found in Zwolle comes from the amount of effluent (volume) and the temperature. The waste water found at the sewage treatment is separated into man made waste water, including industrial and domestic wastewater, and natural 'waste water' resulting from precipitation. All these streams are released into a "bucket", which consists of the area covered by the sewage treatment. The outlet of the bucket is the effluent which is comparable to a hole in the bottom of the bucket.

Next is the temperature. The temperature of the effluent is important for the same reasons as for TESW: when the already used effluent is released into the IJssel, it must meet the same temperature restrictions that

apply for TESW. In short, the temperature of the Ijssel is not allowed to go below 12 °C because of the used effluent, as described in the previous section. The estimate the effluent temperature, a relationship found between air temperature, the capacity of the sewage treatment and the effluent temperature found by Tessel and Pijl (2006) is used. Using both the temperature and the volume flow of the effluent, the total available heat can be modelled.

Volume flow: Effluent production

Different models for simulating effluent production have been proposed in section 2.4.2. A bucket model was found to be a simple model to estimate the amount of effluent. However, this model will not be needed because of the large and steady quantity of effluent available. As the sewage treatment plants are designed to always maintain a steady 'dry-weather' flow, it appears to be most beneficial to use part of this flow as heat source. For Westenholte, the dry-weather effluent volume flow is equal to 0.66 m^3/s (van Haarst, 2021). This would be enough to fill the estimated total heat demand yearly if only run for 2000 hours (assuming a temperature drop of 6 °C). As the amount of dry-weather effluent far exceeds the demand, modelling of the effluent becomes redundant. As the amount of effluent holds no limit, the actual amount which the DH will use is left as a design parameter; the amount of heat which is required of TEWW will determine the amount of effluent used.

Effluent temperature model

The model of the temperature of the effluent is based on the monthly average air temperature and biological capacity as determined by Tessel and Pijl (2006). The effluent temperature has a strong linear correlation with the average monthly air temperature. Tessel and Pijl (2006) evaluated this relationship for over 48 sewage treatments plants in the Netherlands based on monthly average temperatures and found promising forecasting models. Based on the biological capacity of the ST, the parameters of this linear correlation are found, resulting in equations 4.4 and 4.5. For the sewage treatment in Zwolle, their method leads to equation 4.6 when applied to 4.1, but for effluent instead of the temperature of the Ijssel using the biological capacity of C_{bio}=180,000 (Vereniging Nederlandse Watersector, 2021) [g/day] for the sewage treatment in Zwolle and weekly SMA of the air temperature (N = 168 hour).

$$a_0 = 0.97 * \ln(C_{bio}) - 3.3057 = 8.43 \tag{4.4}$$

$$b = 1.345 - 0.0576 * \ln(C_{bio}) = 0.65 \tag{4.5}$$

$$T_{effl} = 8.43 + 0.65 * SMA(T_{air}, N = 168) \tag{4.6}$$

Where $SMA(T_{air}, N = 168)$ is the monthly average temperature [°C] and T_{effl} is the temperature of the effluent. So far this is exactly similar to the method used by Tessel and Pijl (2006). However, contrary to Tessel and Pijl (2006), there will be a change to the inlet air temperature. The SMA temperature of a month is used instead of the hourly air temperature. The SMA is the average of a time period as explained in equation 4.2. This will lead to a more dynamical temperature prediction curve, whilst still meeting the boundary conditions of their method.

In summary, the dry-weather volume flow of the sewage treatment of Zwolle serves as the volume flow of effluent from which thermal energy can be gained. This does require the mixed used and therefore cooled down effluent in the IJssel river to remain above 12 °C in the mixing zone, which is 10 percent of the river volume flow. Determining the window in which heat can be retrieved thus involves the temperature of the effluent. Linear regression analysis with the average weekly air temperature as input used, and the effluent temperature as the output will determine the maximum time the facility will be able to produce.

4.3.4. Equipment

TESW and TEWW use almost identical equipment: piping, pumps, an HEX, and a heat pump. For TESW, it will exchange its heat with the help of an HEX to another intermediate fluid before water will be retrieved from the IJssel through pipes. This intermediate fluid will then go to a heat pump, where the heat will be

upgraded to the temperature suitable to the DH. This process is illustrated in figure 2.6. For TEWW, the HEX will be placed in a bypass of the effluent pipe leading to the IJssel. The secondary fluid or intermediate fluid will then flow through the heat pump, which on its turn releases its heat to the DH.

Using the energy and mass balances, the sizing of the equipment can be determined. To determine the mass flows of the entire system, first, the energy balance needs to be set up. Equation 4.7 states that the amount of heat that the DH requires to fulfil its average heat demand, $\overline{Q}_{DH}$, is filled by Q_s, the amount of heat of the source and the power consumed by the heat pump, $\overline{W}_{HP}$. The energy required by the heat pump can be calculated using the SCOP, as is illustrated in equation 4.8. The required heat from the source can also be calculated using the SCOP, as shown in 4.9. The SCOP is defined as the average COP of the heat over the running hours. The COP of a heat pump is highly dependent on the temperature and can be approximated, as illustrated in equation 4.10, according to the Carnot cycle. Commonly, the efficiency of a heat pump (η_{HP}) is set to 40 percent of the Carnot efficiency (the first part of the equation) Staub et al. (2018).

$$\overline{Q}_{DH} = \overline{Q}_s + \overline{W}_{HP} \tag{4.7}$$

$$\overline{W}_{HP} = \frac{\overline{Q}_{DH}}{SCOP} \tag{4.8}$$

$$\overline{Q}_s = \overline{Q}_{DH} * (1 - \frac{1}{SCOP}) \tag{4.9}$$

$$COP = \frac{\overline{T}_{hot} + 273.15}{\overline{T}_{hot} - \overline{T}_{cold}} * \eta_{HP} \tag{4.10}$$

With the energy balance, the mass balance can be satisfied resulting in the demands of the equipment. The mass flow can be determined from the heat available from the IJssel $\dot{Q}_s$, the average temperature difference $\Delta\overline{T}$ and the specific heat c_p. As previously stated in the literature review above, historically the temperature difference for TESW is between 3 and 6 K, for this study the temperature differences are set to 6 K.

$$\overline{\dot{m}}_s = \frac{\dot{Q}_s}{c_p * \Delta\overline{T}_s} \tag{4.11}$$

With the mass flow, the piping, HEX, pump, and heat pump can now be designed after which the cost can be calculated. The cost of the equipment will be divided into CAPEX and OPEX. The CAPEX will be determined on key figures to estimate costs such as price per length for the piping. The OPEX will be subdivided into maintenance cost and electricity cost, of which the latter depends on two components; the HP and the pump. Equation 4.8 states that the electricity is dependent on two components, the HP and the pump. The electricity consumption of the heat pump is determined by the efficiency illustrated in the COP. To determine the pumping cost, the pressure-drop of each component has to be calculated. In the following, the key figures for the equipment will be set up and the pressure-drop will be calculated to determine the total cost.

Piping

The length of the piping required will vary depending on the location. For the example of Westenholte, the equipment will be placed on the property of the sewage treatment Zwolle, leading to a total piping requirement for TESW of 100 m and TEWW of 10 m, based on its position from the IJssel. The diameter of the piping is determined by the total estimated heat duty and the difference in inlet and outlet temperature and the maximum velocity allowed per pipe, as described in equation 4.12. Kennisinstituut voor Installatietechniek (2012) and table 4.1 show that for the different diameter of piping different maximum velocities are allowed. Assumed is that the installation in this set up will run full power from the moment it is turned on. The material used will be typical HDPE as this is flexible, strong and chemically inert (Spitler & Mitchell, 2016).

$$D = 2 * \sqrt{\frac{max(\dot{Q}_s)}{v_{max} * \rho_w * c_{p,w} * \Delta T * \pi}} \tag{4.12}$$

The OPEX of the piping is determined by the maintenance cost and predominantly from the pressure loss, it creates. Heat loss is ignored in the potential OPEX cost as the water temperature is only slightly warmer than the surrounding air temperature. The pressure drop, Δp [Pa], on the other hand, is significant and can be calculated with f_d, the Fanning friction factor, v_w the velocity of water, L_p the length of the piping and the diameter of the piping using the Darcy-Weisbach equation, illustrated in equation 4.13. Using the dimension of the piping, the velocity can also be calculated through equation 4.12, replacing the maximum of $\dot{Q}_{source}$ with $\dot{Q}_{source}$. The Swamee-Jain equation is used to calculate the friction factor, as illustrated in 4.14 in which Re is the Reynolds number [-] and ϵ is the roughness factor of the piping[m]. In this case, ϵ=0.0015 mm as HPDE falls under smooth polymer piping and is lower than that of steel (0.045 mm).

$$\frac{\Delta p}{L_p} = f_d * \frac{L * \rho_w * v_w^2}{2 * D} \tag{4.13}$$

$$f_d = \frac{0.25}{(log_{10}(\frac{\epsilon/D}{3.7} + \frac{5.74}{Re^{0.9}}))^2} \tag{4.14}$$

The CAPEX of the piping is estimated with the help of pricing from CE Delft (2019) in equation 4.15, based on the minimum and maximum cost. The minimum cost reflects material and installation cost for easily accessible ground such as grassland, where the maximum cost involves asphalt. For Westenholte an average of 0.3 is chosen as it consists mainly of asphalt. Using the insulation of the piping the heat losses of the piping can be calculated according to equation 3.4 for an outside reference temperature of 10 °C. For TESW and TEWW however, the heat losses from piping from source to heat pump will be neglected, as previously mentioned.

$$CAPEX_{pipe} = \alpha_{pipe} * CAPEX_{pipe,min} + (1 - \alpha_{pipe}) * CAPEX_{pipe,max}. \tag{4.15}$$

Table 4.1: Piping cost for polymer and steel piping. The heat loss, U_C, is provided in W per length of piping in meter per Kelvin.

	Steel values from ISSO 7		Polymer values (Thermaflex, n.d.)		Pricing CE Delft (2019)	
DN	U_C [W/(m*K)]	max(v) [m/s]	U_C [W/(m*K)]	max(v) [m/s]	Min [€/m]	Max [€/m]
25	0.165	0.4	0.1198	1.10	€ 430	€ 820
32	0.160	0.5	0.146	1.20	€ 450	€ 830
40	0.194	0.6	0.1679	1.20	€ 470	€ 850
50	0.215	0.7	0.1869	1.40	€ 490	€ 870
65	0.253	0.8	0.2189	1.40	€ 520	€ 900
80	0.261	0.9	0.2257	1.60	€ 560	€ 940
100	0.276	1	0.2329	1.60	€ 610	€ 1,000
125	0.318	1.2	0.2681	1.80	€ 690	€ 1,090
150	0.375	1.3	0.3145	2.10	€ 760	€ 1,180
200	0.401	1.5	0.3413	2.40	€ 910	€ 1,380
250	0.357	1.7	0.357	2.70	€ 1,080	€ 1,620
300	0.456	1.9	0.456	3.00	€ 1,260	€ 1,890
500	0.7	2.7	0.7	4.80	€ 2,120	€ 3,290
600	0.9	3.2	0.9	5.40	€ 2.640	€ 4.230
800	1.6	3.7	1.6	6.00	€ 3.610	€ 6.080

The OPEX of piping used is represented by the pressure loss of the piping. For a high-pressure loss, the pump will require more power, increasing OPEX.

Plate HEX

The HEX for instalment is a countercurrent plate HEX (P-HEX). These can have a very small temperature difference between incoming and outgoing flow, are typically better at conducting heat (6000-7500 [W/(m^2*K)] vs <2500 [W/(m^2*K)]) (White, 1979) and the surface area ratio to volume is higher than other HEX. For designing the P-HEX, the log mean temperature difference (LMTD) method will be used. The temperature difference between the in and outgoing flow is very low compared to other types of HEX and can be

lowered to 1 K. For TESW and TEWW, the temperature difference will be set to 2 K, to minimize the temperature difference between the temperature at the source side and the temperature at the DH side. SS316 is the most common material used for P-HEX in TESW and TEWW installations (IF & Stowa, 2018).

Normally, an HEX is designed based on the heat they are intended to transfer and the overall heat transfer coefficient, resulting in a total surface area, as seen in equation 4.16. This total surface area also forms the base for calculating the CAPEX of a P-HEX. On the other hand, the OPEX is predominantly based on the pressure loss the HEX causes.

$$\dot{Q}_{HEX} = U_{HEX} * A_{HEX} * LMTD \tag{4.16}$$

$$LMTD = \frac{\Delta T_{hot} - \Delta T_{cold}}{ln(\frac{\Delta T_{hot}}{\Delta T_{cold}})} \tag{4.17}$$

As illustrated in equation 4.16, the surface area of the plate heat exchanger is based on the LMTD method since a countercurrent P-HEX is used. The LMTD is defined as in equation 4.17 in which ΔT_h is the temperature difference on the hot side and ΔT_c is the temperature difference on the cold side. The CAPEX is defined in 4.18, which is based on data from Jarić et al. (2015) for an SS316 P-HEX.

$$CAPEX_{HEX} = 262 * A_{HEX}^{0.639} \tag{4.18}$$

As with the piping, the OPEX is expressed in a pressure loss of the HEX. A higher pressure drop of an HEX is directly proportional to the pumping cost. The pressure loss is considered constant at 0.7 bar following Kennisinstituut voor Installatietechniek (2012) and scaled to velocity squared, where for the maximum velocity the pressure drop will be 0.7 bar.

Pump

There are two pumps on the side of the heat source TESW and TEWW; the first is used to pump source material and the second is used to pump between the HEX and the heat pump. Single-suction centrifugal pumps as classified by the DACE pricelist(Freriks, 2011). Equation 4.19 is used to estimate the CAPEX of the pumps, in which $\dot{V}$ is the volumetric capacity [m^3/s] and H_{head} the head [m].

$$CAPEX_{pump} = (-13.4 + 119 * \dot{V} + 119) * (1717–16.8 * H_{head}) + 27302 \tag{4.19}$$

The OPEX is calculated by determining the electricity cost, according to 4.20 (Knepper, 2019), which then is multiplied by the cost of electricity. The pressure drop includes the pressure drop of all the previously mentioned components. The estimated efficiency of the pump is 0.8.

$$\dot{W}_{pump} = \frac{\dot{V} * \Delta p}{\eta_{pump}} \tag{4.20}$$

Heat pump

A large-scale heat pump with ammonia as the refrigerant is used for upgrading heat, similar to the majority of heat pumps in Europe (Pieper et al., 2018). The cost for other equipment can be divided into CAPEX and OPEX. The OPEX of a large-scale heat pump is largely determined by the electricity it requires to upgrade the heat. The CAPEX of the heat pump has been divided by Pieper et al. (2018) into cost for construction, electricity-related investment, consulting and heat source investment. Pieper et al. (2018) compared the CAPEX of heat pumps in Europe based on the heat source, installed thermal capacity and inlet and outlet temperatures of both the heat source and sink. Based on these data the sewage heat pump CAPEX estimate is used to assess all heat pump investment cost since these costs are most representative for the uses of heat source in this case. The CAPEX is then calculated in millions of euro based on the thermal capacity $max(\dot{Q}_{HP})$ of the heat pump in kW, illustrated in equation 4.21.

$$CAPEX_{HP} = (0.6396 * max(\dot{Q}_{HP}) * 10^{-3} + 0.50543) * 10^{6} \tag{4.21}$$

The OPEX of the heat pump is calculated for the COP per hour instead of the SCOP, as described in equation 4.8. The amount of electricity necessary is multiplied by the price of electricity to get the total cost. The

expected average COP is 4.4. In this case, a Carnot efficiency factor of 40 percent will be used to get similar results to a COP of 4.4 as found by Staub et al. (2018).

Total cost

The total cost will be higher than the cost of the individual equipment summed. The investment cost for example will consist of more than just the cost of the material, as other factors such as risk and project cost must also be taken into account. The total cost will be approximated by dividing the CAPEX into continuative sub-department costs for equipment, building, engineering, and consulting, and extra additional cost (which do not fit in the building and engineering cost). Moreover, some costs cannot be anticipated and are covered in unforeseen. These costs are often represented as a factor of the total initial material cost, as illustrated in4.22.

$$CAPEX = (\Sigma CAPEX_i) * \eta_{CAPEX} \tag{4.22}$$

For which η_{CAPEX} equals the product of $\eta_{secondary}$ = 1.21, η_{extra} = 1.05 and $\eta_{unforeseen}$ = 1.3, leading to η_{CAPEX} = 1.65. For the OPEX, maintenance cost is expected to be around 3 percent of the CAPEX per year (Mazhar et al., 2018).

4.3.5. Validation of TESW and TEWW temperature profile

The temperature model set up for the IJssel uses measurement provided by the KNMI for the IJssel temperature of 2019 for Eefde Beneden and weather data of the Hupsel. The Hupsel is one of the main supplying rivers of the IJssel and the Berkel and is located 30 km upstream of the IJssel (KNMI, 2020). These datasets have a limited range with a maximum of 1996-2020, requiring an estimation for the temperature.

The error of the predicted values and the actual values is based on the data of the water temperature, calculated by the model for Hupsel and the actual water temperature. The error is presented in figure 4.1 and the form of covariance, Pearson coefficient and the mean absolute percentage error:

- Pearson coefficient= 0.9836
- Mean absolute percentage error= 1.022 %

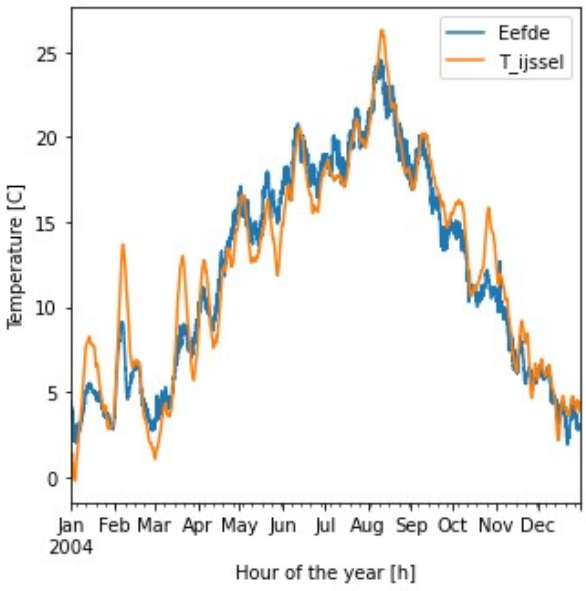

Figure 4.1: Calculated temperature of the Ijssel (T_{IJssel}) and measured temperature of the Ijssel at Eefde (Eefde).

4.4. Model of solar thermal energy

4.4.1. Introduction

Solar thermal energy can be harvested in the Netherlands, which might be unexpected as the Netherlands is not known for its high solar intensity compared to locations closer to the equator. Solar radiation is converted to thermal energy using FPC. As the thermal energy production is highly seasonal, abundant heat will get stored in the ATES. Additionally, thermal energy is of such high levels of temperature that it can be directly used for DH, making DH less dependent on electricity production. Limitations of solar thermal energy include the large space it requires and the low efficiency compared to the total radiation of the sun. As to solve the first major limitation, space requirement, the panels can be ground- or roof-mounted to maximize the harvest grounds. However, ground-mounted solar systems are predominantly cheaper in comparison to roof-mounted systems. Therefore, the space available remains a limiting factor. The second major limitation, low efficiency, is caused by heat losses from the FPC to the surroundings. Lowering the distribution temperatures of the DH network can increase efficiency, limiting heat losses to the surrounding by decreasing the temperature difference between FPC and outside temperature.

For Westenholte, first, the ground-mounted solution will be researched. The system used for collecting solar thermal energy is FPC placed in series to form rows. The rows are in parallel connected to a central HEX, which delivers energy to the DH network. The length and number of the rows depend on the allowed maximum velocity of the heat transferring medium inside the FPC, the pressure drop, and the intensity of the solar radiation. To determine the amount of heat that is available from the sun and the associated costs and CO_2 emissions, the entire setup of the FPC system is explained, to start with a clear understanding of designer demands. Next, the energy and mass balances are solved, which enables a preliminary design of the system. At last, the components involved will be designed individually and the associated costs determined.

4.4.2. Solar thermal harvesting system

To fully comprehend the solar thermal system, the system will be explained from the bottom up; from the ground used to the eventual heat supply and associated cost. The first essential requirement for a solar thermal system is available space where the sunshine can be collected and the FPCs can be placed. The FPC is a type of HEX in which solar irradiation is transmitted to small tubes inside the FPC. Multiple FPCs are then placed in an array to minimize piping between them. As the maximum volumetric flow limits the length of an array, multiple arrays are used to maximize the surface area where the sun can be collected. Next, all transferred heat is directed to a single HEX which transmits the heat to the DH through the FPC's heat transfer medium. Note that a heat pump is not necessary for the STE system, as the heat transferring medium of the FPC is already sufficiently high.

Figure 4.2 illustrates the feasible ground for the installation of FPC in Westenholte, in which the yellow striped areas are the potential areas for ground-mounted FPC and green shaded areas for roof-mounted FPC. The areas are following the destination plan of the township of Zwolle. Initially, only ground-mounted solar panels will be used, as these are cheaper (Mora et al., 2018).). In case the ground-based FPC proof to be unable to provide sufficient heat, the roof-mounted FPC will be looked into.

4.4.3. Physics of solar thermal collectors

With the area for the FPC located, the system of harvesting solar energy can be designed, eventually leading to determination of the costs. To design the total solar thermal energy harvesting system, the first step is to solve the energy balance. Second, the mass balance will be stated with the associated boundary conditions. Finally, elaborating on the solving method will lead to the next section, in which the cost will be calculated based on the heat and mass balances.

$$\dot{Q}_d = A_{FPC} * G * \eta_{FPC} \tag{4.23}$$

Equation 4.23 shows the energy balance in which Q_d is matched by supply, which depends on three main variables, harvesting area A_{FPC}, irradiance G and η_{FPC}. The FPC efficiency has been previously described in equation 2.6. This efficiency illustrates the effect of heat loss by using the average temperature of the FPC T_m and the outside temperature T_a to calculate the heat loss. When filling in equation 4.23 for the heat

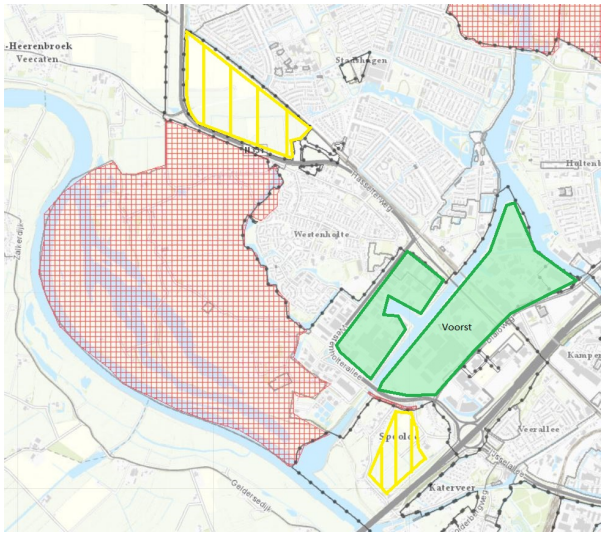

Figure 4.2: Selected areas for use of FPC, based on destination plans by the township of Zwolle. The yellow striped areas are for ground-mounted FPC and the green shaded areas for roof-mounted FPC.

requirement for the DH network will lead to the mass balance, as illustrated by equation 4.24, which solves for the mass flow ($\dot{m}_{array}$).

$$N_{panels,array} = \frac{\Delta T_{DH} * c_p * \dot{m}_{array}}{\eta_{FPC} * G * A_{FPC}} \tag{4.24}$$

The mass flow per array, $\dot{m}_{array}$, is bound by the minimum and maximum flow allowed inside the FPC. For example: $0.4 < \frac{\dot{m}_{FPC}}{\rho_W} < 5$ [m^3/h] for the SolarBoost FPC ACRON SUNMARK (2020). An optimal volume flow should be found based on these boundary conditions and the space available. The dimensioned system will provide steady heat throughout the year but will have a high LCOE, as the energy won is low and it will have a risk of overheating.

To determine the amount of total FPC which can be placed, equation 4.25 will be used, in which N_{panels} refers to the number of panels that can be placed, A_{total} the total amount of area which can be used and A_{FPC} the total area per FPC. It is then further estimated that the total amount of land area used per FPC is equal to 1.5 times A_{FPC}.

$$N_{panels} = \frac{A_{total}}{A_{FPC} * 1.5} \tag{4.25}$$

To estimate the pressure drop, the governing equations for piping will be used. The length of the different piping system will be estimated in the following equations to meet the centralized HEX for all the rows present:

$$L_{field} = L_{FPC} * (N_{panels,array} + 2) \tag{4.26}$$

$$w_{field} = w_{FPC} * (N_{arrays} + 2) \tag{4.27}$$

$$L_{piping} = L_{field} + w_{field} \tag{4.28}$$

In which L_{FPC} is the length of an array, w$_{FPC}$ is the width of an array and L_{piping} the total amount of piping to be used, as illustrated in figure 4.3. The associated pressure drop and cost can be determined through the dimensioned piping.

The pressure drop of the individual FPC is calculated based on the data of the manufacturer or using the Darcy-Weisbach equation (4.13) for the major losses. The minor losses are based on the idea that each solar panel will have several small sets of tubing connected to two main distribution pipes in a U-shape. A K value of 0.5 is considered for the minor losses in each duct, ranging from larger to smaller tubing. For, example, the

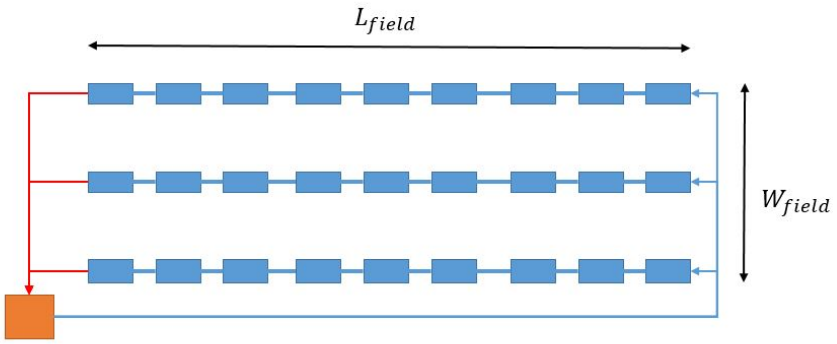

Figure 4.3: Schematic overview of FPC solar thermal installation. Blue boxes are FPC, lines are piping and orange box is central point transferring heat to DH.

FPC SolarBoost 35/10 (ACRON SUNMARK, 2020) has 18 tubes in parallel, with a length of 5.8 m and diameter of 10 mm, and two distribution tubes of 35 mm in diameter. The major pressure losses consist of resistance of the 5.8 m tubings, while the minor losses consist of individual drops for the entrance and a pressure drop for the exit. The total pressure drop will then be the major and minor pressure drops combined, as found in Bava and Furbo (2015) and demonstrated in equation 4.29.

$$\Delta p = \Delta p_{major} + \Delta p_{minor} = \frac{\rho * v^2}{2}(\frac{f * L}{D} + \Sigma K) \tag{4.29}$$

4.4.4. Equipment

With the heat and mass balances satisfied, including the pressure drops over different parts of the system the equipment can be designed.

FPC

The solar panel to be used is the SolarBoost 35/10 for initial estimation. This solar panel is often found in large solar DH systems. The key figures are divided into geometry, efficiency and cost. Concerning the geometry, the panel has an active surface area of 12.51 m^2. It consists of a U-shape arrangement in which smaller tubing is fed in parallel to two distribution pipes. Each of the smaller tubes is 5.8 m long, has a diameter of 10 mm, and is made out of copper. Equation 2.6 determined the efficiency, for which $\eta_0 = 0.838$,$a_1 = 2.46$ and $a_2 = 0.0197$. The CAPEX of the panels is estimated at € 235 /m^2 of the FPC's active area (ACRON SUNMARK, 2020). The maintenance cost of the panels is estimated at 2 percent of the CAPEX instead of the 3 percent of the other heat sources (Atia et al., 2012).

Piping, pumps and HEX

The equations for estimating the price in section 4.3.4 will lead to the CAPEX, OPEX, LCOE and CO_2 emission of the piping, pumps and required HEX. The length of the piping is determined in equation 4.28. The material of the piping will be the same as that used for the DH network. The design and price of the HEX and pumps will be decided according to section 4.3.4, more specifically equations 4.18, 4.19, and 4.20.

Validation of the solar thermal energy model will be based on comparing the LCOE with the literature. This is because the methods used for calculating the heat profile are already widely accepted.

4.5. Model of IWH

4.5.1. Introduction

IWH is thought to be the cheapest heat source available out of the selected heat sources for Westenholte. The SDE++ has estimated that the LCOE of IWH is about € 0.02 /kWh without heatpump and € 0.03 /kWh

with heatpump (Church, 2016). The cost of IWH is small because it is a highly concentrated heat source and temperatures are on average greater than those of natural resources. However, retrieving IWH requires collaboration between the industrial parties and the DH provider. This collaboration has been seen as one bottleneck of IWH, as the industrial parties are not able or not willing to guarantee heat. Two other bottlenecks of IWH are the distance to the heat consumer, increasing the transportation cost, and the idea that supply might be lowered in the future, as companies are required to become more efficient. Additionally, the potential heat available varies greatly per industry and factory, requiring a unique approach per case.

To estimate the IWH potential and bottlenecks for Westenholte, the industrial area of Voorst will be further researched on potential WH. A method similar to the method proposed by Woolley et al. (2018), as explained in section 2.4.4, will be used to estimate the potential IWH for Westenholte. Using literature data and information on the companies present, the heat source is deduced to obtain the amount and expected temperature profile over time of IWH and the phase of matter, air or water. When that amount is known, the calculation will be made on the equipment used, leading to the cost, LCOE, and CO_2 emission.

4.5.2. Methodology of estimating available IWH

To estimate the total available IWH, a further look was given to the industrial area Voorst. Since Voorst is labelled as category four of industrial sites of the Netherlands (IBIS, n.d.), it implies that only a minority of companies fall in the heavy industry label. Looking further into the natural gas usage per postal code from CBS (2014), it shows that not all area codes have excessive heat usage. As not all companies will be used as IWH sources, first, a selection of companies will be made based on the estimated amount of heat consumed per year, after which companies that show waste heat potential are further researched on the quality and quantity of their heat.

In addition to natural gas consumption, CO_2 emissions and visual inspection of air photos serve as methods to identify potential IWH sources. The CO_2 emissions data rapport offered by Rijksoverheid (n.d.) indicates that there are two companies with a significant CO_2 emission: Abbott and ForFarmers. The visual inspection confirms that the companies emitting a relatively large amount of CO_2 also have large cooling systems placed on their roof. Another finding of the visual inspection is that two other companies have cooling equipment installed: Sensus and Agrifirm. Combining the natural gas consumption data, CO_2 emissions an inspection of air photos of Google Maps it became clear that four companies will be of interest for harvesting IWH: Abbott, Agrifirm, Forfarmers and Sensus.

To get to the actual waste heat per company, the total heat demand was estimated based on the natural gas usage, after which historical literature data were used to predict the part of the heat consumption that would eventually become WH. The natural gas consumption is estimated based on the natural gas consumption per postal code by comparing data from CBS (2014). With those data, the total amount of gas usage per company can be estimated for 2014, as illustrated in figures 4.4 and 4.5. Figure 4.4 illustrates the natural gas consumption in the whole of Voorst divided into 2 sections, where figure 4.5 shows the natural gas consumption of different zones of the 6 postal codes. Through deduction, the natural gas usage can be appraised for the selected companies, as seen in columns one and two of 4.2.

.

Table 4.2: Food companies identified with emission data and visually through Google Maps, the method for calculating the gas (using gas per postal code and WH percentages), and the expected temperature.

Companies	Method for estimating natural gas consumption, see figures 4.5 & 4.4	Estimated natural gas consumption [m^3]	Estimated WH [%]	Estimated IWH [m^3 of gas]	Temperature [°C]
Abbott	(East Voorst - 6)/2- heating compensation	6.29E+06	6%	3.77E+05	100-200
Agrifirm	West Voors-sum(1:5)	1.76E+06	60%	1.06E+06	50
ForFarmers	5	2.15E+05	60%	1.29E+05	50
Sensus	(East Voorst - 6)/2- heating compensation	6.29E+06	6%	3.77E+05	100-200
Total		1.45E+07		1.94E+06	

4.5.3. Heat profile

However, the amount of waste heat present does not necessarily mean the WH is useful. The quality of the IWH plays a key role in the associated cost of the IWH source. Starting by estimating the available heat, the

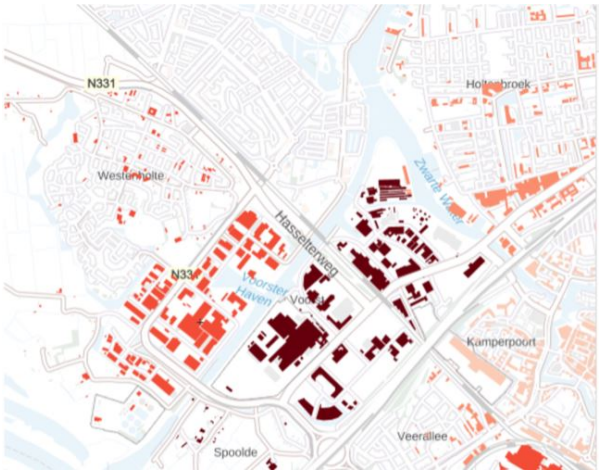

Figure 4.4: Voorst divided into west and east of the Zwolle-IJssel channel based on 4 digits postal codes, (CBS, 2014)

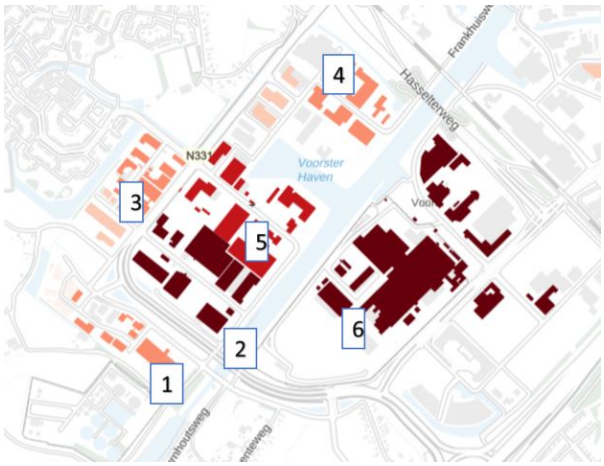

Figure 4.5: : Voorst divided into the 6 postal codes based on 6 digits postal codes accompanied by total gas usage (CBS, 2014).

quality of the WH is divided into two segments: the expected profile of available heat and the medium in which it presents itself, including temperature. Evaluation of these different aspects then allows the formation of the total heat profile.

To estimate the heat profile for the lifespan of DH, an approximation is made for a standard year, which is extrapolated for the rest of the DH life. The approximation for the one year is based on the available natural gas consumption for different industry sectors in the Netherlands, which is only available for the year 2019 (CBS, 2020b). This gas profile describes the weekly gas consumption, using the average consumption per week of 2017 as a reference. However, since the DH network is modelled on an hourly basis, the hourly fluctuations should also be taken into account.

Two working periods were identified for the companies: 12-hour operating workdays with no processes at the weekend and companies producing 24/7. This will be used as leading for the hourly emitted IWH, whereby, if no nightshift were found, it is estimated the shift are from 6:00 to 18:00 hour.

The heat transfer media of the IWH for the four different companies was then researched. For Abbott and Sensus, the product produced is similar and classified, as this information is competition sensitive. Going from the literature, only cooling water is assumed as waste heat in the range of 100-200 °C. The other two companies both produce stockfeed in the form of pellets. The production process could be estimated based on the work of Tumuluru et al. (2016), ergo the form of the IWH carrying medium could also be estimated, as well as the temperature and pressure. The cooling medium is air, and it can be assumed to have a range of

20-90 °C with an average of 70 °C (Tumuluru et al., 2016).

The companies mentioned above were contacted and send a questionnaire to confirm or bust assumptions made. From this questionnaire, quantitative data was shared regarding the WH available regarding the medium in which the IWH is present. This includes the pressure, temperature, and purity, as well as the quantity over time. Thus far, the method resembles the one used by Woolley et al. (2018), however, instead of using the data directly to estimate the surplus of WH, it was merely used for reference. The reason the data could not be used directly is due to privacy concerns. These concerns, however, vanish when it is used to test the newly developed method.

4.5.4. Equipment

The companies selected for Westenholte can now also be divided based on the heat profiles associated. On the one hand, there is a heat profile consisting of 5 days 12-hour production and temperatures varying from 100-200 °C with heat-carrying medium water for the companies Abbot and Sensus. On the other hand, there is 24/7 operation and temperature profiles from 30-90 ° C with air as the heat-carrying medium. The equipment function is the same for both heat profiles: an HEX to exchange heat from the heat-carrying medium combined with a heat pump when the temperature is too low. The large difference for the required equipment is the dimensions required and the medium that it carries. In the following section, for both heat profiles, the equipment will be designed. To start, the equipment will be designed for the water source heat profile of Abbott and Sensus. Next, the equipment will be designed for the air source heat profile for Agrifirm and ForFarmers. Finally, an appraisal of the total cost and emissions for the different companies will lead to the total cost and emissions of IWH. These results will then be evaluated in the following section.

As previously mentioned, the equipment for Abbott and Sensus consists of an HEX and a heat pump if the source temperature is lower than that of the DH. However, as the source temperature is expected to remain mainly between 100-200 °C and only lower for a small period of the year, the heat pump will not be required. This leaves only the necessity for an HEX and a pump. To design the equipment for transferring the heat from waste/cooling to the DH network, the same questions apply as for TESW and TEWW in section 4.3.4. The piping from the source to the HEX is estimated to be 20 m back and forth as they might not be enough room available. The source water will then meet the DH distribution net in the HEX. A pump must be placed in between the source water and the HEX. With all the equipment designed, the total cost can be calculated.

For the remaining two companies, Agrifirm and ForFarmers, the setup will be altered slightly as the source medium is air. Firstly, the air's higher maximum velocity dictates dissimilar pipe dimensions compared to water. The piping should also be different and will thus have different pricing in length and diameter. Secondly, the pump will be changed for a fan to move the air through the piping. Thirdly, the HEX will transfer heat from the air to water. Lastly, a heat pump will be used to upgrade the heat.

Piping

Starting with the piping, the diameter is calculated using the equation for the maximum velocity of 20 m/s (The Engineering Toolbox, n.d.) for air. As the piping's CAPEX is very small in comparison to the heat pump's cost, these can be neglected. The length of the piping will be the same as that for the previous companies; 20 m. For the pressure drop equation 4.13 will be used for 80 °C a density of 1 [kg/m^3] and dynamic viscosity of 1.963*10^{-5} kg/ms.

HEX

The air-to-water HEXs cost are approximated using a simplified method provided by Ferreira (2021) for an estimated mean temperature of the source of 80 °C of the air. The cost are then estimated using equation 4.30.

$$CAPEX_{HEX_{air}} = 14 * 0.65 * \frac{max(\dot{Q} * 10^3)}{\Delta \overline{T}} \tag{4.30}$$

Fan

For the fan, the following equation serves to determine the CAPEX, based on the DACE price sheet (Freriks, 2011). For the electricity consumption of the fan equation 4.32 is used, assuming the air behaves according to the ideal gas law for atmospheric conditions (k=1.41 and p_1=1 bar) (White, 1979) and p_2 calculated by taking the pressure drop over a tube with a length of 10 m and diameter designed to respect the maximum air velocity in the tubing in addition to an HEX pressure drop of 0.1 bar.

$$CAPEX_{fan} = 113000 * max(\dot{V}) + 21000 \tag{4.31}$$

$$W_{fan} = \frac{p_1 * \dot{V} * \frac{k}{k-1} * (\frac{p_2}{p_1}^{\frac{k-1}{k}} - 1)}{\eta_{compressor}} \tag{4.32}$$

Additional cost

In order to use the heat of the companies, financial compensation is expected by the companies. This can be seen as a fee for redeeming the heat. According to Church (2016), a normal compensation per kWh for the usage of the heat is equal to 70 percent of the price paid per kWh of the price paid for natural gas. In this work, the wholesale price of the natural gas is estimated at €0.016 / kWh, resulting in an extra cost of $0.016 * 0.7 = 0.0112e$ /kWh.
Validation of the IWH of the profile is not possible, as the heat profile of the companies is not available.

5

Coupling of heat supply and demand

5.1. Introduction

Obtaining the desired heat from the suppliers to the consumers requires, first of all, a distribution grid of pipes that carry heat. The distribution grid must be constructed in such a way that the consumers in the dwellings always have their demand met. This chapter offers a design of the distribution grid for this case according to ISSO publication 7 from Kennisinstituut voor Installatietechniek (2012), to satisfy this demand, using steel and polymer piping, depending on the grid temperature. Steel piping will be used for 70/40 °C DH network. The 50/30 °C network can use polymer piping. The polymer piping has certain advantages over steel as the maximum velocity is higher and insulation better. To obtain the cost and CO_2 emission of the distribution network, first, the global layout of the network will be determined, second, the heat and mass balances for this layout will be solved, as these will be the input for the last step. In this last step, the equipment will be designed and associated cost and CO_2 emissions calculated.

The second requirement for delivering the heat from the suppliers to the consumers is to solve the difference in time of the heat generation and heat demand. The generation of heat will vary over time, as it depends on the weather, industrial production times, and other influences. Additionally, the heat demand of the consumers for SH and DHW also varies over time, since more people require heat in the evening than during the day, for example for showering. Storage can be used to match the demand and supply. The storage capacity is divided into two time frames; short-term (ST-TES) and seasonal storage. For ST-TES, a large water vessel will be used to overcome differences in supply and demand over a time frame of a day to a week. The long-term storage will be an ATES system, storing energy for a time frame of about half a year. In the following chapter, first, the different time frames are separated, after which both types of storage will be designed and the cost will be determined to get to the overall LCOE.

5.2. Distribution

5.2.1. Introduction

As previously stated, the design methods of ISSO 7 publication from Kennisinstituut voor Installatietechniek (2012) will be used to design a distribution grid connecting the heat supply with the heat demand for Westenholte. The first step for defining a distribution grid for both 70/40 ° C with steel piping and 50/30 ° C with polymer piping is defining the layout. The kind of layout which should be used is provided by the ISSO 7 publication. However, two important design factors are not defined: the total length of the distribution grid and the diameters of piping. The length of the piping will be approximated using the available literature, whereas the diameter of the piping will be appraised based on the existing DH. Following, the heat and mass balances are to be solved as this will inform the cost and energy requirement of the equipment. The last step then will be calculating the cost and energy requirement to determine the total cost and CO_2 emission for all equipment together.

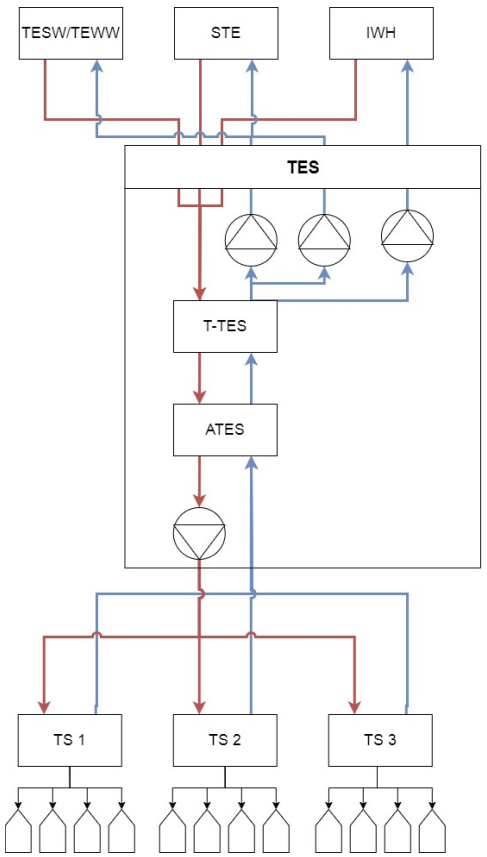

Figure 5.1: Schematic overview heat inside DH distribution network (STE is solar thermal energy).

5.2.2. Lay out distribution system

The piping connecting the heat demand with the supply can be arranged into different layouts. From the literature study and ISSO 7, an indirect distribution network, consisting of a primary and secondary distribution grid, is the best fit for Westenholte. This is the case, as the amount of dwellings in Westenholte far exceeds 800, which is roughly the maximum for direct distribution. The primary network will connect all the heat sources to the main substation, where a secondary network will connect all the consumers to the same substation. A substation is a location where a pump and an HEX transmit the heat from one distribution grid to another distribution grid. This main substation will be, for this case, at the same location where the heat storage is present.

Looking further into the layout; the network is divided into a primary and secondary network. The primary network will consist of sources that are individually connected to the storage substation by a supply and return pipe, except for TEWW and TESW as these remain in the same location. Figure 6.2 schematically illustrates the heat sources and their connection to the grid. For the secondary network, on the other hand, a Y-network will be used as described in chapter 2. For the demand side, however, the total amount of dwellings will be subdivided into 3 sections of each about 800 dwellings as stated in ISSO 7. Each of these sections will include a substation. These smaller distribution grids will then provide heat to the consumers, which is depicted in figure 5.2. Figure 5.1 schematically summarizes this distribution grid.

Each of the substations will contain one HEX and one pump at the “demand” side of the HEX. To come to an estimation of the cost for this distribution network, the total length of the piping per diameter must be known, because the CAPEX of piping is often expressed in € /m per diameter of the piping. Additionally, pumping cost estimation also requires the diameter and length of the piping used, as shown in equations 4.13 and 4.20.

The work of Persson and Werner (2010) serves to estimate the total length of the distribution network for a

total population of 5371 residents. The total area for the whole of Westenholte is 1,24 * 10^6 m^2 which is equal to the build environment area (allecijfers.nl, 2020). The length is then estimated to be 20 km of supply and return pipe. Following, the length of piping per diameter is expected to be equal for all diameters used. The piping for the DH will likely occur in all diameters; from the minimal diameter (the diameter for the typical dwelling with the largest maximal energy consumption) to the maximum diameter (formed by the total heat demand of Westenholte) using equation 4.12.

5.2.3. Heat and mass balance

With the design, length, and diameter of the piping, now the heat and mass balances can be calculated for the distribution network from figure 5.1. Seven pumps and HEXs are present in substations in the distribution network of Westenholte. To estimate the demands on the equipment, the heat and mass balance will be set up, starting from the supply side and following the heat flow to the storage and the demand.

The requirements for calculating the heat and mass balance on the supply side are the length of the piping, as depicted in figure 5.1, the temperature of the DH grid, and the heat flow of each heat source. As the HEX falls under the responsibility of the heat source owner, pumping water through the HEX and piping only requires the pumping energy calculation. Using the heat provided by each source and the temperature difference of the DH network, equation 4.11 serves to calculate the mass flow. With this mass flow, the diameter can be calculated with equation 4.12. The pressure drop over the piping can be calculated with equation 4.13, but should also include the pressure drop of both HEX's, as described in section 4.3.4. Then, equation 4.20 can compute the energy consumption for each pump.

For the substation and storage, one can assume that the supply can release all its heat as provided over time, while the demand can obtain all the heat as required in respect to time, as the storage used will guarantee the match. On the demand side, the storage substation is connected to three other substations, for which the pumping energy should be calculated. The connection contains the main pipe for supply and return, which is then split up into three, each going to a separate substation. After that, the pressure loss is calculated by estimating the pressure drop that only one substation would cause, as they are placed in parallel. The piping diameters can be estimated through equation 4.29, assuming that the heat demand of each substation is equal.

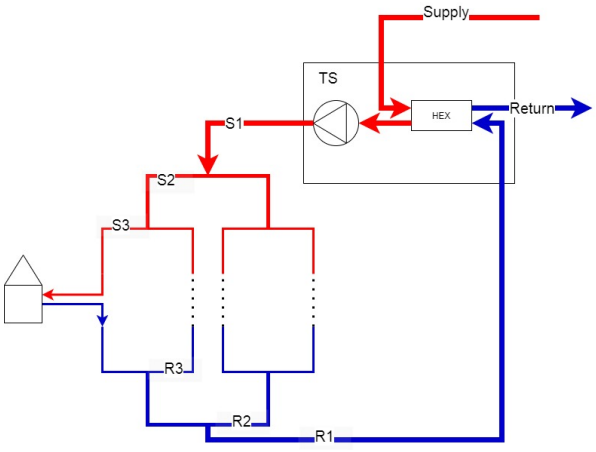

Figure 5.2: Schematic overview heat inside DH distribution network of heat transfer stations (TS). S1 and R1 have the same diameter as have S2 and R3 etc. Inside the dwelling a local hex transfers the heat to the local distribution network.

The network becomes more complex between the substations and the dwellings. So far the length per diameter of piping is known, as the lengths are all equal. To calculate the pressure drop over the network from the substations to the dwellings, the length of piping to and from a single dwelling should also be known. The reason is that the dwelling with the highest pressure drop must be met, so the distribution network should be able to provide for this dwelling. This thus sets the minimum pressure drop, as all the dwellings are placed in parallel in a ring-type network. However, contrary to the literature study, the dwellings are all attributed with

a pressure valve to control the local heat flow into the dwelling instead of a pump.
When assuming a perfect network, the following equations and boundary conditions provide the average pressure drop over a single dwelling: equation 5.2 provides the number of parallel pipes which are required to carry the maximum heat load. The maximum heat load per diameter of piping is calculated using equation 5.1 and illustrated in table 5.1, in which $v_{max,DN}$ is the maximum velocity per diameter of piping, A_{DN} the surface area per diameter, ρ_w the density of water, $c_{p,w}$ the specific heat of the water and ΔT_{DH} the temperature difference of the supply and return of the DH. Multiplied, these lead to the maximum heat flow per diameter $\dot{Q}_{max,DN}$.
The length leading to one dwelling is estimated by putting all the pieces of pipe required to get to one dwelling and their associated speed in series and calculating the pressure drop. The length per diameter of piping is calculated by dividing the total length of piping with a certain diameter by a factor that determines the amount of which need to be placed parallel to transport the whole heat demand. This factor is calculated according to equation 5.2. Placing all of the lengths per diameter in series, and calculating the maximum heat load per diameter will lead to the pressure drop. This pressure drop is the major loss of the network, as described in equation 4.29. The minor losses are estimated as 10 percent of the major losses. With the pressure drop and the volumetric flow for each substation, the energy consumption of the pumps can be calculated according to equation 4.20.
For example, if the total length of piping of DN 250 is 100 m and of DN 125 as well, transporting heat from one central point to six subpoints. The maximum heat transport capacity of DN 250 is 10.5 kW and of DN 125 1.86 kW for a Δ T of 30 °C. To transport the same amount of heat one DN 250 is carrying would require 10,500/1,860 = 6 tubes to be placed in parallel. Thus to get from the central point to one subpoint would require 100 m of DN 250 and 100/6 = 16.7 m of DN 125. Then the pressure drop for all of these segments is calculated as if the pipe was a perfect fit for the heat load: the maximum heat load it has to transport equals the maximum heat load the tube can carry. Adding up all of these pressure drops leads to the total pressure drop. This gives a pressure drop of 100 m DN 250 for a heat load with a peak of 10.5 kW and 16.7 m for a heat load with a peak of 1.86 kW.

$$\dot{Q}_{max,DN} = v_{max,DN} * A_{DN} * \rho_w * c_{p,w} * \Delta T_{DH} \tag{5.1}$$

$$N_{pipes} = \frac{max(\dot{Q}_D)}{\dot{Q}_{max,DN}} \tag{5.2}$$

$$L_{dwelling} = L_{DN} / N_{pipes} \tag{5.3}$$

Table 5.1: Maximum heat load of piping, calculated according to equation 5.1.

	$\dot{Q}_{max,DN}$[kW]			
	Steel		Polymer	
DN \ΔT	30	20	30	20
25	25	16	68	45
32	51	34	122	81
40	95	63	190	127
50	173	115	346	231
65	334	223	585	390
80	570	380	1,013	676
100	990	660	1,583	1,056
125	1,860	1,240	2,780	1,860
150	2,890	1,930	4,680	3,120
200	5,940	3,960	9,500	6,330
250	10,500	7,000	16,700	11,100
300	16,900	11,300	26,700	17,800
500	66,800	44,500	118,700	79,200
600	110,000	80,000	190,000	130,000
800	230,000	160,000	380,000	250,000

5.2.4. Total cost

The total cost and CO_2 emission will be calculated as described in section 4.3.4. This will include the cost estimation of the pumps and HEXs used. However, for the piping of the distribution system, the maintenance cost is lower in comparison to the other parts of the DH with 2 percent per year of the piping CAPEX, according to ISSO 7. This is because the piping does not contain moving parts, contrary to, for example, a pump.

5.3. Thermal energy storage

TES resolves the time dependency of heat demand and supply. The TES will be divided into two time scales: short-term TES (ST-TES) and seasonal/long-term TES. ST-TES can compensate for the daily and weekly variations, which occur, for example, because the generation of heat during the day is often higher than demand. For this type of TES, T-TES allows cheap loading and unloading of heat. The seasonal storage is necessary as during the summer months energy will be generated in excess, while during the winter months energy demand surpasses that of the supply. The literature study suggested that SH-TES is the best TES solution. For long-term storage, the ATES method will be used because the storage space is the cheapest available. Since loading and unloading into the aquifers are more costly compared to the T-TES, this method cannot be used for fast unloading and loading as a result of daily variations. T-TES, on the other hand, suits fast loading and unloading of heat and will be used for ST-TES.

To eventually come to the total cost and CO_2 emission of both storage solutions, first, the heat balance will illustrate the differences in time of heat supply and demand. The difference will then be subdivided into short-term and long-term differences. Second, solving the mass balance and thereby calculating the equipment demands will lead to designs for both the ATES and the T-TES solutions. At last, the cost and CO_2 emission will be determined based on the cost for both designs. These will be validated for Westenholte in chapter 6.

5.3.1. Energy balance

The ATES will be able to store the excess heat that is created by seasonal differences and release the heat once the demand surpasses the supply, where the ST-TES will only act as a short-term buffer to smoothen the (un)loading of the ATES and the load on the piping. The ST-TES will dampen the peaks in heat demand and supply. Since the pumping cost during peak demand is cubically proportional to the cost, this can make a significant impact (Guelpa & Verda, 2019).

To obtain the excess heat supplied by the heat sources and the demand that cannot be met, $\dot{Q}_{\Delta}$, the levelized heat supply ($\dot{Q}_{l,s}$, calculated in equation 5.5) will be subtracted from the heat demand ($\dot{Q}_d$), as seen in equation 5.4. The levelised heat supply is calculated according to equation 5.5. This scales the total amount of supply to be equal to the total amount of demand, whilst the supply maintains the old heat profile. By using the levelized heat supply, only the timing differences between the heat production and demand are being stored, as the total heat demand equals the total heat supply. $\dot{Q}_{\Delta}$ thus provides the redundant heat when positive and the reluctant heat when negative. From $\dot{Q}_{\Delta}$, the two different time frames, short term, $\dot{Q}_{ST-TES}$, and long term, $\dot{Q}_{ATES}$, are computed.

$$\dot{Q}_{\Delta} = \dot{Q}_{l,s} - \dot{Q}_d \tag{5.4}$$

$$\dot{Q}_{l,s} = \frac{\dot{Q}_s}{\Sigma_i(Q_{s,i})} * \Sigma_i(Q_{d,i}) \tag{5.5}$$

In this case, the T-TES will act as a buffer for 24 hours, as most periods of demand and supply are 24 hours. This means that the net energy stored over the past 24 hours should be equal to zero. An easy way of calculating the result for a buffer of 24 hours is by using the SMA for the heat difference for 24 hours. Equation 4.2 shows the SMA, for which t is the current time in hours, N is the period and p is the time series for which the SMA is calculated. With a window from the past 12 hours and the future 12 hours, the SMA equals a perfect prediction of the heat flow, as the weather can also reasonably be predicted for 24 hours. This means that only the perfect amount of heat is stored or provided because of the mathematical property of an average. The SMA will be the result of applying the T-TES, so the signal automatically sets the heat that the ATES

should be able to store or provide, $\dot{Q}_{ATES}$, as illustrated by equation 5.6. The amount of heat that then has to be stored by the ST-TES, $\dot{Q}_{ST-TES}$, can be calculated according to equation 5.7. With the storage demand split into short and long-term storage, the design of both storage solutions can be determined. This method is appropriate for the tank model, which will be explained in section 5.3.3, as the model assumes a perfectly steady temperature of the supply of the proposed DH distribution and no heat losses in the tank.

$$\dot{Q}_{ATES} = SMA(\dot{Q}_{\Delta}, N = 24) \tag{5.6}$$

$$\dot{Q}_{ST-TES} = \dot{Q}_{\Delta} - \dot{Q}_{ATES} \tag{5.7}$$

5.3.2. ATES

To get to the design of the ATES, first, the functioning of the ATES will be further defined by examining the working of the ATES and the losses that occur. Solving the heat and mass balances will enable one to design the equipment and obtain the total volume required for the ATES. Finally, with the solved heat and mass balances, the cost and CO_2 emission of the equipment can be calculated leading to the cost and CO_2 emission of the ATES system. The CAPEX will be based on the total volume of the ATES, where the OPEX is based on energy consumption.

Figure 5.3 depicts the functioning of an ATES. As can be seen, when there is an abundance of energy, water from the cold well will be pumped through an HEX, thus gaining heat from the DH network, and raising the temperature. The warm water is then pumped into the hot well, where it will be stored until the heat demand of the DH exceeds the supply. To regain the heat, the water from the hot well will be pumped to the cold well, passing a heat pump where it will release its heat. In the heat pump, the heat is extracted and upgraded for use by the DH. Historically, LT-ATES is widespread throughout the Netherlands, with storage temperatures of 10 °C for the cold and 17 °C for the hot well (de Wit-Blok, 2017). The depth of the aquifers ranges between about 20-300 m, with some exceptions (Fleuchaus et al., 2018). This form of TES is known in the Netherlands for having one of the lowest costs among long TES and relatively small space requirements, and being the only permitted form of ATES. Typically, ATES storage capacity ranges from 10 MWh to 10,000 MWh and heating power from 0.5 MW to 200 MW (de Wit-Blok, 2017). This suffices as the total heat demand of Westenholte has a maximum of approximately 10 MW.

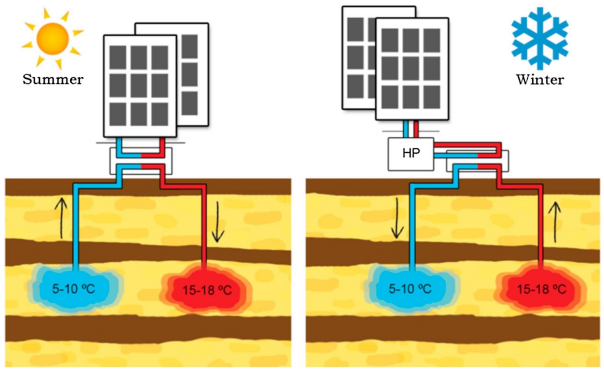

Figure 5.3: Schematic representation of LT-ATES in which the storage of water takes place in the sand between two impermeable layers. In the summer, it is charged using an HEX and, in the winter, discharged with a heat pump. Adapted from Bloemendal et al. (2018).

The heat balance will be solved to obtain the heat stored in the ATES. Thus far, only the heat demand from the ATES is known and depicted in equation 5.8, as the levelized heat supply ($\dot{Q}_l$, is used to calculate Q_{Δ}. Calculation of the amount of heat required to provide the final heat should account for the heat pump as well as the efficiency of the ATES system. The demand which should be provided by the ATES is illustrated in equation 5.8. Equation 5.9 gives the demand that should be provided by the ATES. The heat directly output by the ATES then remains. This heat becomes less as heat losses occur (Bloemendal et al., 2018). The input of the ATES must be more than the output as a result of this efficiency. Equation 5.10 shows how the heat input

of the ATES is calculated from the heat demanded from the ATES $\dot{Q}_{d,ATES}$. The total input can then be calculated according to equation 5.11. The heat, including losses, that is "stored" in the ATES can be calculated by summing the previous in and output of this heat.

$$\dot{Q}_{d,ATES} = \dot{Q}_{ATES} \; for \; \dot{Q}_{ATES} > 0 \tag{5.8}$$

$$\dot{Q}_{ATES,out} = \dot{Q}_{d,ATES} - \dot{W}_{el} \tag{5.9}$$

$$\dot{Q}_{ATES,in} = \frac{\dot{Q}_{ATES,out}}{\eta_{ATES}} \tag{5.10}$$

$$\dot{Q}_{ATES,in} = \frac{\dot{Q}_{d,ATES}}{\eta_{ATES}} * (1 - \frac{1}{COP - 1}) \tag{5.11}$$

Mass balance and cost

Next up for investigation are the mass balances. The ATES can be divided into two stages: loading and unloading. In the loading phase, energy from the DH will be put into the ground with the help of an HEX. By law, the heat and volume going in and out of the ATES should be equal over a full year. In hindsight, for Westenholte, this would mean the heat input over a full year must average to zero. This can be calculated by subtracting the $Q_{ATES,in}$ which heat should be stored and released by the SMA of the heat profile of $Q_{ATES,in}$ of a year (8760 hours), as illustrated in equation 5.12. By subtracting the yearly SMA, the mean of the total heat profile per year will be zero, meaning all energy stored is released in the same year. This then satisfies the regulations set by the Dutch authority. However, this technique is based on hindsight, meaning it can only be used with known data and only roughly estimates the storage capacity. The volume flows for (un)loading can be calculated with equation 4.11, for water for a temperature difference of 7 °C and $\dot{Q}_{ATES,in}$. A negative mass flow indicates that the mass is being pumped from the hot well to the cold well.

$$Q_{ATES,yearly} = Q_{ATES,in} - SMA(Q_{ATES,in}, N = 8760) \tag{5.12}$$

With the volume flow, the pumping cost can be determined for the ATES system. Haichar (2018) prescribes that the maximum diameter and velocity for each utilized ATES well must be accounted for, leading to multiple wells and pumps. The maximum diameter for an aquifer is estimated to be 0.3 m and the velocity 0.52 m/s. The number of aquifers is then calculated by dividing the total volume flow by the maximum volume flow for one aquifer. The energy it takes to pump the water is estimated in equation 4.20. The pressure drop the gravity causes has a net-zero effect, as the water is pumped the same amount up as down, the gravity does not cause pressure differences.
Besides, the pressure drops caused by friction forces and the HEX's are still present and should be added to this pressure drop. When the soil is assumed as water, the pressure drop for both loading and unloading is the same: pumping water into the aquifer causes an increased pressure that equals the increased pressure drop due to the conservative force field properties of gravity.

The CAPEX of the ATES will be based on the total volume of the ATES. The cost of the ATES can be calculated using the volume equivalent water of the ATES, calculated in equation 5.13 (de Guadalfajara et al., 2014), in which V_{stored} is the total volume equivalent of water stored and α_{TES} is a variable dependent on the type of storage (α_{TES}= 0.25 is assumed for ATES and α_{TES}=1 for T-TES). The CAPEX is then calculated using equation 5.14. This equation has been verified for ATES data using de Wit-Blok (2017).

$$V_{stored} = \frac{max|\Sigma_{t=0}^{t} Q_{ATES,yearly}|}{c_{p,w} * \rho_w * \Delta T_{ATES}} \tag{5.13}$$

$$CAPEX = \alpha_{TES} * 4660 * V_{stored}^{0.615} \tag{5.14}$$

The OPEX of the ATES system consists of the cost for electricity of the heat pump and other pumps. The pumping cost is calculated based on the pressure drop. For the pressure drop, it is assumed the cold and hot aquifers are separated by 100 m and the depth is 80 m. With this pressure drop and the volume flow, equation 4.20 can calculate the electricity consumption for a single aquifer. The electricity consumption for the heat

pump is obtained through equation 4.8 with input $\dot{Q}_{ATES,out}$ and COP for the temperatures (10+17)/2 = 13.5 ° C and supply temperature for the DH network.

5.3.3. Short term SH-TES

How the T-TES balances heat demand and supply over 24 hours is illustrated in section 5.3.1. The tank stores the thermal energy by holding hot and cold water in the same tank in a stratified manner. Additionally, the T-TES can act as a pressurization vessel when directly connected to the DH distribution system. Loading of the tank is done by letting the supply piping fill the tank with hot water, while the return pipe is draining the tank. Vice versa for unloading of the tank. Figure 5.4 depicts the above described T-TES.

The cost is determined in largely the same manner as for the ATES: the volume of the tank determines the total CAPEX and the OPEX mainly consists of the friction losses and minor losses at the distributor. Additionally, when using the moving boundary model from Dumont et al. (2016), the layer of water separating the hot water and the cold water, the thermocline, takes up some space in the tank and reduces its efficiency. Learning the cost of the T-TES starts with determining the tank design, including its efficiency, leading to the volume. Next, the loading and unloading of the tank will be modeled, leading to the energy consumption of the T-TES. At last, the cost and CO_2 emission are calculated based on the volume of the tank and the energy consumption.

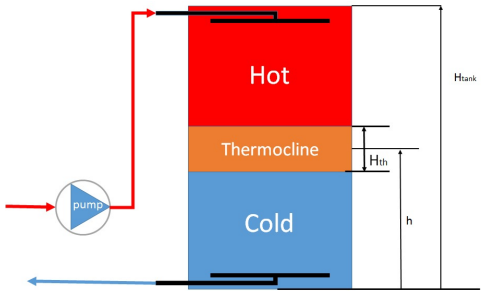

Figure 5.4: Schematic overview of a stratified T-TES, showing the hot and cold side, thermocline, and diffusers.

Design of T-TES

The design of the T-TES is based on the moving boundary model of Dumont et al. (2016) for a stratified water tank. The model proposed by Dumont et al. has low computational demand while providing relatively high accuracy. This model is based on the usage of a stratified tank divided into two sections: a hot section and a cold section. These sections are separated with a boundary layer that is infinitely thin and where no heat transfer takes place, as can be seen in Dickes et al. (2015) and is described by the equations 5.15 and 5.16.

$$Q_{hot} = (H_{tank} - h(t) - 0.5 * H_{th}) * A_{tank} * \rho_w * c_{p,w} * \Delta T \tag{5.15}$$

$$Q_{cold} = (h(t) - 0.5 * H_{th}) * A_{tank} * \rho_w * c_{p,w} * \Delta T \tag{5.16}$$

$$H_{th} = L_{th} * H_{tank} \tag{5.17}$$

For this model to be used, first, the total volume of the water inside the tank needs to be obtained in order to calculate CAPEX and OPEX of the T-TES. An initial estimation for the volume of water required can be made using the work of Gadd and Werner (2015) and Guelpa and Verda (2019). In their research, 6 m^3 of water was used for storage per TJ generated heat to fulfil the annual heat supply. This initial estimate leads to a volume of around 750 m^3. Additionally, Guelpa and Verda (2019) have estimated that 17 percent of the average daily heat load is required in storage, which is 16 m^3 for when ΔT = 30 °C. Equation 5.13 assesses the volume of the tank without the thermocline separating the hot and cold sides. For a reference case for the DH of Westenholte, where each source is providing a quarter of the heat, the demand is as-is and the temperature of the DH is 70/40 ° C, the volume lowers to 700 m^3 for 95 percent of the maximum based on $\dot{Q}_{T-TES}$. This illustrates the method used to model the heat flow for the T-TES provides a good approximation.

The method used to calculate the 700 m^3 however does not include the volume of the thermocline inside the tank. Therefore, an adaptation on the model is proposed for H_{th}, in which a transition layer or thermocline is used, as the thermal energy capacity is overestimated. The transition layer can be adapted to account for the thermal efficiency of the TES and reduces the thermal storage capacity to approximate the encountered experimental values better, which Dickes et al. (2015) encountered. A value for the non-dimensionalized thickness was found to be approximate L_{th}=0.4. This can then be used to calculate the total required volume of water for the tank, and therefore all other dimensions required for calculating the CAPEX and OPEX, as will be elaborated in the following sections.

(Un)loading

(Un)loading the tank with heat requires pumping energy. In case of a heat surplus, the tank will gain hot water from the DH network and feedback the cold water, maintaining the same volume. In case of a heat shortage, the hot water will be put back into the DH network and the colder water will be fed into the tank. Because the tank is connected directly to the DH this will happen automatically: a surplus of heat will cause extra pressure in the distribution piping. The extra pressure from a decreased demand leads to a sudden lower flow rate, while the pumps are still running at a previously indicated flow rate. This is because the closed flow valves at the dwellings leave no opportunity for the DH to discard the volume. The extra pressure in the distribution net then finds a way out by filling the tank. Diffusers are used to slowly fill/drain the tank, preventing distortions that could break the thermocline. This process happens vice versa when extra cooling is required of the sources with the return line. Direct connection to the DH also means that the supply temperature will equal the hot water as the return temperature will equal the colder water. The amount of pumping energy can be estimated by calculating the pressure drop formed by friction and gravity, similar to the ATES.

Cost

Equation 5.14 serves to calculate the total CAPEX of the T-TES, for α_{TES}=1, according to de Guadalfajara et al. (2014). Next, equation 4.20 gives the electricity consumption for the previously calculated pressure drop during (un)loading and the associated volumetric flow for a pipe with the diameter as determined in 4.12. This electricity is then multiplied by the electricity price to obtain the OPEX.

6

Total model

6.1. Introduction

So far, the different sub-models have been constructed independently from one another. In this chapter, the models will be merged to form the complete DH model. The goal of the DH model is to answer the main research question. It does so by calculating the KPIs, previously determined in chapter 2, for various scenarios and researching the influences of DH temperature and the different heat sources. Location-bound variables should remain constant to determine the effect of these two variables. Therefore, a distinction is made between constants, which are variables for the case study, and variables such as the DH temperature. The model is, first, initialized with constant location-bound data which does not change with a run of the model for the case study: the neighborhood of Westenholte. Next, the variables of specific scenarios are entered into the DH model after which the result for that scenario can be calculated.

To get a starting point for finding the optimal configuration of heat sources, two base case scenarios per submodule will be calculated for Westenholte, summarized: the conservative 70/40 °C scenario and the progressive 50/30 °C scenario. For these base cases, the total heat supply per source is equal for all sources so they can easily be compared, whilst the temperature causes the main differences in the resulting KPIs.

The DH model will be constructed by composing each submodule for the base case scenario to obtain the KPIs per submodule. These KPIs will then be validated with the current literature. Using the validation, the total output of the DH model can be calculated with an amount of certainty. The results of the base scenarios are then compared with an all-electric heated reference model, which is developed in the last part of the chapter. Chapter 7 offers a discussion for optimization of the DH based on the resulting KPIs of the base scenario and the all-electric reference model.

6.2. Model

The total model is largely based on the heat flow model shown in figure 6.1. However, instead of the weather being the sole input of the model, various parameters each play a role. Two kinds of parameters will be distinguished: initial and variable parameters. Initial parameters are constant per location and cover, for example, the number of dwellings that the case study represents. Variable parameters are subject to change throughout a case study, these will include the DH temperature.

In the following section, the DH model is constructed based on figure 2.3, after which the two base scenarios are composed. Second, the different submodules are individually calibrated for Westenholte, the variables for the scenarios are determined and then run for the base case scenarios. The variables are chosen in line with the model's goal of obtaining the KPIs for different demand distributions over the heat sources. The submodules will be initialized and run according to the flow of figure 6.1 and be compared to finally arrive at the output. To assure the assumptions made are correct, each submodule will be validated with the literature.

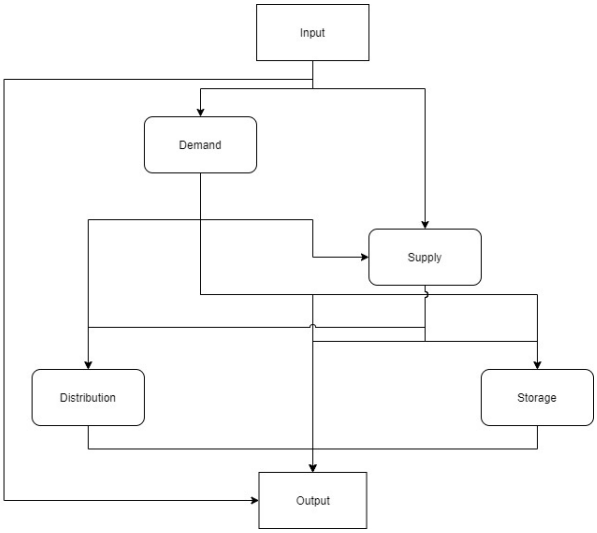

Figure 6.1: Schematic overview DH model

6.2.1. Functioning and goal of the DH model and scenarios

Figure 6.1 depicts the DH model and provides the information flows between the submodules. Compared to the heat flow model in figure 2.4, this new model has an additional input and output submodule. The input module, as illustrated in the figure, provides the variables that are open for research, such as the temperature of the DH network. This submodule is the single central point of the DH network where variables (independent of location) are loaded for the whole model. The input module is nested in all other submodules. After running the submodules in the flow illustrated in figure 6.1, the output submodule can merge the results of all the different submodules to get the final KPIs for the total DH. Based on these KPIs, the total DH network can be evaluated on the effects caused by the variables loaded into the input submodule. The last stage starts with an elaboration on the goal of the base scenarios. The total functioning of the model is explained with help of these base scenarios, illustrating the location-dependent variables and the scenario variables.

Developing the different scenarios and setting up the DH model requires, first, a confined area. This case study involves the area of Westenholte, so the different scenarios can be developed. Two base scenarios are developed for initial research on the temperature effects of a DH in Westenholte: the conservative 70/40 °C and the progressive 50/30 °C. The goal of the 70/40 °C scenario is to be the least invasive without large disruption of current designs of DH and in the dwellings of consumers. For example, this scenario will not need an electrical boiler for its DHW. The 50/30 °C progressive scenario, however, is designed to minimize the CO_2 emission. For instance, insulating the dwellings could limit the demand. These scenarios offer a view at the effect of the different temperature regimes whilst also providing an equal ground for comparison of the heat sources. Both cases are locally implemented for each submodule. Using the base scenarios, the global functioning of the model is explained, after which the variables per submodule are determined for both base scenarios. The total amount of variables for the network is then illustrated in table 6.1.

As illustrated in figure 6.1, the DH model starts with the input module. This module contains global location-constant parameters relevant for all the submodules and all the variables which can be altered based on the scenarios, as this is the submodule influencing all the other modules. The demand will be determined from the input module. For the demand, the insulation of the dwellings is not location-bound and will differ per scenario. Insulation does not affect the conservative case, and thus will not be considered. However, the progressive case has a benefit from insulation: less heat to be generated directly means less CO_2 emission.

The total heat supply is calculated through the demand and the input modules. This must include how much each heat source will need to produce in respect to the total heat demand, to study the effect of using different sources and of the heat loss of the overall network on the heat production. The amount of heat supply per source can thus be varied. It is even possible to completely exclude certain sources. For the conservative case, the peak supply will consist of a gas boiler and the baseload will be covered by equal amounts

of each heat source. For the progressive scenario, the peak load is provided by the ATES, limiting CO_2 emission from the boiler. The baseload will be the same to research the effect of the different scenarios without the varying heat supply.

With the demand and supply, the storage and distribution network can be determined. The storage will not vary over iteration and only needs to be initialized. However, the distribution grid includes two options, steel or polymer piping. The conservative scenario will use steel piping as is mostly used by DH so far. The progressive scenario likely will benefit from the polymer piping, since the heat losses are slightly lower. Table 6.1 provided below gives a clear overview of all the variables used in the base scenario.

Table 6.1: Values for the variables of the base scenarios. The running period for both scenarios is from 2005 to 2020.

	Scenarios	conservative	progressive	unit
Heat demand	Insulation	No	Yes	[-]
Heat supply	Peak load boiler	Yes	No	[-]
	IWH	22	31	[%]
	TEWW	24	24	[%]
	STE	27	23	[%]
	TESW	27	22	[%]
Distribution	Piping material	ST/PUR/PE	PB-h/PUR/HDPE	[-]
	Supply temperature	70	50	[C]
	Return temperature	40	30	[C]

6.2.2. Input

At the beginning of the model, the input submodule offers location-based data such as the weather, but mainly supports altering key/design constants of the entire DH network, as defined in the previous section. Different scenarios can therefore be simulated to come to the ultimate solution. For example, this model allows changing the temperatures of the DH distribution model.
The input module consists of three main groups of key parameters used to describe the DH distribution network: the distribution of heat provided by the different sources and input to financial parameters previously described in section 4.3.4 and general key characteristics of the entire DH model.

Starting with the latter, general key characteristic parameters for the DH consist of the specific heat value and the weather. Heino's data for the period of 2005-2020 describes the weather and includes solar irradiation and temperature. For more on the financial parameters for the DH model, refer to section 4.3.4. The specific CO_2 emission is part of the main KPI and is also included in this group at 441 g CO_2/kWh of electricity (European Enviroment Agency, 2020).

The variables loaded into the input submodule include the distribution temperature, dwelling insulation, and extra required heat production to compensate losses. The distribution temperature was already set to research 50/30 and 70/40 °C networks, these are only the minimum and maximum of the DH and can be altered as well. The second adjustable variable is the insulation of the housing stock. This will reduce the demand profile and produce investment costs that are calculated in the demand section. Lastly, the fraction of heat supplied per heat source is set based on the percentage of the total heat supply for each heat source, depicted in table 6.1.

In addition to distributing the heat demand over the sources, the input module also estimates the amount of heat loss in the DH as a percentage of the demand. The heat loss is then encountered in the heat production. The total heat loss is divided into two parts, the heat loss of the ATES and the heat loss of the distribution grid, as the tank is assumed to be 100 percent efficient. The heat loss of the ATES is calculated according to section 5.3.2 and of the distribution grid according to section 4.3.4. The supply to demand ratio can then be calculated using equation 3.4 for a constant ground temperature of 10 °C (Kennisinstituut voor Installatietechniek, 2012) and the ATES efficiency as described in equation 5.11. However, the heat loss depends on the amount of heat stored, which can only be determined based on the match between the supply and de-

Table 6.2: Demand output for a lifetime of 30 years for the 2215 dwellings of Westenholte.

Scenarios	Conservative	Progressive	[unit]
Demand	110	74	TJ/year
CAPEX	0	37,3	M€
OPEX	0	0,217	M€/year
LCOE	0	0.072	€/kWh

mand profiles. These profiles are known after the input model, making an iteration round required to get to the exact heat production, but before calculating the storage and distribution. However, the results reflected in this work already account for this correction and are thus the final results.

6.2.3. Demand

The heat demand is the first to be calculated based on the input. The input of the heat demand only consists of the input model, which provides the weather data and defines whether or not the dwellings need insulation. Additionally, the demand module initializes its data before running the model. This data provides the types of dwellings according to Agentschap NL (2011b), based on its envelope and construction year, and reference heat usage of these types. It also includes the number of dwellings found in Westenholte based on the four typical dwellings formed in chapter 3 and listed in appendix A in table A.1.

The process of calculating the heat demand starts with estimating the standard insulation per dwelling. The standard insulation is based on the reference gas consumption of the entire neighbourhood (CBS, 2018). A lower reference value indicates that extra insulation is used, illustrating the effect of insulation. The heat demand is then calculated by the insulation values, the weather, and the values of the four typical dwellings. The heat demand is categorized in solar heat, heat losses, and DHW heat demand per typical dwelling – calculated simultaneously. At last, the heat demand of the entire neighborhood is estimated by multiplying the number of dwellings per typical dwelling with its heat demand.

Each scenario has different insulation of the dwellings and utilization of the electric boiler. A lower distribution temperature of the DH than the allowed DHW temperature would require electrical boilers and insulation measures need to be taken. Both costs are determined based on Technim (n.d.) and Knepper (2019). The cost of the boiler is based on the CAPEX per unit at €2000.- and the OPEX energy consumption of the boiler and the consumer electricity price of € 0.22/kWh. The DHW heat demand will be used to determine this energy consumption and provide the OPEX. The insulation only involves the CAPEX as, after insulation, it is considered to be maintenance-free. The total cost of the submodule heat demand will thus consist of the insulation and boiler costs, including the installation cost, extra costs, and unforeseen costs, as discussed in section 4.3.4.

The output thus consists of the heat demand per typical dwelling, the total heat demand of the whole neighbourhood and the CAPEX of the applied insulation. The heat demand is used in all the following modules of the DH model.

The output of the heat demand modules for both cases is compared for the years 2013-2020 to the average heat demand based on the average gas consumption for a normal dwelling without insulation (allecijfers.nl, 2020). With a combustion efficiency of η_{gas} = 94.2 percent (Energy Matters, 2014) the average heat demand for the past seven years for a dwelling in Zwolle is estimated at 44.0 GJ, which is slightly higher than normal. For the model this amounts to 49.7 GJ for one dwelling per year. The 8.0 percent difference is fairly low.

6.2.4. Supply

Following the flow chart in figure 6.1, the next step is calculating the heat supply model. First, the heat demand is used to determine the amount of heat supply required, using the expected heat losses of the system. With the total supply in place, the total demand per heat source is determined through the input module. The required heat supply is divided into baseload and peak load. The required peak load is delivered either by a gas boiler or the ATES and the baseload by the RES and IWH. From these submodules, the heat sources provide the heat supply profile. This, in turn, leads to the sources' CAPEX, the OPEX, and the electricity use,

which only applies to the output submodule to produce the final output.

First of all, the amount of heat supply needs to be determined based on expected losses of the DH grid. In this study, the 100 percent efficient tank leaves the ATES' storage losses and the distribution grid's heat losses as the two major heat losses. Based on initialization, the heat losses are calculated using equations 5.11 and 3.4. Converting the heat losses will allow the heat supply to compensates for the heat losses in the input submodule. However, as the loss of the ATES depends on the difference in time of supply and demand, it requires an iteration round to get the perfect match. The starting value for this iteration will be that 25 percent more heat is required to account for the heat losses, based on an ATES efficiency of 75 percent. This ratio will then be adjusted to the ATES heat losses for each scenario.

The division between peak load and baseload is based on using a division in quantiles. The heat demand required is first ordered in size. The lower quantile, covering the lower 95 percent of the total amount of heat required is taken as the baseload. For Westenholte this will mean that up to a heat load of 9 MW is considered baseload and consists of heat provided by the RES and the TES. If the heat load is above 9 MW, the peak load provide the heat. This comes down to about 1000 hours per year of which the peak supply is also used. The peak load can be shut off and be replaced with a larger ATES providing this heat, as is done for the progressive case to limit CO_2 emission.

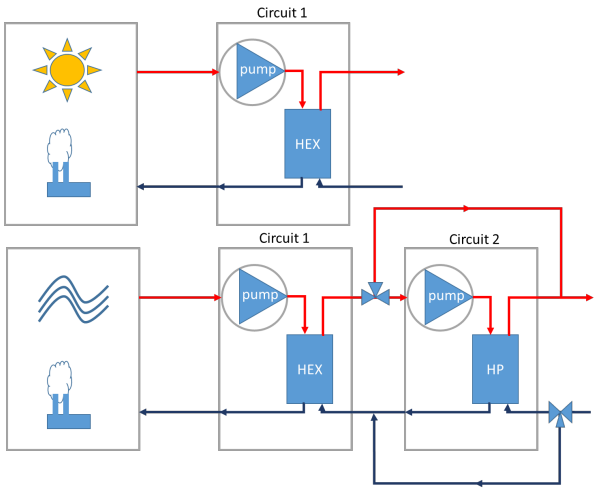

Figure 6.2: Schematic overview heat sources of DH network for solar thermal energy (yellow sun), TEWW and TESW (waves) and IWH (factory).

The RES and WH used are all calculated similarly. Starting, the amount of heat to be used is calculated, accompanied by the temperature and volume flow of the source material. With these values, the cost is calculated based on the equipment. Two types of heat sources are differentiated; on the one hand, the sources where the maximum temperature is always above the distribution temperature, and on the other hand, the sources below the distribution temperature. The first type only requires an HEX, piping, and pump and is defined as circuit one in this study and illustrated in 6.2. For the second type of heat source, circuit one is used but supplemented with a second circuit that consists of piping, a pump, and a heat exchanger. The equipment will be adapted according to the source material.

Using the equations in section 4.3.4 and finance values from the input module, the total heat supply, CAPEX, OPEX, and electricity consumption will be calculated. This will include the rough material cost as primary cost, secondary cost such as small buildings facilitating the installation, extra cost and unforeseen cost as discussed in section 4.3.4. The total heat supply will be considered in both distribution and storage. Only the distance from the source to the point of extraction by the DH is taken into consideration for this setup. Table 6.3 shows the results of the conservative base scenario, which are elaborated on in the following sections.

Table 6.3: Heat supply various heat profiles definitions and KPIs for a lifetime of 30 years.

	TEWW	STE	TESW	IWH	
Heat production	30.55	35.19	35.40	25.73	TJ/year
Maximum capacity	1.26	4.88	2.16	0.82	MW
production time	6,757	2,002	4,548	8,760	h
Electricity consumption	2,641.98	0.13	3,166.34	24.19	MWh/ year
CAPEX	2.04	7.14	2.97	1.40	M€
OPEX	245.36	149.48	320.31	117.49	k€
LCOE	0.04	0.06	0.05	0.03	€/kWh

TEWW,TESW

TESW and TEWW have fairly similar inputs for both sources. Both TESW and TEWW use the air temperature to estimate the source temperature. The total heat potential can be calculated by assessing the available amount of source water. Both sources are limited by the amount of effluent that can be dumped. Lastly, the heat source uses both circuits.

The local inputs for both sources thus will be the air temperature of Heino. Additionally, the effluent temperature is computed based on the capacity the sewage treatment can handle, according to equation 4.6. The available volume for the effluent is the dry weather capacity to 0.66 m^3/s and for the TESW, a maximum of 0.16 m^3/s has been set according to the largest TESW installation found in the Netherlands. Water can be dumped back into the Ijssel at 12.3 °C, assuming a flow of 340 m^3/s for the IJssel and a maximum flow of both TEWW and TESW of 0.66 + 0.16 = 0.82 m^3/s is 12.14 °C to meet the proposed regulations of IF and Stowa (2018).

Additionally, both heat sources are placed on the land owned by Waterschap at the same location. Both the effluent and the IJssel are easily accessible while it remains as close to Westenholte as possible. The length of the piping to the sources also reflects this proximity: estimated at 100 m of tubing for TESW and about 10 m for TEWW.

The amount of heat is controlled by limiting the input of the sources. Less volume will mean less water to obtain heat from. As each heat source provides roughly a quarter of the heat flow (table 6.1), for the TESW this will mean that only an effluent volume flow of 0.0343 m^3/s and Ijssel volume flow of 0.0343 m^3/s leading to 30 TJ per year of heat for the conservative 70/40 °C scenario are returned to the IJssel. This value is then adjusted to provide the percentage of heat for the progressive scenario.

The output for both installations is calculated for a quarter of the total heat demand of both base scenarios, leading to the CAPEX, OPEX, LCOE, and electricity consumption. A summary of these results is illustrated in table 6.3.

The cost of TESW is € 0.047 per kWh, which only 7 percent higher than the estimated € 0.044 per kWh by SDE++. Heat supply for one year is illustrated in figure 6.3. What is clearly illustrated in this figure is the effect of the heat pump, as the heat from the heat pump decreases when the temperature increases. Assuming a constant supply of heat from the IJssel, the only variation is the heat added by the heat pump when upgrading the heat. During summer, when the source temperature is high, the efficiency of the heat pump is higher, resulting in less additional heat. This process reverses in the winter.

However, since the effluent has a higher temperature, the operation hours are 6,700 hours instead of 6,000 for TESW. This also reflects in the LCOE, which is with €0.042/ kWh slightly lower than that of TESW. In perspective to the SDE++ model, with approximated the LCOE at €0.028/ kWh, the price is 50 percent higher per kWh.

STE

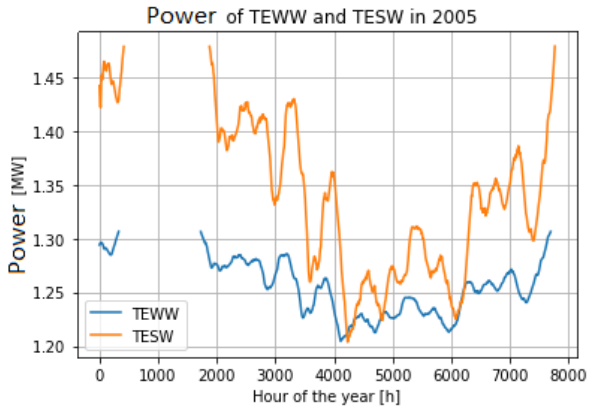

Figure 6.3: Power available from TEWW and TESW of 2005. In the cold months, roughly hour 0 to 2000, the temperature is below 12.5 °C and no heat is available from the water sources because the water from which heat is extracted cannot be dumped back to the IJssel per government rule.

The solar heat source does not require the second circuit from figure 6.2 to provide heat, only the first circuit, because of the beneficial source temperature. Multiplying the designated area to install the FPC with solar radiation and efficiency gives the STE heat. The efficiency is calculated based on the air temperature and the DH temperature. The FPC is placed in arrays based on the available heat. With the setup complete, the required pumps and HEX can be calculated.

For Westenholte, both the location for installation as well as the preferred FPC for iteration are preselected. The location is shown in figure 4.2 and the FPC is the solar boost HQ, with relevant parameters as listed in section 4.4.3.

As the area of the FPC is still open for selection, the total FPC area might vary. With the input parameter in which an indication can be provided of what part of the total area can be used, the heat source can be scaled. For the base cases/scenarios, this will mean only 26584 m^2 of the active area of FPC will be installed, leading to a power profile as illustrated in figure 6.4.

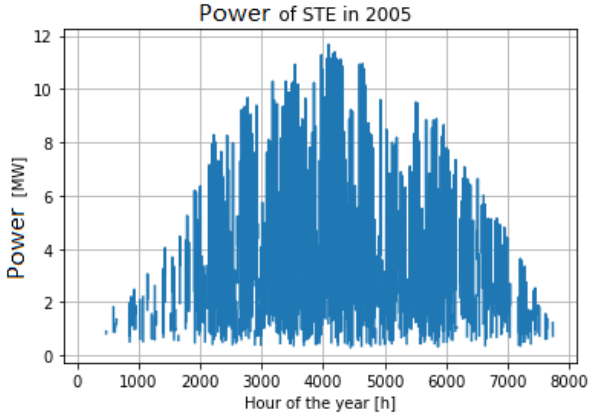

Figure 6.4: Power available from solar thermal for 2005

From this heat source, the output will be OPEX, CAPEX, electricity consumption and total heat. Table 6.3 shows these results. In comparison to the SDE++ model, which had an LCOE of 0.095 € /kWh, this seems very reasonable and even a bit on the low side by 80 percent. However, their model is slightly different as it only offers 600 hours of full operation against the 2,000 hours that model of this study is active. This drastically decreases the influence of the CAPEX on the LCOE, making it a logical approximation. In comparison to (Perez-Mora et al., 2018), which estimated the LCOE at € 0.050 /kWh, it is the same. An increase in plant size most likely will reduce its LCOE.

Table 6.4: KPIs of the companies making IWH source for the base scenario

	Abbott	Agrifirm	ForFarmers	Sensus	
Tj/year	13.3	13.1	1.6	13.3	TJ/year
CAPEX	37.2	3580	1363	37.2	k€
OPEX	43.1	227.9	74	43.1	k€/year
Electricity consumpion	0	197.6	24.1	0	MWh
LCOE	0.012	0.126	0.365	0.012	€/kWh

IWH

The companies providing the IWH were previously selected during a feasibility study. The heat profile is obtained based on the gas consumption, the temperature range of the source, operating hours, the WH percentage of the total gas consumption, and whether the source material is water or air.

For Westenholte the selected companies are shown in table 6.4, with the WH percentage, working hours, type of source and temperature profile. For each company, the length of piping from the source to the delivery point has yet to be determined.

To research the effect of the IWH, the total amount of heat that will be retrieved from the companies can be altered. In the input, the percentage of WH is determined. However, as it will not be beneficial to install IWH retrieving equipment for only half of the available IWH, this has been made discrete. The order in which the IWH would be disconnect from the DH in the case the amount of IWH would be reduced is according to the following; first ForFarmers then Agrifrim, Sensus and Abbott at last.

The output for the DH will be OPEX, CAPEX, electricity consumption and heat generated. For the whole DH for the conservative base scenario, this is presented in table 6.3. The heat profile is provided in figure 6.5, gained according to figure 6.2. With all the equations, the following results are obtained, as provided in

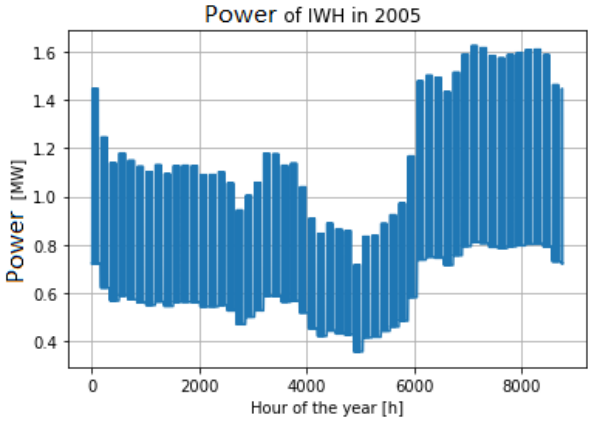

Figure 6.5: Power available from IWH for 2005

table 6.4. The LCOE for the air source company is exceptionally high, whereas the LCOE of the companies providing heat in water sources follows the SDE++ of €0.03/kWh.

6.2.5. Distribution

Each heat supply will be connected separately to a central point in order to prevent co-dependence of the supply piping. The central point will match the supply and demand in time by use of storage. Three substations are connected to the central point to which the heat will be pumped, after which a subnetwork for each substation serves to transmit the heat to the dwellings. The substations each will consist of an HEX and a

Table 6.5: Distribution grid cost of conservative scenario. Distribution costs from sources to storage, storage to demand, and the total are illustrated in figure 5.1.

	CAPEX [M€]	OPEX [k€]	LCOE [€/kWh]
TEW	6.4	132.3	0.0092
STE	8.9	178.7	0.0127
IWH	5	101.1	0.0071
Demand grid	18.2	398.7	0.0265
Total	38.4	810.8	0.0555

pump.

Pumps at the center of each heat source will draw the heat from that source to the central point. The HEX is already placed and is part of the source. From the HEX of the source, water is pumped to the central point. For each heat source, the diameter and length of piping are equal for the different sources and are estimated at supply and return of 3 km, as all heat sources are roughly in a circle of radius 1.5 km.

Water is transported from the central point to the substations, which then transfer the heat through an HEX to the separated consumer network. The consumer network is designed according to Persson and Werner (2010). Over the total length of 20 km, the length of piping per diameter of the piping is evenly distributed.

The only variable for the DH network is the piping material. The material used is dependent on the temperature of the DH network; polymer piping for the progressive and steel for the conservative. However, primary tests have shown that polymer piping can also be used for 70/40 °C networks, on the condition that the pressure does not exceed 8 bar. The investment cost of both different types of piping is expected to be the same per piping diameter. This is because the difference in the source material is small compared to the variance in installation cost. Placing the piping underneath asphalt has a much higher cost than under grassland. For the whole network, it is assumed the ground in which the piping is placed will be equal asphalt and grassland.

The results of the conservative scenario are illustrated in table 6.5. The LCOE of the distribution was found to be 0.056 € /kWh, which is in the range stated by Mazhar et al. (2018) of 0.051-0.1065 € /kWh for 1.1 euro per pound.

6.2.6. Storage

The storage is formed by heat demand and supply. The goal of the storage is to match heat supply and demand in time. This process is highly influenced by the profiles of both the demand and supply. However, the design method is the same and thus indifferent to the heat supply and demand and other input variables used.

Designing the supply starts with taking the difference between the demand and the supply and splitting this into a 24 hours signal, of which the mean over 24 hours is zero, and a yearly signal, of which the mean over one year is zero. The yearly signal will then be used to design the ATES system and the 24-hour signal to design the ST-TES solution.

The ST-TES consists of a tank stratifiedly filled with water. The tank depends on the signal it receives to cover the maximum peak. Furthermore, the T-TES temperature equals that of the DH network. The main cost of this tank is found in the CAPEX, which is directly related to the tank volume and thus to the match between supply and demand. For both cases, the water equivalent volume of the tank follows the method discussed in chapter 5 for the base cases, including the CAPEX and the OPEX. As seen in table 6.6, the size of the tank almost directly matches the estimated amount provided by Guelpa and Verda (2019).

The depth of the ATES is estimated at 100 m and the temperature at 10 - 17 ° C. The efficiency is about constant and an estimated at 80 percent (de Wit-Blok, 2017). The size of the ATES is directly dependent on the seasonal match between supply and demand and the cost is also primarily determined by the CAPEX, which

relies on the size of the ATES. In table 6.6 the size and cost of the ATES are illustrated for the conservative scenario.

Table 6.6: TES results for conservative 70/40 °C base scenario

	Volume [m^3]	CAPEX [M€]	OPEX [k€]	LCOE [€/kWh]
ATES	1,350,000	6.9	43	0.007
T-TES	775	0.4	12	0.001
Total	1,350,775	7.3	55	0.008

6.2.7. Output

The output of all the submodules is provided in OPEX, CAPEX, LCOE, heat electricity, and electricity consumption. Simply adding the individual CAPEX of all submodules gives the final CAPEX, idem ditto for the OPEX. However, as the LCOE is not calculated for the total heat of the network but per submodule, this has to be recalculated. The CO_2 emission is calculated for all the heat sources by multiplying the electricity with the CO_2 equivalent. The results of both base scenarios are provided in table 6.7 and are discussed in chapter 7.

6.3. Individual reference model

A reference scenario that does not rely on the decentral use of natural gas serves to put the results of the DH network into perspective. According to section 2.6, an individual decentralized all-electric scenario gives the most fitting alternative to a DH system. In order to compare these two systems, the KPI for both systems are calculated and compared. The KPIs of the DH system have already been calculated for the base scenarios in the previous chapter. However, the KPIs of the decentralized system are not. To come to these KPIs, the following section will design the decentralized all-electric reference scenario and set up a model to provide the KPIs, after which the latter is calculated. In the literature study in section 2.6, it was found that an air source heat pump seemed to be the best solution as a heat source, without the need for natural gas. In the following section, first, the design of a system based on a heat pump for an individual dwelling will be set up, second, the total electricity consumption will be calculated and lastly, the cost of the decentralized solution will be calculated and contrasted to the current price per kWh and that of the DH network.

For the design of a decentralized heating solution, the scenario with solutions competitive with DH is that of an individual electrical heat pump, supplemented with an electric boiler to fulfil the SH and DHW demand per dwelling. In this scenario, the heat pump will supply the required heat for the SH of the dwelling. The electrical boiler will provide heat for the DHW requirement. This design was also largely previously used as a reference scenario by Knepper (2019) and requires high insulation of the dwellings for the heat pumps to function effectively. When the demand is too high, the heat pump won't be able to subtract enough heat out of the air to heat the house (ECN & TNO, 2016). The required airflow would be too large to be economically viable. A normal temperature for an air source heat pump to produce heat is 35 - 55 °C (ECN & TNO, 2016).

Table 6.7: Results of conservative and progressive scenario's

	CAPEX [M€]		OPEX [k€/y]		LCOE [€/kWh]	
Scenario	Conservative	Progressive	Conservative	Progressive	Conservative	Progressive
IWH	1.40	1.39	117	115	0.0292	0.0288
TEWW	2.04	1.72	246	145	0.0445	0.0498
STE	7.14	2.64	150	56	0.0627	0.0406
TESW	2.97	2.36	321	186	0.0522	0.0603
Total supply	13.55	8.11	833	502	0.0564	0.0527
Demand	0.00	40.26	0.00	185	0	0.0783
Storage	14.50	11.34	48	33	0.0279	0.0326
Distribution	38.44	35.86	405	578	0.0955	0.1491
Total	66.49	95.57	1,286	1,298	0.1844	0.3848

Since this temperature is lower than the required 65 °C by law, an electric boiler will be used to upgrade this heat to 60 °C. Concluding, the all-electric scenario will consist of an air source heat pump, an electrical boiler and additional insulation of all dwellings.

6.3.1. Design of decentralized all-electric reference scenario

To simulate the previous illustrated model, standard values for air-source domestic heat pumps and electric boilers will be used from ECN and TNO (2016). The input of this model will be provided by the already established heat demand model. From the heat demand module, the signals of the central heating demand and the DHW heating demand are separated. Secondly, for both the signals the electricity consumption is calculated. For the heat pump, this implies that first the COP will be calculated based on the outside temperate, after which the electricity consumption can be calculated based on the heat demand using equation 4.10 for a Carnot efficiency of 0.4. For the electric boiler, only the efficiency will need to be considered to get the electrical demand. With the electricity demand per typical dwelling, the total demand can be calculated as a third step. Finally, the CAPEX, OPEX, LCOE and CO_2 will be calculated using the same pricing construction as for the DH network, except the electricity price. For normal consumers, this price is doubled, as tariffs differ per user size.

Starting from the CAPEX, which consists of the insulation cost, the heat pump cost and the electrical boiler cost, the CAPEX of the heat pump is estimated at € 5,100.- including installation, the boiler is then estimated at € 1000.- euro per dwelling. The insulation cost is previously determined in 3.1 and for the whole of Westenholte are estimated at on average € 7,800.- per dwelling.

The OPEX is determined by the maintenance and operation costs, where the operational cost is largely determined by the electricity for the boiler and the heat pump. The electricity price for an average dwelling is estimated at €0.22 in comparison to € 0.053. The maintenance cost then consists of 3 percent per year of CAPEX of the heat pump, where the insulation and electrical boiler are considered to last the 30 year lifetime.

6.3.2. Output

The following CAPEX and OPEX, LCOE and CO_2 emission are found for the “all-electric” individual heating by heat pump and boiler scenario for Westenholte, which are illustrated in table 6.8. The CAPEX thus consist of the costs for insulation, heat pumps, and electrical boilers per dwelling and include the secondary, extra, and unforeseen costs discussed in section 4.3.4. Notably, the average heat price of gas is roughly € 0.085 /kWh.

Table 6.8: KPI of reference all-electric scenario, including the average COP of the heat pump

	Ref_model	Unit
CAPEX	29	M€
OPEX	2.4	M€/year
LCOE	0.22	€/kWh
CO_2	49	ton/year
SCOP	2.7	

7

Discussion and optimization

7.1. Introduction

In this chapter, the optimal distribution of heat load over the heat sources will be conceptualized, calculated and evaluated. To conceptualize the optimal scenarios, first, the results of chapter 6 will be discussed. The previously chosen variables per scenario are evaluated on their impact on the KPIs. This evaluation will result in a prognosis on how the distribution of heat load could optimize the KPIs for the two different scenarios. After the prognoses, a sensitivity analysis will be performed for both scenarios with variable heat loads per source. The result of the sensitivity analysis will then be evaluated with the prognoses to conclude the distribution of the heat load over the heat sources.

7.2. Discussion results of chapter 6

Three scenarios were simulated in the DH model in chapter 6: the conservative scenario, the progressive scenario, and the individual scenario. The KPIs of these scenarios will be compared in this chapter. Per submodules of the DH model, the impact of various parameters on the KPIs will be evaluated: CAPEX, OPEX, LCOE, and CO_2 emissions. The total KPIs from the scenarios will be compared and lead to a prognosis on the optimal distribution of the heat load at the sources.

7.2.1. Demand

Starting with the first submodule of the DH model: the heat demand. The most impactful difference between the scenarios from the heat demand module's parameters is the effect of the insulation, which reduces the heat demand significantly; from 110 to 70 TJ per year. This difference of roughly 40 TJ/year will have a large impact on the total cost between the scenarios.

Looking at the impact on the KPI, a reduction in heat supply will instigate a reduction in all costs related to heating the dwellings as well as a reduction in CO_2 emissions. However, even when assuming a constant LCOE of all other submodules, the additional investment cost of the insulation logically will increase the LCOE of the total system. All in all, the € 0.052 paid per saved kWh of heat roughly equals the price for kWh of natural gas. These costs should be covered by the decrease in demand, as the consumption is less and the total cost and consumption of the DH are reduced.

The other parameter concerned with the heat demand is the additionally required boiler for DHW. The CAPEX of the boiler remains insignificant in comparison to the cost of the insulation. However, the OPEX is significant, as the heat DHW demand does not change with insulation. The electric boiler needs to upgrade the temperature with 60–(50 − 2) = 12 K of which is approximately 20 percent of the total heat required to upgrade normal tap water to hot tap water. Because the boiler is relatively inefficient compared to a heat pump, a large amount of electrical power is needed for the heating, instigating a large increase in CO_2 emissions. Section 7.2.5 offers a comparison of these values to other submodules of the total DH model.

7.2.2. Supply

The KPIs of the different heat sources can be fully compared for both scenarios. As all heat sources produce similar amounts of heat per scenario, it is an ideal starting point for the comparison of the different sources and their KPIs. Starting with the CAPEX, figure 7.1a shows that the largest CAPEX belongs to solar thermal energy, which is strongly dependent on the amount of heat that needs to be produced. A reduced production allows a reduced CAPEX. This decline in CAPEX is visible for all other sources, except for IWH, as this production does not differ per scenario.

For the supply, the scenarios can fully be compared for all the KPI. As all heat sources produce roughly the same amount of heat per scenario, it is an ideal starting point for the comparison of the different sources and their KPI's. Starting with the CAPEX, as illustrated in figure 7.1a, the largest CAPEX belongs to solar thermal energy, which is strongly dependent on the amount of heat that needs to be produced. Since the production has been reduced, also the CAPEX has been reduced. For all other sources, this decline in CAPEX can also be seen, except for IWH, as this production does not differ per scenario.

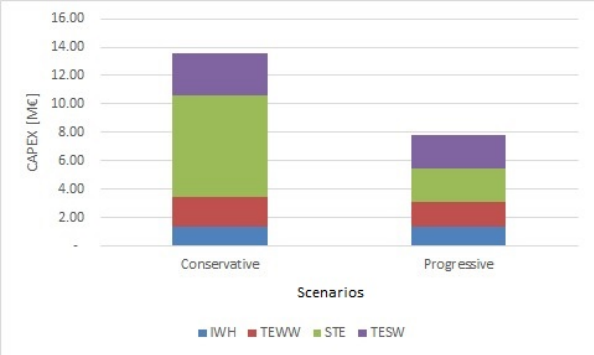

(a) CAPEX of different heat sources for progressive and conservative base scenarios

(b) OPEX of different heat sources for progressive and conservative base scenarios

Figure 7.1: Cost of heat sources for base scenarios

The OPEX illustrated in figure 7.1b also decreases significantly with a lowered heat demand, as less heat needs to be provided by the heat sources. The other reason for a lower OPEX in the progressive scenarios, compared to the conservative scenarios, is the higher efficiency of the heat pump at all sources, except solar thermal energy. The most notable difference in the OPEX between the individual heat sources is found between the water-based sources and the solar thermal energy: Solar thermal energy has roughly half of the operational cost compared to the water-based sources. This can be explained by the difference in heat production method. The water-based sources need a heat pump to upgrade the heat, which consumes a large amount of electrical energy. On the contrary, a heat pump is not required for solar thermal energy, significantly reducing the cost.

Figure 7.2: LCOE of different heat sources for progressive and conservative base scenarios

The LCOE is evaluated for the heat produced per source over a lifetime of 30 years. The effect of the heat

pump dependent heat source is most notable in figure 7.2, as the cost is scaled to produced heat. Both the heat pump dependent water-based sources have a higher LCOE for the progressive scenario compared to the conservative scenario. This however differs for the solar thermal energy source. For this source, the efficiency of this source increases as heat losses reduce with a lower DH temperature, resulting in a decrease in the LCOE with a lower distribution temperature. This compensated for the linear price decrease per installed MW of solar thermal energy, resulting in an overall higher advantage of temperature difference versus the decrease in size of the source.

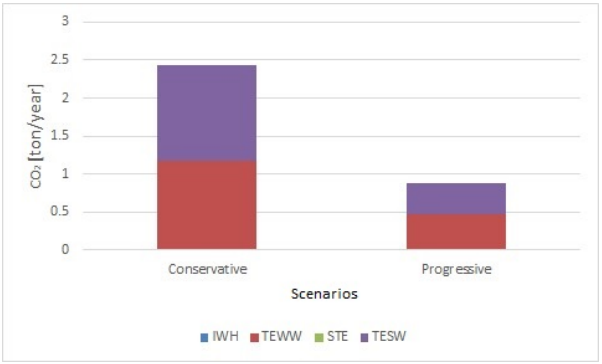

Figure 7.3: CO_2 of different heat sources for progressive and conservative base scenarios

Figure 7.3 shows that the CO_2 production of the IWH and solar thermal energy are negligible in comparison to the heat pump dependent water-based sources. The decrease in heat demand and increase in heat pump efficiency are both dominant factors in the lowering of the total emitted CO_2 as a result of the electricity consumption.

For the heat supply of the reference scenario, the CAPEX of the heat-producing heat pump for the whole of Westenholte is estimated at € 29,000,000.- . The CAPEX of the heat source is higher than the combined CAPEX of all other heat sources used in the DH. The lower source temperatures (temperature of air versus the water-base sources) also decreases the efficiency of the heat pump and results in a higher OPEX at € 2,400,000.- as the efficiency of the heat pump is far lower due to lower source temperatures. Additionally, the electricity cost € 0.22 /kWh, is far higher than the industrial electricity price of €0.053 /kWh. The CO_2 is also higher due to the lower HP efficiency but is roughly equal to the total DH model.

Based on the sensitivity analysis of the heat sources, the water-based sources present the lowest overall CAPEX, while STE offers the lowest overall CAPEX as well as CO_2 emission. When considering the overall cost, the water-based sources also produce a lower LCOE. Thus, a balance needs to be found in cost and CO_2 emission.

7.2.3. Storage

The relative differences in the KPI of TES are provided in figure 7.4. It presents lower CAPEX and OPEX yet higher LCOE for the progressive scenario. As an increase in volume reduces the price per m^3 of storage for both types of TES, the larger the storage, the smaller the relative CAPEX per amount of heat stored, which is also illustrated by equation 5.14. On the contrary, the OPEX is reduced linearly with a reduction in total stored volume. The combination of the increase in the relative cost of CAPEX is enough to increase the LCEO. The reduction in heat demand does have a positive effect on absolute CO_2 emission, as illustrated in the most right part of figure 7.4. The progressive scenario thus will have a large LCOE no matter the amount of heat. The difference in KPIs between scenarios is already slightly less as the peak supply of the progressive scenarios already reduces the total required storage volume. In case the scenarios would have equal peak supply, an absence of the peak supply for the progressive scenario, the KPIs would differ even more.

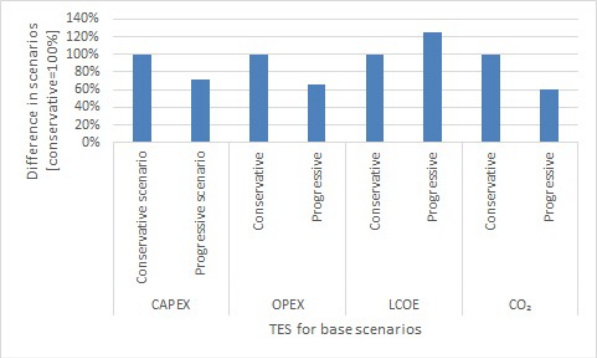

Figure 7.4: KPI of TES for progressive and conservative base scenarios

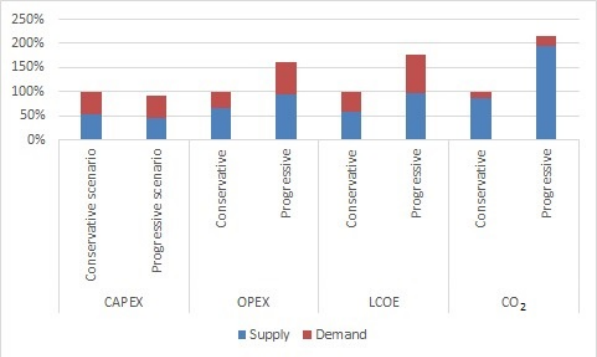

Figure 7.5: KPI of distribution for progressive and conservative base scenarios

7.2.4. Distribution

The cost of distribution is separated into the cost of the supply part of the distribution grid and the cost of the demand part of the distribution grid. The supply part connects the heat sources to the storage facility and the demand part connects the storage facility to the dwellings, also illustrated in figure 5.1. This division enables a clear overview of the different impact the scenarios make. In figure 7.5, the KPIs are illustrated relative to the total KPIs of the conservative scenario. Starting with the CAPEX, it becomes visible the supply and demand of both cases are relatively the same. However, the CAPEX of the progressive scenario shows a slight decrease in cost. This, most likely, is a result of the decrease in heat demand. When comparing the CAPEX of the supply and demand distribution grid, the diameter and length of the piping present a relatively simple explanation for the same CAPEX: The wider the diameter, the higher CAPEX of the piping. Even though the total length of the supply grid is lower than that of the demand grid, the diameter of the supply grid is far larger, resulting in roughly similar costs for both.

For the OPEX and CO_2 emission, the effect of the difference in temperature regime is most obvious as both increases with a decrease in temperature of the DH network. More water has to be transported for the same amount of heat. This effect is so large that even the reduced heat demand does not compensate for this change. When contrasting the supply and demand grids, the demand has both notably lower OPEX as CO_2 emission because the piping is placed in parallel, requiring less pumping power compared to the sources. The relative distance from storage to the dwelling thus becomes far shorter, even the total piping length is significantly longer than that of the supply. This reduction in length reduces the required pumping power.

Finally, an increase of LCOE for the progressive scenario is obvious as both the CAPEX and OPEX are higher and the heat supply is lower. The ratio of demand and supply remains the same for both cases. Figure 7.5 serves to clarify that the supply part of the distribution exceeds half of the KPIs of the total and thus will have a significant impact.

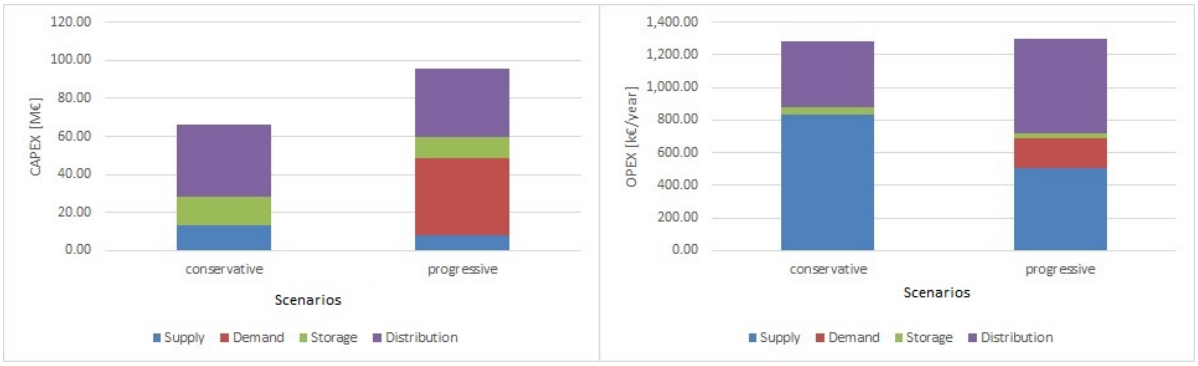

(a) CAPEX of progressive and conservative base scenarios

(b) OPEX of progressive and conservative base scenarios

Figure 7.6: Cost of progressive and conservative base scenarios

7.2.5. Total comparison of scenarios

The results of both base scenarios from table 6.7 are depicted in the figures 7.6a, 7.6b, 7.7 and 7.8. However, instead of the total amounts of each KPI, the relative amount is provided. The relative amount is the value of the KPI divided by the amount of the total for that KPI of the conservative scenario. For example for the CAPEX of the demand of the progressive scenario is roughly 30 percent of the total CAPEX of the conservative scenario. The relative presentation provides a more easy comparison method as the absolute values do. What the following figures predominately illustrate's is a summary of the previous DH sections. As the main research question revolves around comparing the LCOE and CO_2, the latter will be dealt with in this section.

Altogether, the progressive demand appears more expensive than the conservative scenario, this is illustrated for both the CAPEX, OPEX and also the LCOE. However, the CO_2 emission is significantly reduced in comparison to that in the conservative scenario. The most obvious reason for this reduction is the decrease in heat demand resulting from the insulation used by dwellings in that scenario. Additionally, the progressive scenario does not use a natural gas-based heat source for the peak load. The second reason less CO_2 is produced is that the heat pumps in the heat sources are more efficient with a lower distribution temperature, as explained in section 2.2.1.

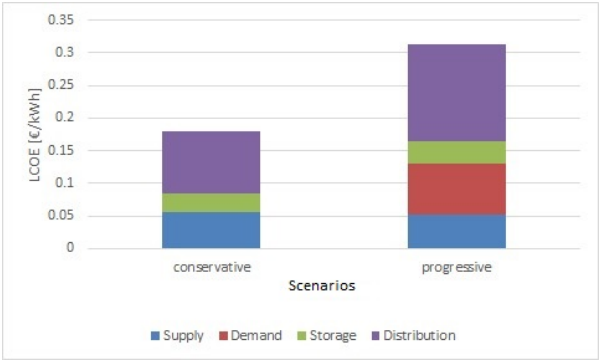

Figure 7.7: LCOE for progressive and conservative base scenarios

The reduction of CO_2, however, comes with a price: adaptation to a lower DH distribution temperature. This includes both the insulation to facilitate a lower distribution network, as well as the boilers required to upgrade the heat. As illustrated in figures 7.6a, 7.6b for both the OPEX and the CAPEX, the cost are respectively what makes the total cost of the progressive network higher. The real question which thus remains is whether or not the LCOE should be the lowest or the CO_2.

Based on these findings, it is expected that IWH in combination with TESW or TEWW will have the lowest overall price for the DH. IWH scores best on all KPIs but is unable to provide enough heating for the whole of Westenholte. TEWW and TESW present fewer distribution costs than solar energy, as the heat profile has

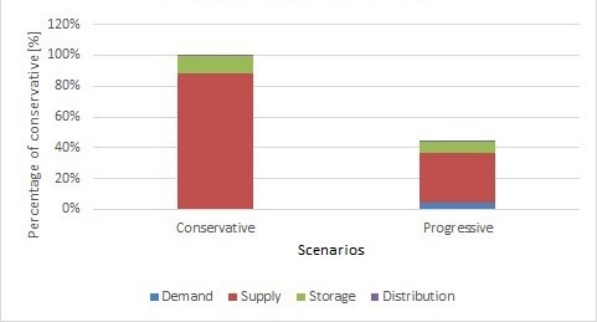

Figure 7.8: CO_2 for progressive and conservative base scenarios

lower variance and because they share the same location. The latter effect might be able to compensate for the higher LCOE of the water-based heat sources.

7.3. Optimization of heat sources

To answer sub-question 6 of what is the optimal scenario of heat load over the heat the DH model will be optimized for both LCOE and CO_2 by performing a sensitivity analysis. This will be done by decomposing the model into submodels, after which the KPIs are calculated per submodule for the different heat load distribution scenarios and DH temperatures. The KPIs of the submodules are then added to come to KPIs of the total model resulting in the final optimal heat load distribution over the heat sources for the lowest LCOE and CO_2 emissions for the two different temperature regimes.

The model constructed in the programming language Python is not computational fit to analyze the whole system. Therefore, the submodules are individually optimized, whilst still obtaining results similar to optimization of the entire model. The optimization method and model are further illustrated in appendix B. The final optimized result from the appendix is discussed in the following section, these studies will be combined to provide the optimal distribution for the different supply temperatures and LCOE and CO_2.

7.3.1. Optimal distribution of heat load over sources

The result of the optimization of appendix B is presented in figures 7.9 for the total cost and 7.10 for the CO_2 emission.

The DH network is optimized by varying the amount of heat provided per heat source. This results in different costs and CO_2 emissions per scenario. Since IWH was found to be the cheapest and least CO_2 emitting heat source, the maximum amount of IWH will be applied to all scenarios analyzed. This leaves three heat sources supplying distinct heat totals: TESW, TEWW, and solar thermal energy. The heat loads of these sources will vary from providing all heat for the entire DH per one source to being excluded from the used sources. For example, this could mean that IWH will provide 25 percent of all heat required, TEWW 75 percent, and no other heat sources. However, it could also mean that in addition to the IWH only TESW or solar thermal heat will be used.

For example, this could mean that IWH will provide 25 percent of all heat required, TEWW 75 percent, and no other heat sources. However, it could also mean that in addition to the IWH only TESW or solar thermal heat will be used.

Results of optimization

The total DH cost, CAPEX in addition to all the OPEX over the DH's lifetime, is optimized for the total lifetime of a DH network in figure 7.9. In figure 7.9 and 7.10 the total cost and CO_2 emission for the various heat distribution scenarios: The y-axes depict the percentage of the heat amount from either TEWW or TESW. Besides IWH, the upper left corner shows the sole use of TESW, while the lower-left corner depicts the sole use of TEWW. The x-axis illustrates the amount of solar within the total heat supply mix: Left in the figure,

only solar thermal energy is used in addition to IWH. An equal contribution of all heat sources, in addition to IWH, can thus be found in the middle of the figure. The resulting values are then scaled from 0 to 1, as illustrated in the color bar next to the figures. The zero represents the lowest value and 1 the highest.

Discussion of optimization

In figure 7.9, what is first notable is that the solar thermal energy source leads to the most expenses. This also does not happen gradually but step-wise. This most likely results from the distribution cost, which follow a similar pattern. The cost of distribution increase relatively stepwise as wider dimensions of piping result in higher CAPEX in steps. The second conclusion which can be drawn from the figure is that the difference between using TEWW, TESW or a combination of both is minor. Ultimately, these figures thus provide profit for primarily using TEWW/TESW for the lowest cost.

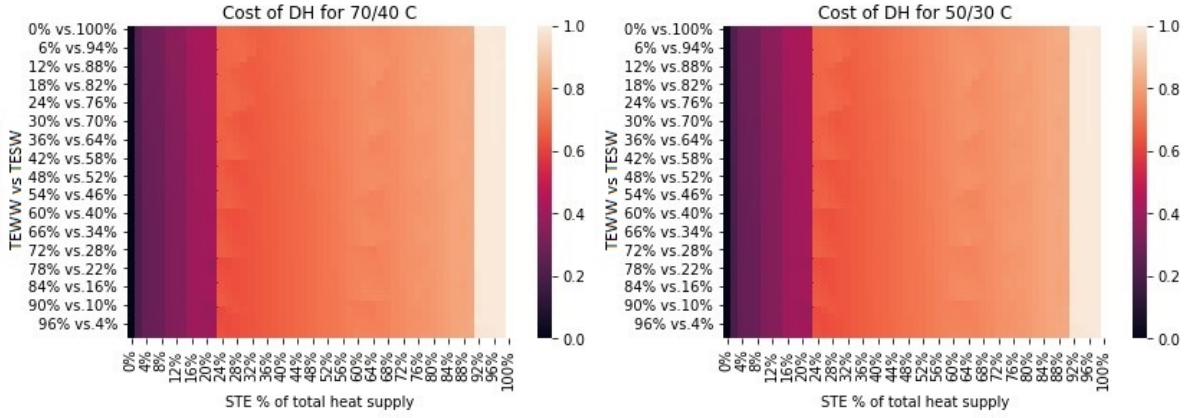

(a) Relative cost of 70/40 °C DH of Westenholte

(b) Relative cost of 50/30 °C DH of Westenholte

Figure 7.9: Relative cost of DH of Westenholte. The y-axis presents the percentage of TEWW vs TESW and the x-axis presents the amount of solar thermal energy versus amount of TESW and TEWW. 1 is for the highest possible cost and 0 the lowest.

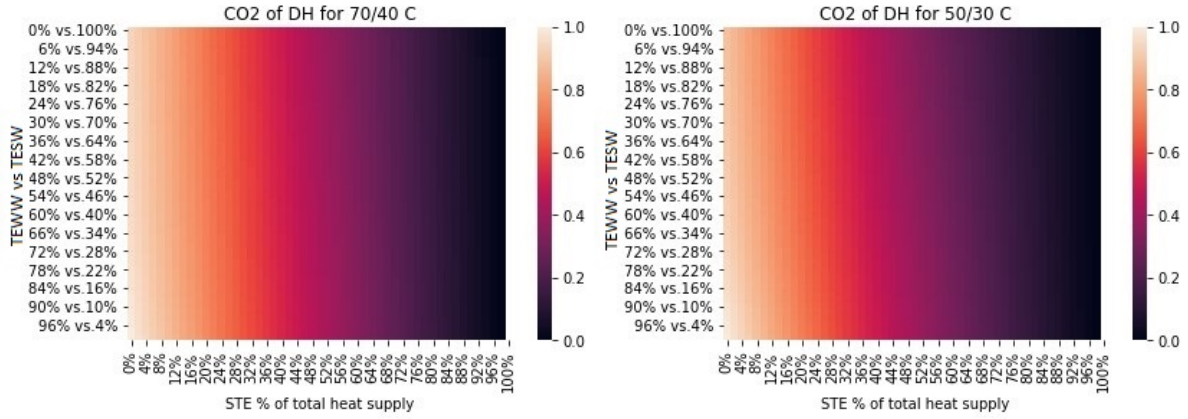

(a) Relative CO_2 emission of 70/40 °C DH of Westenholte

(b) Relative CO_2 emission of 50/30 °C DH of Westenholte

Figure 7.10: Relative CO_2 emission of DH of Westenholte. The y-axis presents the percentage of TEWW vs TESW and the x-axis presents the amount of solar thermal energy versus amount of TESW and TEWW. 1 Is for the highest possible CO_2 emission and 0 the lowest.

The result of the cost optimization, as described in the previous paragraph, stands in great contrast with the CO_2 emission. Figures 7.10 shows that the CO_2 emission is the lowest when primarily using solar thermal energy. The transition from TEWW/TESW to solar thermal energy also happens gradually, opposed to the cost, because heat sources TEWW and TESW are the primary producers of CO_2 emission and solar thermal energy the lowest. When the heat load from the water-based heat sources is gradually shifted to the solar thermal energy, so will the CO_2 emission while solar thermal energy is the lowest. When the heat load from

the watery heat sources is gradually shifted to solar thermal energy, the CO_2 emissions will consequently decrease. The key difference here is that the total cost is primarily influenced by the distribution cost, which increases step by step, whilst the CO_2 emission is mainly influenced by heat production, which increases gradually. Overall, a trade-off is illustrated between cost and CO_2 emission. It will be up to the designer of the network which they consider to be of the highest importance. This conclusion reflects the prognoses almost perfectly.

The lowest cost scenario for both temperature scenarios comes down to 25 percent IWH, 55 percent TEWW and 20 percent TESW, in addition to a peak supply. This leads to the respective CAPEX, OPEX, LCOE and CO_2 emission illustrated in table 7.1. For a minimal CO_2 emission, the heat load mixture consist of 25 percent IWH and 75 percent solar thermal energy, leading to the KPIs also included in table 7.1.

Table 7.1: Results of optimization of heat load over heat sources

Scenario	Minimalized	CAPEX [M€]	OPEX [M€/year]	LCOE [€/kWh]	CO_2 [ton/year]
Conservative	LCOE	52.02	1.156	0.1492	34.67
	CO_2	79.17	1.092	0.2051	4.3
Progressive	LCOE	88.13	1.257	0.358	16.19
	CO_2	102.64	1.165	0.4015	2.76

Comparison of DH network to the all-electric reference scenario

Starting the KPI comparison of the all-electric reference scenario versus the optimized scenarios with the CAPEX, directly a large difference is encountered: the largest difference in CAPEX is estimated at € 70,000,000. This is explained by the additional equipment required for the DH network. However, the OPEX of the DH network is lower than half of the OPEX of the reference scenario, also leading to lower LCOE for the progressive scenario. This difference can most likely cause by the increased efficiency of heat generation, as also the CO_2 emission of the optimized DH scenarios is lower than that of the reference scenario. Since the CO_2 predominantly is produced as a result of the electricity production, less energy is required to produce the same amount of heat, since this emission is lower for the optimized DH than that of the reference scenario. This conclusion is also established in the heat production discussion, found in section 7.2.2.

8

Conclusion and recommendations

8.1. Introduction

In the previous chapters, the KPIs of the DH network for Westenholte for the heat sources TEWW, TESW, solar thermal energy, and IWH were optimized for the two temperature regimes 70/40 °C and 50/30 °C. In this chapter, the conclusions for these optimizations will be summarized and connected to the other conclusions drawn previously. First, the answers will be provided per sub-research question, as formulated in section 1.2. Subsequently, the sub research question, the main research question will be answered, providing the final conclusion. The recommendations for further research regarding the multi-RES DH network will be provided per chapter, to stimulate continued research on the feasibility of multi-source DH networks.

8.2. Conclusion

The purpose of this research is to find an alternative to the natural gas-fueled heating systems of dwellings for the neighbourhood of Westenholte. The reason for replacing this system is to prevent GHG emissions resulting from the combustion product of natural gas (CO_2), in addition to the greenhouse effect that natural gas has.

DH for Westenholte with RES

The proposed solution is to replace this GHG intensive system with a DH network, which was compared to a decentralized all-electric solution for reference. Neither solution requires the vast amount of natural gas needed by the traditional system, so both could lead to the desired reduction in CO_2 emissions. The DH network, on the one hand, adopts central renewable heat sources, of which the heat is then distributed to the dwellings. The decentralized all-electric solution, on the other hand, will use an individual heat pump and electrical boiler per dwelling for heat generation.

Research effect of temperature and heat sources on KPI

However, constructing and using a DH network would involve a large investment with total costs that might be higher than that of the traditional, CO_2 emission-intensive, heating system. For this reason, the cost of a new DH should be minimalized. To investigate both the cost and CO_2 emission, the following KPIs were selected: CAPEX, OPEX, LCOE to quantify the cost and CO_2 emission to indicate the difference in GHG emissions.

Two temperature regimes of the distribution temperature of the DH were calculated and optimized for the neighborhood of Westenholte. Using a lower temperature (50/30 °C) in comparison to the more conventional temperature (70/40 °C) would successfully reduce the KPIs. Lowering the distribution temperature would raise the heat pumps' efficiency, so reducing the overall cost.

Additionally, the DH could probably be made less GHG-emitting and cheaper by using multiple renewable heat sources. As the heat profile over time differs per heat source, a combination of the energy sources

would offer a better match with the heat demand profile, reducing the required heat storage and associated CO_2 emission and cost.

To research the latter two suspicions, a DH model was created, calculating the KPIs. Several sub-questions needed to be answered to come to a state-of-the-art model. Finally, optimization of the results led to an answer to the main question.

8.2.1. Answering sub-questions

Sub-question consumer end :

1. How can the demand for domestic buildings, set for 2022 and the near future, be modelled for the temperature regimes low and middle on an hourly basis for three or more years?

The heat demand of the DH network was modeled through an appropriate combination of historic and deterministic modeling. Specifically, the methods found most suitable for modeling the heat demand are based on these two categories. For both categories, a tradeoff between the accuracy versus computational cost and availability for data resulted in an optimal heating degree day method based on typical dwellings. However, an additional deterministic element to the model prevented an inaccurate fit of the heat demand and the solar heat supply. The model was able to accurately predict the heat demand for 15 years, based on the weather data available from the KNMI and the dwelling data from the RVO. Furthermore, the demand could be predicted for both temperature regimes by incorporating insulation into the dwellings for the lower temperature regime.

Sub questions heat supply :

2. What is the state of the art of the components for the different RES used to acquire energy for DH?

For the RES, the state for the art of the mechanical model was found as depicted in figure 6.2. For TESW, an open type of configuration was found to provide the best overall results. The water for this setup was pumped from the river the IJssel into a P-HEX which then transported the heat to a heat pump. The heat pump transported the heat on its turn to the distribution grid of the DH. For TEWW, instead of river water, the effluent of the sewage treatment is used. Harvesting IWH is fairly similar to that process. When the source material, which was either air or water, drops below the DH temperature, a HEX would transport the heat to the heat pump after which the upgraded heat was presented to the DH network.

In contrast to the above-mentioned source, in case the source temperature raised higher than that of the DH, no heat pump was required to upgrade the heat. For the IWH and solar thermal energy heat sources, such situations were found. The step of the heat pump could just be skipped for IWH. However, the solar thermal energy required a different approach, as FPC is used to harvest heat from the sun. A grid of FPCs was designed, heating the thermal fluid in several FPCs, after which the thermal fluid was led to a central location to exchange its heat using a P-HEX to the distribution grid. Figure 6.2 schematically illustrates this process.

3. What is the most suitable modelling method for each individual RES?

Different methods were examined to find the best method for modeling the RES. In general, the first step was to estimate the gross heat potential and the total heat potential for the DH network following a heat pump model. The model for the gross heat potential for TEWW and TESW was based on a combination of simple linear regression models. For solar thermal energy, the method as described in the common European standard most accurately approached the computational time allotted for the model. For IWH, the average waste heat profile of the food section and the gas usage found on the postal code allowed for a rough estimation. The cost was then calculated based on the setup in combination with a heat pump model as depicted in figure 6.2, consisting of (a) pump(s), P-HEX, piping and a heat pump (if required).

Coupling of demand and supply :

4. What is the most optimal type of distribution network to supply heat to consumers?

In general, the optimal type of distribution found was the ring network because it kept pressure differences fairly low. Polymer turned out to be the ideal piping material for the lower temperature regime of the DH, as maximum velocity is relatively high at the same cost. For the medium temperature regime of the DH, the best material to be used was ST/PUR/PE, as this the most conventional and the best in the used design method according to the Kennisinstituut voor Installatietechniek (2012).

5. What is the most optimal type of storage to compensate the mismatch in heat supply and demand?

The best type of storage seasonal storage was the ATES combined with T-TES for short-term storage. The ATES offers relatively cheap storage and does not require a vast amount of space above ground, thus an ideal seasonal storage method for the densely populated area of Westenholte. It is also an established technology in the Netherlands of TLR 9. T-TES proved to be the best fitting short-term storage, as its charging and discharging cost is small. This type of storage also eliminates the need for pressure vessels acting as a pressure buffer. In addition, it decreases the pipe diameter, as well as the cost of the ATES.

6. How can an optimal configuration of the different heat sources be found, minimizing CO_2 emissions and LCOE?

The optimal source configuration for both scenarios for the baseload was adopting three of the four companies suitable for IWH. Dividing the remaining heat load allowed for 20 percent TESW and 80 percent TEWW while the LCOE was to be kept to a minimum. If the CO_2 was to be minimized, the optimal configuration was that of IWH in combination with solar thermal energy. These results were found for both temperature regimes.

8.2.2. Answering the main question

What are the LCOE and CO_2 emission of multi-source DH systems with supply/return temperatures of 70 / 40 °C and 50 / 30°C and decentralized all-electric heat pump systems for space heating and DHW heating of the 2177 dwellings of Zwolle's district Westenholte?

The multi-source DH system of 70/40 ° C has an optimal LCOE of 0.15 €/kWh for a heat load distribution for the baseload where 25 percent of the heat load is covered by IWH, 60 percent by TEWW and 15 percent by TESW in addition to a peak load heat source. The CO_2 emission on the other hand was found to be the lowest for heat load distribution of 25 percent IWH and 75 percent solar thermal energy of 4.3 ton CO_2/year, for an LCOE of 0.21 €//kWh.

The multi-source DH system of 50/30 ° C has an optimal LCOE of 0.35 €//kWh for a heat load distribution where 25 percent of the heat load is covered by IWH, 60 percent by TEWW and 15 percent by TESW. The CO_2 emission on the other hand was found to be the lowest for heat load distribution of 25 percent IWH and 75 percent solar thermal energy of 2.76 ton CO_2/year, for an LCOE of 0.40 €//kWh.

The reference case was found to have an LCOE of 0.22 €/kWh and a CO_2 emission of 49 ton/year. This makes the reference solution financially on the same scale as the DH, however, the CO_2 emission is far higher.

These results lead to the conclusion that, financially, a conservative scenario with a heat load distribution of 25 percent IWH, 60 percent TEWW and 15 percent TESW in addition to a peak load supply is the best solution financially. Regarding the emissions, the best solution is a progressive scenario with a heat load distribution of 25 percent IWH and 75 percent solar thermal energy. The latter solution would lead to an emission of 2.76 ton CO_2/year, but this reduction in CO_2 emission would trigger a 100 percent price increase.

8.3. Recommendations

This research has as the main goal to provide techno-economic analysis of a DH for two temperature regimes, with the focus on the use of multiple RES to lower the cost and CO_2 emissions. For further research into this topic, recommendations resulting from this study will be provided per chapter.

8.3.1. Literature
This study intends to answer whether or not a combination of heat sources would be beneficial in reducing cost and CO_2 emission. However, whilst studying the available literature, it has become clear that more research is required to provide a good indication of the feasibility for a multi-source DH varying in DH grid temperature.

8.3.2. Demand
The heat demand was greatly simplified as the heat demand will differ per dwelling over time. A more extensive model including solar energy and consumer behavior per dwelling would be beneficial. Both factors are incorporated in the model to a certain extent, however, they could still significantly reduce or increase the overall heat demand of the DH network.

The error of the model producing the heat demand was found to be ± 3 percent in absolute heat demand, which does not reflect all inaccuracies. The heat demand profile is only verified with the absolute total heat demand, so the total heat used over time. Verification should, however, also include comparing two heat profiles over time for Westenholte.

Additionally, the model used for the dwellings from the RVO was accurate around the date of creation but can now be considered slightly outdated, as it does not incorporate dwellings built after 2006. The error of this model is both prevailing into what extend dwellings can be insulated, as well as the cost for this insulation, including inflation compensation and subsidy of the government for these measures. Although, the latter roughly cancel each other out (Milieucentraal, 2021).

8.3.3. Supply
For the water-based heat sources, TEWW and TESW, the temperature and volume flow are reasonably well approximated. The estimated cost as seen in equation 4.22, however, could be improved. The secondary cost, indicating the cost of the additional required equipment to facilitate the core equipment, is calculated by utilizing the multiplication factor of the raw material cost. Even though this will suffice as an initial approximation, the overall accuracy is not satisfactory. As this method of cost calculation is used for the entire network, the overall cost should be defined more accurately. This includes all the secondary, extra and unforeseen cost, and also the maintenance costs per year as a percentage of the CAPEX.

The solar thermal energy model provides a sufficient initial approximation, as also determined by the European Union (European Solar Thermal Industry Federation, 2012). However, the presented method lacks dynamic modeling of the heat losses occurring when using the FPC. These heat losses include, for example, the heat-up time in the morning and the cooling-down time in the evening. Extra factors should be taken into consideration to compensate for this lack of calculations.

The second proposed improvement involves the location of the FPC. The placement of the FPCs on the ground near Westenholte will, most likely, face resistance of the inhabitants of the dwellings in or nearby Westenholte. This issue could be prevented by placing the FPC on a rooftop. However, that would require a more extensive assessment of whether or not the FPC can be placed on top of the roof.

The IWH approximation is largely based on assumptions for the quality and profile of the IWH, as IWH is largely classified for public use. A method should be developed to deal with a classification method that both enhances the information, whilst preventing a harmfull impact on the competitive position of companies. This would not only help with the current DH and its accuracy but also could increase the total use of IWH in all future DH networks.

8.3.4. Coupling of heat demand and supply
Distribution

As for the distribution, a couple of improvements could be made. To start, the layout of the distribution grid was based on a more general approach for a random DH network. This layout should be optimized to include the specific geography of Westenholte. For the distribution network of the heat sources, the layout of

each heat source has an own piping network to the central storage point, which might result in a larger cost when compared to a ring network. Secondly, the material used for the distribution of the medium regime network was steel. If possible, replacing steel with polymer piping could reduce the distribution cost. Lastly, the OPEX was calculated based on a perfect network in which the maximum velocity is only reached once or twice in the lifetime of the grid. This is an unlikely scenario for a realistic DH network.

TES

The functioning of both TES solutions has been simplified and assumptions were made. The most significant of these assumptions is the efficiency of the storage system. In contrast to the real-world ATES system, in the model, a constant efficiency over time is assumed. Additionally, the efficiency is also assumed for an average ATES found in the Netherlands. Both attributes of the efficiency should be locally investigated in order to come to a more realistic model. The design of the TES and the resulting CAPEX for both storage types was calculated using a basic general equation and might differ depending on the location. Further research should include a method that can easily assess the cost on local parameters more easily without a large computational burden.
Additionally, this general approach lacks information on efficiency and pumping cost. The efficiency was determined based on the general efficiency for the Netherlands and does not increase with time, which is unlikely. The pumping cost also did not include the pressure drop over the filter used in the ATES to regain water from the aquifer, which might increase the cost. Although these changes will, most likely, not cause any significant changes in the cost to the model, further research should investigate the latter.

8.3.5. Total model

For the total model, key assumptions are made for the electricity price and the associated CO_2 emissions. The electricity price is assumed to be fixed over time, however, as the coverage of DH over the whole of the Netherlands increases, this price will become higher as demand increases. In this study, the CO_2 intensity of the electricity is approximated by taking the average over 2018. As the price of the electricity fluctuates, so does the CO_2 emission intensity. Therefore, to improve the model for both the price and the CO_2 emission, also the cost and CO_2 emission should be modelled on an hourly basis.
Additionally, to further improve the model, cooling of dwellings should also be incorporated. With the expected temperature rise according to the Paris agreement, the demand for cooling will increase significantly. To research the feasibility of DH, this could play a key part, as demand for the DH would be throughout the year instead of only during the colder days.

A

Appendix A

Table A.1: Archetype buildings based on type of building and year of construction with current gas usage, improved gas usage and associated cost and total window area according to Agentschap NL (2011a).

Type of dwelling		Construction period		Gas usage [m^3]	Improved gas usage [m^3]	Improvement cost	Window area [m^2]
house	Detached	0	1964	4.731	1.496	15.510	28,3
house	Detached	1965	1974	4.110	1.602	16.870	35,3
house	Detached	1975	1991	2.616	1.581	16.490	34,7
house	Detached	1992	present	1.882	1.702	2.580	39,6
house	Semi-detached	0	1964	3.453	1.194	13.400	26
house	Semi-detached	1965	1974	3.046	1.233	13.990	31,3
house	Semi-detached	1975	1991	1.915	1.234	14.230	26,4
house	Semi-detached	1992	present	1.497	1.296	3.680	29
house	Terraced	0	1945	3.337	1.106	11.480	22,9
house	Terraced	1946	1964	2.246	953	7.880	23,2
house	Terraced	1965	1974	2.030	1.050	8.980	27,1
house	Terraced	1975	1991	1.542	1.037	8.240	21,1
house	Terraced	1992	present	1.135	1.077	1.000	23,6
Apartment building	'maisonette'	0	1964	2.693	799	7.810	20,3
Apartment building	'maisonette'	1965	1974	1.493	767	7.900	20,3
Apartment building	'maisonette'	1975	1991	1.081	763	6.830	16
Apartment building	'maisonette'	1992	present	833	798	450	18,4
Apartment building	'galerij'	0	1964	875	513	3.550	20,7
Apartment building	'galerij'	1965	1974	1.339	807	5.340	20,7
Apartment building	'galerij'	1975	1991	747	513	5.214	15
Apartment building	'galerij'	1992	present	606	583	770	17,2
Apartment building	'portiek'	0	1945	1.489	510	11.201	15
Apartment building	'portiek'	1946	1964	1.162	532	6.084	31,6
Apartment building	'portiek'	1965	1974	981	550	3.700	19,5
Apartment building	'portiek'	1975	1991	849	644	4.110	13,9
Apartment building	'portiek'	1992	2005	774	675	2.390	16
Apartment building	'overig'	0	1964	1.140	525	5.634	16,2
Apartment building	'overig'	1965	1974	1.329	829	4.900	19,6
Apartment building	'overig'	1975	1991	782	530	5.304	14,9
Apartment building	'overig'	1992	present	691	669	50	1,9

B

Appendix B

B.1. Method

Normally, for optimization, a sensitivity analysis would be performed for all different combinations of the whole DH model, after which the cheapest or least CO_2 emitting heat load distribution scenario would be selected. However, since this would take too much computational time, simplifications are made to the model. The method used for the optimization of the KPI by varying the distribution of the heat load over the different sources is still performed, however, individually per simplified submodule. These resulting KPI will then later be combined to form the final analysis of the simplified DH, but with a similar optimum as for the whole DH model. As the demand model can not be optimized by varying the heat load, this submodule will be overlooked.

Starting with the sensitivity analysis of the heat sources, each model is put in the form as defined in equation B.1. These equations will then provide the KPI dependent on the heat load the heat source should produce per scenario. In equation B.1 the KPI_k is are the KPI for heat source k, calculated by function f_k for heat load Q_{HS}. The total heat load will thus be varied, resulting in a different cost per sources, however, the total heat load should still match the demand of the DH system. For example, all heat sources are responsible for 25 percent of the heat demand which is 110 TJ/year. This ratio of heat load over the heat sources may vary in performing the sensitivity analysis. The KPIs are dependent on the quantity of heat load, so will they change when the heat load is changed, besides the influence of the DH temperature.

What might be noted is the lack of heat source IWH. This is because the IWH is very limited in optimization as it has only four options and cannot scale up. Additionally, IWH found by using all companies except ForFarmers has provided the lowest cost and CO_2. Since this heat source has the lowest KPI, it is considered inherent to the system and will not be optimized.

$$KPI_k = f_k(Q_k) \textit{ for k in TESW, TEWW and STE} \tag{B.1}$$

For the distribution, the KPI will be calculated in a similar matter. However, the cost of the demand part of the distribution can be excluded, as these will not change with changing heat load per heat source. The KPI can then be calculated as stated in equation B.2. The KPI of the distribution is formed by two functions: f_{STE}, which is the function that calculates the transport cost based on the heat load for solar thermal energy, Q_{STE} and f_{TEW} which calculates the distribution cost for the watery heat sources load of Q_{TESW} and Q_{TEWW}. As these heat sources are on the same location, only one distribution network is required to transport this heat, leading that the KPI are results of both heat load of watery sources.

$$KPI_{Distribution} = f_{TEW}(Q_{TESW}, Q_{TEWW}) + f_{STE}(Q_{STE}) \tag{B.2}$$

For the storage, however, no linear combination of heat source influence can be formed. This is because the storage is calculated based on the difference of the heat supply profile over time and the demand profile.

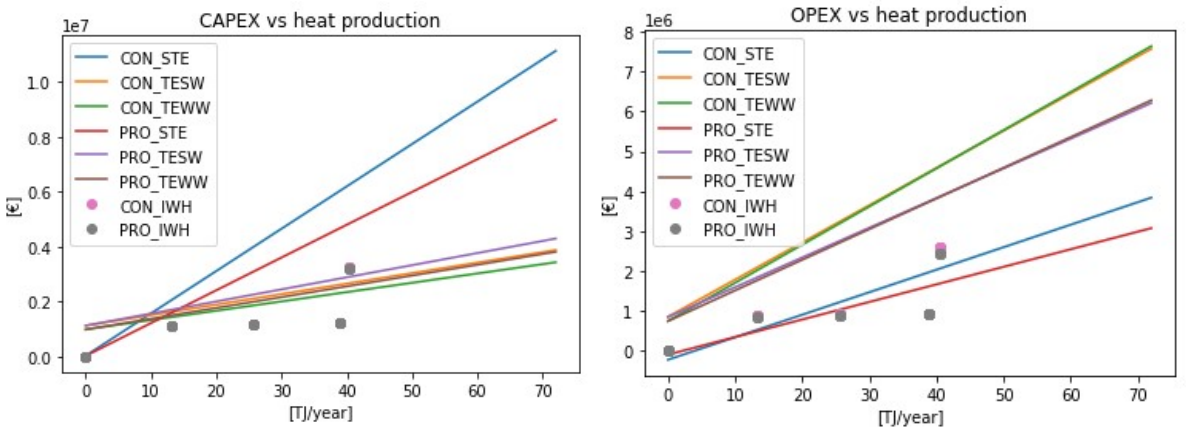

(a) CAPEX of heat source for temperature regimes illustrated in progressive and conservative base scenarios.

(b) CAPEX of heat source for temperature regimes illustrated in progressive and conservative base scenarios.

Figure B.1: Cost of heat source for progressive (PRO) and conservative (CON) temperature regime

The equation used for the supply is illustrated in B.3.

$$KPI_{TES} = f_{TES}(Q_{TESW}, Q_{TEWW}, Q_{STE}) \tag{B.3}$$

The total DH model is then calculated using the output module to form the KPI of the whole system. The output module simply adds the different KPI of the submodules to come to the final KPI, except for the LCOE. Since all the variables are changed for the LCOE, this has to be recalculated to come to the LCOE of the whole system.

B.1.1. Heat sources

In this section, the different KPI per heat sources will be approximated on the heat output per heat source to come equation B.1. As the KPI are dependent on the temperature of the DH, for both temperature regimes a model will be constructed. In figures, the CAPEX, OPEX and CO_2 emission per source are illustrated for a varying heat load as part of the total heat demand of the 70/40 °C DH system.

What is found from performing the sensitivity analysis is that the CAPEX and OPEX can be reasonably approximated using a linear approach since the Pearson number has only a deviation of 0.0001 percent of the perfect 1. Table B.1 illustrates the inputs describing the system when using a equation B.4 for the α and β factors provided by the table. The KPI is calculated dependent on the values used.

Nota bene the low total cost and CO_2 emission of IWH. This re-emphasizes why these heat sources in all cases will be used: compared to other heat sources is IWH the cheapest and lowest CO_2 intensive source.

$$KPI = \alpha * Q + \beta \tag{B.4}$$

Table B.1: Alpha and beta factor for linear equation leading to specific KPI of the heat source

		CAPEX		OPEX		CO2	
		alpha	beta	alpha	beta	alpha	beta
Conservative	STE	3.70E-05	3.32E+04	1.36E-05	-2.29E+05	4.64E-05	-4.51E+06
	TESW	9.16E-06	1.13E+06	2.24E-05	8.48E+05	2.85E-01	1.46E+02
	TEWW	8.14E-06	9.91E+05	2.30E-05	7.44E+05	3.11E-01	-7.53E+02
Progressive	STE	2.86E-05	2.81E+04	1.06E-05	-1.01E+05	3.74E-05	-2.06E+06
	TESW	1.06E-05	1.13E+06	1.79E-05	8.45E+05	1.79E-01	-3.06E+03
	TEWW	9.42E-06	9.87E+05	1.85E-05	7.41E+05	2.07E-01	1.09E+03

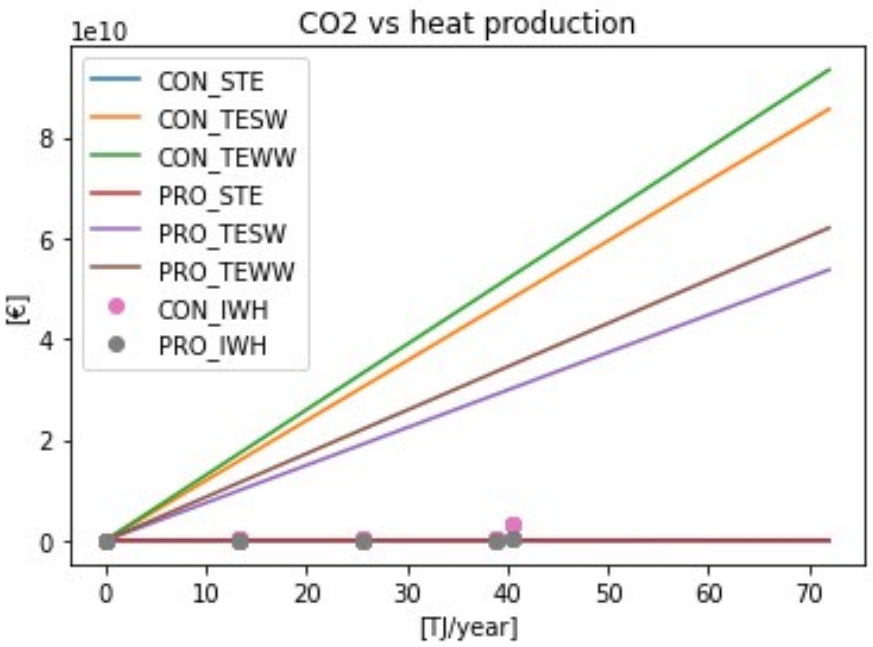

Figure B.2: CO2 of heat source for progressive (PRO) and conservative (CON) temperature regime

B.1.2. Distribution

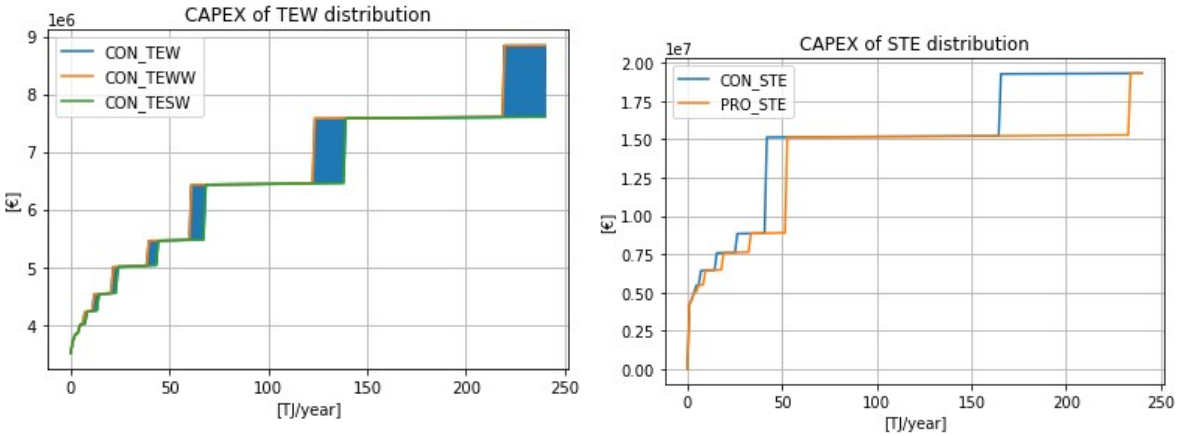

(a) CAPEX of heat distribution from watery source to storage point for 70/40 °C.Blue shaded area reflect possible ratios of TEWW/TESW of total heat supply.

(b) CAPEX of heat distribution from solar thermal energy.

Figure B.3: CAPEX of heat distribution of TEWW,TESW and solar thermal energy

For the distribution, the two distribution points are considered; the distribution of the heat from the water-based source to the storage point and that for the solar thermal based heat source to heat source. Both these heat sources are individually connected to the central storage point. The reason these distribution grids are selected comes from the fact that only the KPI of these distribution grids will change when the distribution of the heat load is altered. The KPI of the part connecting the storage to the dwellings of Westenholte will be unchanged by a different distribution of heat load over the heat sources, as the storage act as a buffer, preventing the change of equipment for the distribution grid.

Starting with the KPI of the distribution grid transporting the heat from the watery heat sources to the central storage point: In figure B.3, the CAPEX of the distribution point is illustrated. The CAPEX of the distribution grid is bound by either the graphs of the CAPEX if only one source was present, so either only TEWW or TESW. As illustrated in the figure, the CAPEX, if only TEWW was gained, is overall slightly higher than if only

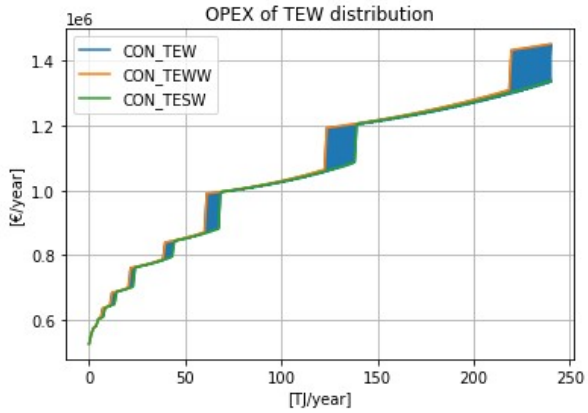

(a) OPEX of heat distribution from watery source to storage point for 70/40 °C. Blue shaded area reflect possible ratios of TEWW/TESW of total heat supply.

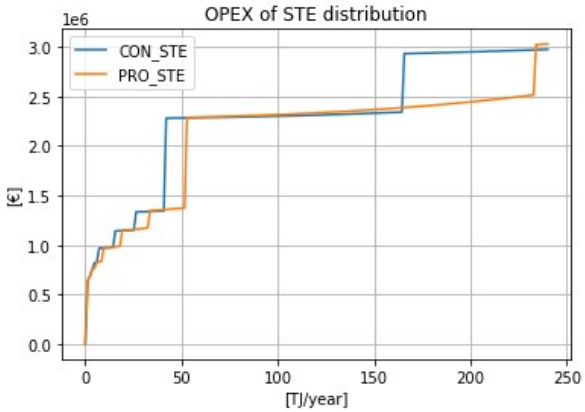

(b) OPEX of heat distribution from solar thermal energy.

Figure B.4: OPEX of heat distribution of TEWW,TESW and solar thermal energy

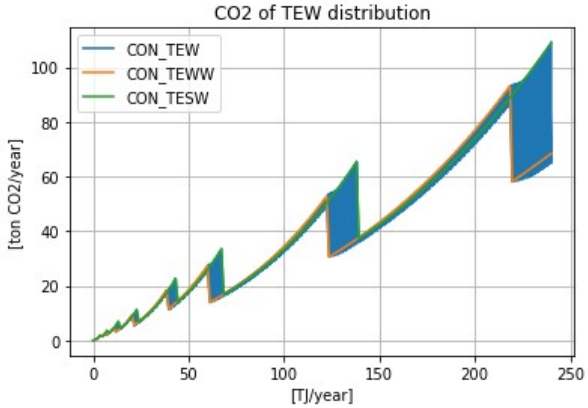

(a) CO_2 production of heat distribution from watery source to storage point for 70/40 °C. Blue shaded area reflect possible ratios of TEWW/TESW of total heat supply.

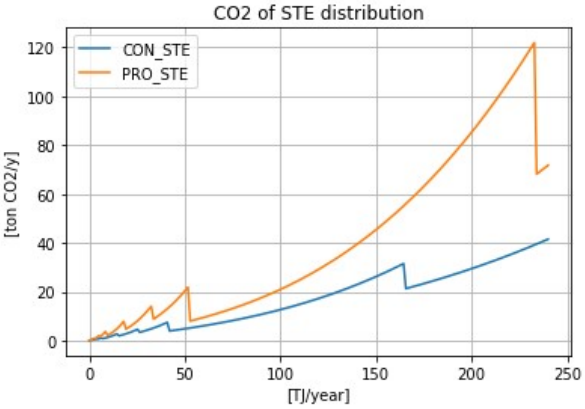

(b) CO_2 production of heat distribution from solar thermal energy.

Figure B.5: CO_2 production of heat distribution of TEWW,TESW and solar thermal energy

TESW was gained. The blue area found in between these graphs is a possible configuration of both sources. For the OPEX, the same effect is illustrated. The sudden move up in cost is explained by an increase in piping diameter. The increased pipe diameter significantly increases the CAPEX. Since the OPEX is dominated by the maintenance cost, this jump can also be identified in figure B.4. The CO_2 production however drops when piping size is increased, as the power required to pump the water decreases because the overall velocity decreases, illustrated in figure B.5.

B.1.3. Storage

The cost is determined by the profile of the heat supply and the demand. The supply should match the demand, making it impossible to determine the cost of the supply per source. However, the contribution of the heat of each heat source can be varied to calculate the KPI of the TES. As the two temperature regimes show great similarities, only 70/40 °C will be provided. In figure B.6a the CAPEX is illustrated for the 70/40 °C scenario. It illustrates that the CAPEX of the ATES is the lowest for dominance of TEWW in the total heat supply. This can be explained as TEWW is the source that gives the most steady heat supply over the year.

The OPEX, figure B.6b however is the lowest for dominance by TESW. The heat pumps upgrading the heat at the end of the year must play a crucial role in this differentiation in CAPEX and OPEX. The extra heat generated by the heat pumps must smoothen the peak in demand, reducing the overall OPEX. Since the OPEX is

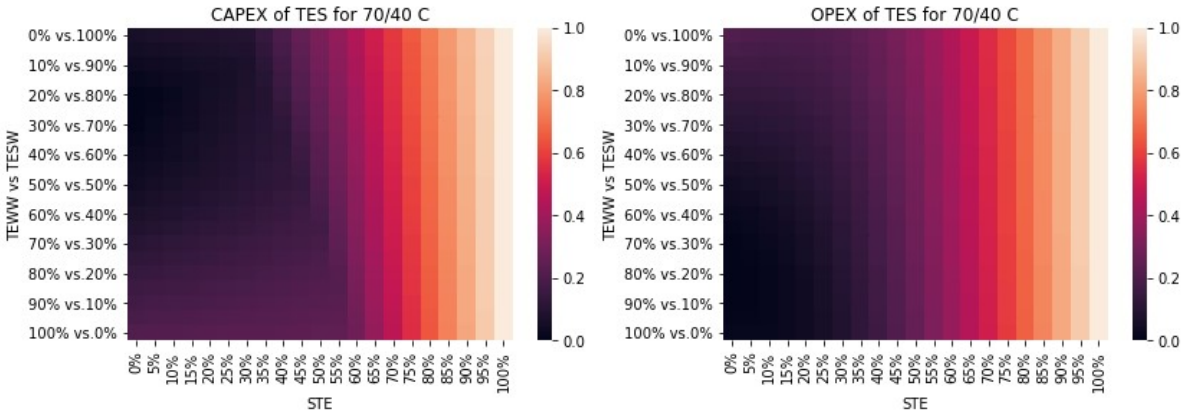

(a) Relative CAPEX of TES for different heat load distribution for 70/40 °C

(b) Relative OPEX of TES for different heat load distribution for 70/40 °C

Figure B.6: Relative CAPEX and OPEX of TES for 70/40 °C DH temperature with on the y-axis percentage of TEWW vs TESW and on x-axis amount of solar thermal energy versus amount of TESW and TEWW. 1 Is for the highest possible cost and 0 the lowest.

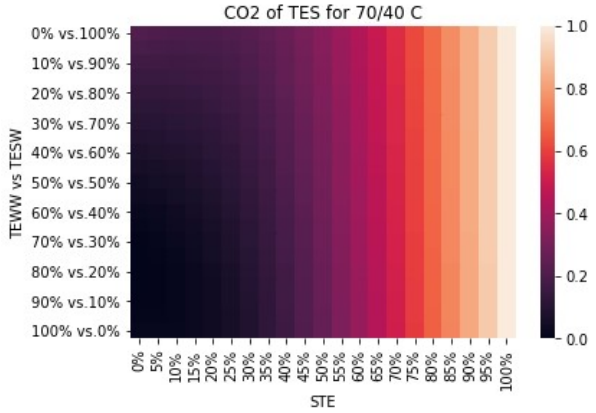

Figure B.7: CO_2 emission of TES for 70/40 °C DH temperature with on the y-axis percentage of TEWW vs TESW and on x-axis amount of solar thermal energy versus amount of TESW and TEWW. 1 Is for the highest possible CO_2 emission and 0 the lowest.

lower for a scenario dominated by TESW, it follows that also less CO_2 is emitted, as seen in figure B.7.

Bibliography

ACRON SUNMARK. (2020). *Arcon-Sunmark HT-SolarBoost 35/10* (tech. rep.). arcon-sunmark.

Afstandmeten.nl. (2020). Afstandmeten.nl. https://afstandmeten.nl/

Agentschap NL. (2011a). *Voorbeeldwoningen 2011* (tech. rep.).

Agentschap NL. (2011b). Voorbeeldwoningen 2011 bestaande bouw. *Voorbeeldwoningen 2011*, 1975–1991.

Ahmed, K., Pylsy, P., & Kurnitski, J. (2016). Hourly consumption profiles of domestic hot water for different occupant groups in dwellings. *Solar Energy*, *137*, 516–530. https://doi.org/https://doi.org/10.1016/j.solener.2016.08.033

Ajah, A. N., Patil, A. C., Herder, P. M., & Grievink, J. (2007). Integrated conceptual design of a robust and reliable waste-heat district heating system. *Applied Thermal Engineering*, *27*(7), 1158–1164. https://doi.org/https://doi.org/10.1016/j.applthermaleng.2006.02.039

allecijfers.nl. (2020). Informatie Wijk 21 Westenholte: https://allecijfers.nl/wijk/wijk-21-westenholte-zwolle/

Atia, D. M., Fahmy, F. H., Ahmed, N. M., & Dorrah, H. T. (2012). Optimal sizing of a solar water heating system based on a genetic algorithm for an aquaculture system. *Mathematical and Computer Modelling*, *55*(3-4), 1436–1449. https://doi.org/10.1016/j.mcm.2011.10.022

Bava, F., & Furbo, S. (2015). Numerical model for pressure drop and flow distribution in a solar collector with horizontal U-connected pipes. *ISES Solar World Congress 2015, Conference Proceedings*, (November), 870–879. https://doi.org/10.18086/swc.2015.10.01

Bayer, P., Saner, D., Bolay, S., Rybach, L., & Blum, P. (2012). Greenhouse gas emission savings of ground source heat pump systems in Europe: A review. *Renewable and Sustainable Energy Reviews*, *16*(2), 1256–1267. https://doi.org/https://doi.org/10.1016/j.rser.2011.09.027

Bedir, M. (2017). Occupant behavior and energy consumption in dwellings: An analysis of behavioral models and actual energy consumption in the dutch housing stock. *A+ BE| Architecture and the Built Environment*, (16), 1–266.

Best, I. (2018). Economic comparison of low-temperature and ultra-low-temperature district heating for new building developments with low heat demand densities in Germany. *International Journal of Sustainable Energy Planning and Management*, *16*, 45–60.

Bloemendal, M., Jaxa-Rozen, M., & Olsthoorn, T. (2018). Methods for planning of ATES systems. *Applied Energy*, *216*, 534–557. https://doi.org/https://doi.org/10.1016/j.apenergy.2018.02.068

Boilermarkt.nl. (2021). 150 Boiler Stiebel Eltron Medium Line. https://www.boilermarkt.nl/Grote-Boilers/Elektrische-Boiler-Medium-Line-Stiebel-Eltron-Horizontaal-Ophangen/Stiebel-Eltron-Boiler-150L-PSH-Comfort-150-Uni/

Bonilla-Campos, I., Nieto, N., del Portillo-Valdes, L., Egilegor, B., Manzanedo, J., & Gaztañaga, H. (2019). Energy efficiency assessment: Process modelling and waste heat recovery analysis. *Energy Conversion and Management*, *196*, 1180–1192. https://doi.org/https://doi.org/10.1016/j.enconman.2019.06.074

Caissie, D. (2006). The thermal regime of rivers: a review. *Freshwater biology*, *51*(8), 1389–1406.

CBS. (n.d.). Energieverbruik particuliere woningen; woningtype en regio's. https://opendata.cbs.nl/statline/#/CBS/nl/dataset/81528NED/table?dl=3A0A4

CBS. (2014). CBS Aardgas- en Elektriciteitslevering 2014 WMS. http://nationaalgeoregister.nl/geonetwork/srv/dut/catalog.search#/metadata/b4a19fe1-ea82-423f-83e8-ece0aa466a25

CBS. (2018). Energielevering aan bedrijven en instellingen per wijk. https://www.cbs.nl/nl-nl/maatwerk/2019/46/energielevering-aan-bedrijven-en-instellingen-per-wijk

CBS. (2020a). Opendata CBS. https://opendata.cbs.nl/#/CBS/nl/navigatieScherm/thema?themaNr=84632

CBS. (2020b). Wekelijks gasverbruik industrie per sector. https://www.cbs.nl/nl-nl/maatwerk/2020/25/wekelijks-gasverbruik-industrie-per-sector

CE Delft. (2019). overzicht aanpassingen Vesta MAIS.

Chowdhury, J. I., Hu, Y., Haltas, I., Balta-Ozkan, N., Matthew, G. J., & Varga, L. (2018). Reducing industrial energy demand in the UK: A review of energy efficiency technologies and energy saving potential in selected sectors. *Renewable and Sustainable Energy Reviews*, *94*, 1153–1178. https://doi.org/https://doi.org/10.1016/j.rser.2018.06.040

Church, K. (2016). Energy sources for district heating and cooling. *Advanced district heating and cooling (dhc) systems* (pp. 121–143). Elsevier.

Colla, M., Ioannou, A., & Falcone, G. (2020). Critical review of competitiveness indicators for energy projects. *Renewable and Sustainable Energy Reviews*, *125*(December 2019). https://doi.org/10.1016/j.rser.2020.109794

de Boer, T. J. (2018). *Optimization of a District Heating Network with the Focus on Heat Loss* (tech. rep.). TU Delft.

de Guadalfajara, M., Lozano, M., & Serra, L. (2014). A Simple Method to Calculate Central Solar Heating Plants with Seasonal Storage. *Energy Procedia*, *48*, 1096–1109. https://doi.org/10.1016/j.egypro.2014.02.124

Dénarié, A., Calderoni, M., & Aprile, M. (2018). Multicriteria Approach for a Multisource District Heating BT - Smart and Sustainable Planning for Cities and Regions. In A. Bisello, D. Vettorato, P. Laconte, & S. Costa (Eds.). Springer International Publishing.

Descamps, M. N., Leoncini, G., Vallée, M., & Paulus, C. (2018). Performance assessment of a multi-source heat production system with storage for district heating. *Energy Procedia*, *149*, 390–399. https://doi.org/https://doi.org/10.1016/j.egypro.2018.08.203

de Wit-Blok, M. (2017). Duurzame warmte 'de meerwaarde van (hogetemperatuur)warmteopslag voor warmtenetten. *Uneto-Vni*.

Dickes, R., Desideri, A., Lemort, V., & Quolin, S. (2015). Model reduction for simulating the dynamic behavior of parabolic troughs and a thermocline energy storage in a micro-solar power unit. (July).

Doracic, B., Novosel, T., Pukšec, T., & Dui, N. (2018). Evaluation of Excess Heat Utilization in District Heating Systems by Implementing Levelized Cost of. https://doi.org/10.3390/en11030575

Dugdale, S. J., Hannah, D. M., & Malcolm, I. A. (2017). River temperature modelling: A review of process-based approaches and future directions. *Earth-Science Reviews*, *175*, 97–113. https://doi.org/https://doi.org/10.1016/j.earscirev.2017.10.009

Dumont, O., Carmo, C., Dickes, R., & Georges, E. (2016). Hot water tanks : How to select the optimal modelling approach ? Hot water tanks : How to select the optimal modelling approach ? (June).

Dürrenmatt, D. J., & Wanner, O. (2014a). A mathematical model to predict the effect of heat recovery on the wastewater temperature in sewers. *Water Research*, *48*(1), 548–558. https://doi.org/10.1016/j.watres.2013.10.017

Dürrenmatt, D. J., & Wanner, O. (2014b). A mathematical model to predict the effect of heat recovery on the wastewater temperature in sewers. *Water Research*, *48*, 548–558. https://doi.org/https://doi.org/10.1016/j.watres.2013.10.017

ECN, & TNO. (2016). Technology factsheet,Air Source Heat Pump. https://doi.org/10.2790/057687

EDUgis. (n.d.). Edugis. http://kaart.edugis.nl/?x=674262.31972174&y=6895151.0010328&z=15&layers=Achtergrondlagen%0A%20:OpenStreetMap:OpenStreetMap;Gebouwen%0A%20:Panden%20e.d.:panden%20-%20bouwjaar

Elshof, P. I. (2016). Changing energy demand in the residential sector due to decentralized generators and the electrification of heating and driving.

Energy Matters. (2014). Rendement ketel.

European Commission. (2019). The European Green Deal. *Annex to the Communication from the Commission to the European Parliament, the European Council, the Council, the European Economic and Social Committee and the Committee of the Regions*.

European Enviroment Agency. (2020). Greenhouse gas emission intensity of electricity generation. https://www.eea.europa.eu/data-and-maps/daviz/co2-emission-intensity-6#tab-googlechartid_googlechartid_chart_111_filters=%7B%22rowFilters%22%3A%7B%7D%3B%22columnFilters%22%3A%7B%22pre_config_date%22%3A%5B2018%5D%7D%3B%22sortFilter%22%3A%5B%22index_2018%22

European Solar Thermal Industry Federation. (2012). Understanding and using collector test standard EN 12975. *QAiST*, 80.

Fang, H., Xia, J., & Jiang, Y. (2015). Key issues and solutions in a district heating system using low-grade industrial waste heat. *Energy*, *86*, 589–602. https://doi.org/https://doi.org/10.1016/j.energy.2015.04.052

Fang, H., Xia, J., Zhu, K., Su, Y., & Jiang, Y. (2013). Industrial waste heat utilization for low temperature district heating. *Energy Policy*, *62*, 236–246. https://doi.org/https://doi.org/10.1016/j.enpol.2013.06.104

Ferreira, C. I. (2021). Contents Lecture 10- course ME 45165 2021.

Fleuchaus, P., Godschalk, B., Stober, I., & Blum, P. (2018). Worldwide application of aquifer thermal energy storage – A review. *Renewable and Sustainable Energy Reviews*, *94*(November 2017), 861–876. https://doi.org/10.1016/j.rser.2018.06.057

Freriks, A. (2011). DACE price booklet.

Friedel, P., Jong, A. d., & Horstink, M. (2014). *Eindrapportage veldtesten, Energieprestaties van 5 warmtetechnieken bij woningen in de praktijk.* (tech. rep.). RVO. https://www.lente-akkoord.nl/wp-content/uploads/2014/01/Praktijkprestaties-van-warmtetechnieken-bij-huishoudens.pdf

Gadd, H., & Werner, S. (2015). 18 - Thermal energy storage systems for district heating and cooling. In L. F. Cabeza (Ed.), *Advances in thermal energy storage systems* (pp. 467–478). Woodhead Publishing. https://doi.org/https://doi.org/10.1533/9781782420965.4.467

Guelpa, E., & Verda, V. (2019). Thermal energy storage in district heating and cooling systems: A review. *Applied Energy*, *252*, 113474. https://doi.org/https://doi.org/10.1016/j.apenergy.2019.113474

Guzzini, A., Pellegrini, M., Pelliconi, E., et al. (2020). Low Temperature District Heating: An Expert Opinion Survey. *Energies*, *13*(4), 810.

Haichar, A. e. (2018). *Concept of a HT-ATES system well design on the TU Delft campus* (Doctoral dissertation November). Delft University of Technology.

Hansen, K. (2019). Decision-making based on energy costs: Comparing levelized cost of energy and energy system costs. *Energy Strategy Reviews*, *24*, 68–82. https://doi.org/https://doi.org/10.1016/j.esr.2019.02.003

Hart, O. E., & Halden, R. U. (2020). Modeling wastewater temperature and attenuation of sewage-borne biomarkers globally. *Water Research*, *172*, 115473. https://doi.org/https://doi.org/10.1016/j.watres.2020.115473

Hepbasli, A., Biyik, E., Ekren, O., Gunerhan, H., & Araz, M. (2014). A key review of wastewater source heat pump (WWSHP) systems. *Energy Conversion and Management*, *88*, 700–722.

Hoogervorst, N. (2016). *Toekomstbeeld klimaatneutrale warmtenetten in Nederland* (tech. rep.). Planbureau voor leefomgeving.

Hoogervorst, N., Langeveld, T., Bemmel, B. v., Molen, F. v. d., Polen, S. v., Ta-vares, J., & van den Wijngaart, R. (2020). *Startanalyse aardgasvrije buurten* (tech. rep.). Planbureau voor de leefomgeving.

Huang, J., Fan, J., & Furbo, S. (2019). Feasibility study on solar district heating in China. *Renewable and Sustainable Energy Reviews*, *108*, 53–64. https://doi.org/https://doi.org/10.1016/j.rser.2019.03.014

IBIS. (n.d.). Landelijke informatie IBIS Bedrijventerrein. https://www.ibis-bedrijventerreinen.nl/

IF, T., & Stowa. (2018). Leeswijzer bij de studie naar kansen " Thermische Energie uit Afvalwater ".

Jarić, M., Budimir, N., Rakonjac, I., & Budimir, S. (2015). *Manufacturing costs of gasketed and brazed plate heat exchangers*. https://www.researchgate.net/publication/331152845_Manufacturing_costs_of_gasketed_and_brazed_plate_heat_exchangers

Kemna, R., & Acedo, J. (2014). Average EU building heat load for HVAC equipment. *Final Report of Framework Contract ENER C*, (August). http://scholar.google.com/scholar?hl=en&btnG=Search&q=intitle:Average+EU+building+heat+load+for+HVAC+equipment#0

Kennisinstituut voor Installatietechniek. (2012). *ISSO-publicatie 7 Grondleidingen voor warmte- en koudetransport*.

Klimaatwet. (n.d.). https://wetten.overheid.nl/jci1.3:c:BWBR0042394&z=2020-01-01&g=2020-01-01%0A

Kluck, J., van den Bulk, J., Flameling, T., & de Brauw, H. (2011). *Thermische energie uit afvalwater in Zwolle* (tech. rep. No. 25). STOWA. Stationsplein 89 3818 LE Amersfoort.

Knepper, S. (2019). *Meeting heat demands in existing dutch homes using low temperature district heating* (tech. rep.). TU Delft.

KNMI. (2020). Klimatologie Uurgegevens van het weer in Nederland - Download. http://projects.knmi.nl/klimatologie/uurgegevens/selectie.cgi

Kranz, S., & Bartels, J. (2010). Simulation and Data Based Optimisation of an Operating Seasonal Aquifer Thermal Energy Storage. *Proceedings World Geothermal Congress, Bali, Indonesia*, (April), 1–6.

Kretschmer, F., Simperler, L., & Ertl, T. (2016). Analysing wastewater temperature development in a sewer system as a basis for the evaluation of wastewater heat recovery potentials. *Energy and Buildings*, *128*, 639–648. https://doi.org/10.1016/j.enbuild.2016.07.024

Kruit, K., Schepers, B., Roosjen, R., & Boderie, P. (2018). *Nationaal potentieel van aquathermie* (tech. rep.). CE Delft.

Kuosa, M., Kontu, K., Mäkilä, T., Lampinen, M., & Lahdelma, R. (2013). Static study of traditional and ring networks and the use of mass flow control in district heating applications. *Applied Thermal Engineering*, *54*(2), 450–459. https://doi.org/https://doi.org/10.1016/j.applthermaleng.2013.02.018

Laajalehto, T., Kuosa, M., Mäkilä, T., Lampinen, M., & Lahdelma, R. (2014). Energy efficiency improvements utilising mass flow control and a ring topology in a district heating network. *Applied Thermal Engineering*, *69*(1), 86–95. https://doi.org/https://doi.org/10.1016/j.applthermaleng.2014.04.041

Langeveld, J. (2004). *Interactions within wastewater systems* (Vol. PhD).

Lee, K. S. (2010). A review on concepts, applications, and models of aquifer thermal energy storage systems. *Energies*, *3*(6), 1320–1334. https://doi.org/10.3390/en3061320

Lensink, S. (2020). EINDADVIES BASISBEDRAGEN.

Li, H., & Nord, N. (2018). Transition to the 4th generation district heating - Possibilities, bottlenecks, and challenges. *Energy Procedia*, *149*, 483–498. https://doi.org/10.1016/j.egypro.2018.08.213

Lund, H., Werner, S., Wiltshire, R., Svendsen, S., Thorsen, J. E., Hvelplund, F., & Mathiesen, B. V. (2014). 4th Generation District Heating (4GDH): Integrating smart thermal grids into future sustainable energy systems. *Energy*, *68*, 1–11.

Lund, R., Østergaard, D. S., Yang, X., & Mathiesen, B. V. (2017). Comparison of low-temperature district heating concepts in a long-term energy system perspective. *International Journal of Sustainable Energy Planning and Management*, *12*, 5–18.

Mangold, D., Schmidt, T., & Müller-Steinhagen, H. (2004). Seasonal thermal energy storage in Germany. *Structural Engineering International: Journal of the International Association for Bridge and Structural Engineering (IABSE)*, *14*(3), 230–232. https://doi.org/10.2749/101686604777963739

Martin, C., & Vanrolleghem, P. A. (2014). Analysing, completing, and generating influent data for WWTP modelling: A critical review. *Environmental Modelling and Software*, *60*, 188–201. https://doi.org/10.1016/j.envsoft.2014.05.008

Mazhar, A. R., Liu, S., & Shukla, A. (2018). A state of art review on the district heating systems. *Renewable and Sustainable Energy Reviews*, *96*, 420–439. https://doi.org/https://doi.org/10.1016/j.rser.2018.08.005

McKenna, R. C., & Norman, J. B. (2010). Spatial modelling of industrial heat loads and recovery potentials in the UK. *Energy Policy*, *38*(10), 5878–5891. https://doi.org/https://doi.org/10.1016/j.enpol.2010.05.042

Milieucentraal. (2021). Subsidie voor isolatie | Milieu Centraal. https://www.milieucentraal.nl/energiebesparen/energiesubsidies-en-leningen/subsidie-voor-isolatie/

Miró, L., Gasia, J., & Cabeza, L. F. (2016). Thermal energy storage (TES) for industrial waste heat (IWH) recovery: A review. *Applied Energy*, *179*, 284–301. https://doi.org/https://doi.org/10.1016/j.apenergy.2016.06.147

Mitchell, M. S., & Spitler, J. D. (2013). Open-loop direct surface water cooling and surface water heat pump systems—A review. *HVAC&R Research*, *19*(2), 125–140.

Mora, N. P., Bava, F., Andersen, M., Bales, C., Lennermo, G., Nielsen, C., Furbo, S., & Martínez, V. (2018). Solar district heating and cooling : A review. (May 2017), 1419–1441. https://doi.org/10.1002/er.3888

Niessink, R. (2019). *TECHNOLOGY FACTSHEET AQUATHERMAL - LOW TEMPERATURE HEAT FROM SURFACE WATER* (tech. rep.).

Niewold, F. (2019). *Kengetallen aquathermie* (tech. rep.). IF technology.

Østergaard, D. S. (2018). Heating of existing buildings by low-temperature district heating.

Paardekooper, S., Lund, R. S., Mathiesen, B. V., Chang, M., Petersen, U. R., Grundahl, L., David, A., Dahlbæk, J., Kapetanakis, I. A., Lund, H., et al. (2018). Heat Roadmap Netherlands: Quantifying the Impact of Low-Carbon Heating and Cooling Roadmaps.

Pakere, I., Lauka, D., & Blumberga, D. (2018). Solar power and heat production via photovoltaic thermal panels for district heating and industrial plant. *Energy*, *154*, 424–432. https://doi.org/https://doi.org/10.1016/j.energy.2018.04.138

Papapetrou, M., Kosmadakis, G., Cipollina, A., La Commare, U., & Micale, G. (2018). Industrial waste heat: Estimation of the technically available resource in the EU per industrial sector, temperature level and country. *Applied Thermal Engineering*, *138*, 207–216. https://doi.org/https://doi.org/10.1016/j.applthermaleng.2018.04.043

Perez-Mora, N., Bava, F., Andersen, M., Bales, C., Lennermo, G., Nielsen, C., Furbo, S., & Mart\'\inez-Moll, V. (2018). Solar district heating and cooling: A review. *International Journal of Energy Research*, *42*(4), 1419–1441.

Persson, U., & Werner, S. (2010). Effective width - The relative demand for district heating pipe lengths in city areas. *12th International Symposium on District Heating and Cooling*, 128–131.

Pieper, H., Ommen, T., Buhler, F., Lava Paaske, B., Elmegaard, B., & Brix Markussen, W. (2018). Allocation of investment costs for large-scale heat pumps supplying district heating. *Energy Procedia*, *147*, 358–367. https://doi.org/10.1016/j.egypro.2018.07.104

Pieper, H., Ommen, T., Elmegaard, B., & Brix Markussen, W. (2019). Assessment of a combination of three heat sources for heat pumps to supply district heating. *Energy*, *176*, 156–170. https://doi.org/10.1016/j.energy.2019.03.165

Pinel, P., Cruickshank, C. A., Beausoleil-morrison, I., & Wills, A. (2011). A review of available methods for seasonal storage of solar thermal energy in residential applications. *Renewable and Sustainable Energy Reviews*, *15*(7), 3341–3359. https://doi.org/10.1016/j.rser.2011.04.013

Rezaie, B., & Rosen, M. A. (2012). District heating and cooling: Review of technology and potential enhancements. *Applied energy*, *93*, 2–10.

Rijksoverheid. (n.d.). Emissieregistratie. http://www.emissieregistratie.nl/erpubliek/erpub/facility.aspx

Sakhaei, S. A., & Valipour, M. S. (2019). Performance enhancement analysis of The flat plate collectors: A comprehensive review. *Renewable and Sustainable Energy Reviews*, *102*, 186–204. https://doi.org/https://doi.org/10.1016/j.rser.2018.11.014

Sarbu, I., Mirza, M., & Crasmareanu, E. (2019). A review of modelling and optimisation techniques for district heating systems. *International Journal of Energy Research*, *43*(13), 6572–6598.

Sayegh, M. A., Jadwiszczak, P., Axcell, B. P., Niemierka, E., Bryś, K., & Jouhara, H. (2018). Heat pump placement, connection and operational modes in European district heating. *Energy and Buildings*, *166*, 122–144. https://doi.org/https://doi.org/10.1016/j.enbuild.2018.02.006

Schepers, B., & van Lieshout, M. (2011). *IPO Nationale Routekaart Restwarmte* (tech. rep.). CE Delft.

Schmidt, D., Kallert, A., Blesl, M., Svendsen, S., Li, H., Nord, N., & Sipilä, K. (2017). Low Temperature District Heating for Future Energy Systems. *Energy Procedia*, *116*, 26–38.

Schweiger, G., Kuttin, F., & Posch, A. (2019). District Heating Systems: An Analysis of Strengths, Weaknesses, Opportunities, and Threats of the 4GDH. *Energies*, *12*(24), 4748.

Segers, R., Oever, R., Niessink, R. J. M., & Menkveld, M. (2019). Warmtemonitor 2017.

Sociaal-Economische Raad. (2018). Voorstel voor hoofdlijnen van het Klimaatakkoord. *Den Haag: Klimaatberaad*.

Spitler, J. D., & Mitchell, M. S. (2016). Surface water heat pump systems. *Advances in ground-source heat pump systems* (pp. 225–246). Elsevier.

Statline. (n.d.). Aardgas en elektriciteit, gemiddelde prijzen van eindverbruikers. https://opendata.cbs.nl/statline/#/CBS/nl/dataset/81309NED/table?fromstatweb

Staub, S., Bazan, P., Braimakis, K., Müller, D., Regensburger, C., Scharrer, D., Schmitt, B., Steger, D., German, R., Karellas, S., Pruckner, M., Schlücker, E., Will, S., & Karl, J. (2018). Reversible heat pump-organic rankine cycle systems for the storage of renewable electricity. *Energies*, *11*(6). https://doi.org/10.3390/en11061352

STOWA. (2018). Handreiking Aquathermie. https://www.stowa.nl/sites/default/files/assets/PUBLICATIES/Publicaties%0A2018/STOWA%0A2018-47%0Ahandreiking%0Aaquathermie.pdf

Tagliafico, L. A., Scarpa, F., & De Rosa, M. (2014). Dynamic thermal models and CFD analysis for flat-plate thermal solar collectors - A review. *Renewable and Sustainable Energy Reviews*, *30*, 526–537. https://doi.org/10.1016/j.rser.2013.10.023

Talebi, B., Mirzaei, P. A., Bastani, A., & Haghighat, F. (2016). A review of district heating systems: modeling and optimization. *Frontiers in Built Environment*, *2*, 22.

Technim. (n.d.). Warmtepompboiler AQUA1 PLUS 200HT €650,- subsidie. https://www.technim.nl/sanitair/warmtepompboilers/warmtepompboiler-aqua1-plus-200ht/

Tessel, P., & Pijl, P. v. d. (2006). COMMUNAAL AFVALWATER OP TEMPERATUUR HOUDEN VOOR ACTIEVER SLIB IN RWZI'S.

The Engineering Toolbox. (n.d.). Typical Air Duct Velocities. https://www.engineeringtoolbox.com/flow-velocity-air-ducts-d_388.html

Thermaflex. (n.d.). Catalogus Flexalen. https://thermaflex.com/nl/download/bestand/214

Thomsen, P. D., & Overbye, P. M. (2016). Energy storage for district energy systems. *Advanced district heating and cooling (dhc) systems* (pp. 145–166). Elsevier.

Tian, Z., Zhang, S., Deng, J., Fan, J., Huang, J., Kong, W., Perers, B., & Furbo, S. (2019). Large-scale solar district heating plants in Danish smart thermal grid: Developments and recent trends. *Energy Conversion and Management*, *189*, 67–80. https://doi.org/https://doi.org/10.1016/j.enconman.2019.03.071

Tumuluru, J. S., Conner, C. C., & Hoover, A. N. (2016). Method to produce durable pellets at lower energy consumption using high moisture corn stover and a corn starch binder in a flat die pellet mill. *Journal of Visualized Experiments*, *2016*(112), 1–13. https://doi.org/10.3791/54092

van Haarst. (2021). Zwolle RWZI. https://www.hvanhaarst.nl/Betonspecialisten/Zwolle_RWZI.html

Van Miltenburg, R. M. (2016). Integration of decentralized solar collectors in Dutch district heating networks.

Vereniging Nederlandse Watersector. (2021). RWZI - Zwolle. https://www.watersector.nl/rwzi/150/rwzi

Vesterlund, M., Toffolo, A., & Dahl, J. (2017). Optimization of multi-source complex district heating network, a case study. *Energy*, *126*, 53–63. https://doi.org/https://doi.org/10.1016/j.energy.2017.03.018

Virtanen, P., Gommers, R., Oliphant, T. E., Haberland, M., Reddy, T., Cournapeau, D., Burovski, E., Peterson, P., Weckesser, W., Bright, J., van der Walt, S. J., Brett, M., Wilson, J., Millman, K. J., Mayorov, N., Nelson, A. R. J., Jones, E., Kern, R., Larson, E., … SciPy 1.0 Contributors. (2020). {SciPy} 1.0: Fundamental Algorithms for Scientific Computing in Python. *Nature Methods*, *17*, 261–272. https://doi.org/10.1038/s41592-019-0686-2

Wang, H., Wang, H., Zhou, H., & Zhu, T. (2018). Modeling and optimization for hydraulic performance design in multi-source district heating with fluctuating renewables. *Energy Conversion and Management*, *156*, 113–129. https://doi.org/https://doi.org/10.1016/j.enconman.2017.10.078

Weeda, M., & Niessink, R. (2020). *Waterstof als optie voor een klimaatneutrale warmtevoorziening in de bestaande bouw* (tech. rep.). TNO.

Weeren, B.-J. v., Bos, S., Noij, L., & Rens, G. v. (2018). *PORTFOLIO THERMISCHE ENERGIE UIT AFVALWATER; WAARDEVOLLE LESSEN UIT DE PRAKTIJK* (tech. rep.). Stichting Toegepast Onderzoek Waterbeheer. https://www.stowa.nl/publicaties/portfolio-thermische-energie-uit-afvalwater-waardevolle-lessen-uit-de-praktijk

Wells, S. A., Bashkatov, D., & Makinia, J. (2005). Modeling and evaluating temperature dynamics in wastewater treatment plants. *World Water Congress 2005: Impacts of Global Climate Change - Proceedings of the 2005 World Water and Environmental Resources Congress*, *40792*(November 2014), 137. https://doi.org/10.1061/40792(173)137

White, F. M. (1979). *Fluid mechanics*. Tata McGraw-Hill Education.

Woolley, E., Luo, Y., & Simeone, A. (2018). Industrial waste heat recovery: A systematic approach. *Sustainable Energy Technologies and Assessments*, *29*, 50–59. https://doi.org/https://doi.org/10.1016/j.seta.2018.07.001

Yang, B., Jiang, Y., Fu, L., & Zhang, S. (2018). Experimental and theoretical investigation of a novel full-open absorption heat pump applied to district heating by recovering waste heat of flue gas. *Energy and Buildings*, *173*, 45–57. https://doi.org/https://doi.org/10.1016/j.enbuild.2018.05.021